ANALYTICAL, NUMERICAL AND EXPERIMENTAL INVESTIGATION OF THE
DISTORTION BEHAVIOR OF STEEL SHAFTS DURING THROUGH-HARDENING

A THESIS SUBMITTED TO
THE GRADUATE SCHOOL OF NATURAL AND APPLIED SCIENCES
OF
MIDDLE EAST TECHNICAL UNIVERSITY

BY

BETÜL PELİN MARADİT

IN PARTIAL FULFILLMENT OF THE REQUIREMENTS
FOR
THE DEGREE OF MASTER OF SCIENCE
IN
METALLURGICAL AND MATERIALS ENGINEERING

SEPTEMBER 2010

Approval of the thesis:

ANALYTICAL, NUMERICAL AND EXPERIMENTAL INVESTIGATION OF THE DISTORTION BEHAVIOR OF STEEL SHAFTS DURING THROUGH-HARDENING

submitted by **BETÜL PELİN MARADİT** in partial fulfillment of the requirements for the degree of **Master of Science in Department of Metallurgical and Materials Engineering, Middle East Technical University** by,

Prof. Dr. Canan Özgen   _____
Dean, Graduate School of **Natural and Applied Sciences**

Prof. Dr. Tayfur Öztürk   _____
Head of Department, **Metallurgical and Materials Engineering**

Prof. Dr. C. Hakan Gür   _____
Supervisor, **Metallurgical and Materials Engineering Dept., METU**

Dr. Thomas Lübben   _____
Co-Supervisor, **Foundation Inst. for Materials Science (IWT), Germany**

Examining Committee Members:

Prof. Dr. Tayfur Öztürk   _____
Metallurgical and Materials Engineering Dept., METU

Prof. Dr. C. Hakan Gür   _____
Metallurgical and Materials Engineering Dept., METU

Prof. Dr. İshak Karakaya   _____
Metallurgical and Materials Engineering Dept., METU

Prof. Dr. Rıza Gürbüz   _____
Metallurgical and Materials Engineering Dept., METU

Dr. Caner Şimşir   _____
Manufacturing Engineering Dept., Atılım University

Date: 17.09.2010

I hereby declare that all information in this document has been obtained and presented in accordance with academic rules and ethical conduct. I also declare that, as required by these rules and conduct, I have fully cited and referenced all material and results that are not original to this work.

Name, Last name: Betül Pelin Maradit

Signature:

ABSTRACT

ANALYTICAL, NUMERICAL AND EXPERIMENTAL INVESTIGATION OF THE DISTORTION BEHAVIOR OF STEEL SHAFTS DURING THROUGH-HARDENING

Maradit, Betül Pelin

M.Sc, Department of Metallurgical and Materials Engineering
Supervisor: Prof. Dr. C. Hakan Gür
Co-Supervisor: Dr. Thomas Lübben

September 2010, 164 pages

Distortion (undesired dimension and shape changes) is one of the most important problems of through hardened steel components. During quenching, anisotropic dimensional changes are inevitable due to classical plasticity and transformation induced plasticity. Moreover; various distortion potential carriers are brought into material during production chain.

This study consists of analytical, numerical and experimental investigations of quench distortion. In numerical and analytical part, sensitivity analysis of the quenching model, and dimensional analysis of distortion were conducted by utilizing experimentally verified simulations. In sensitivity analysis, effect of uncertainties in input data on simulation results were determined, whereas; in dimensional analysis, the influence of various dimensionless numbers that govern quench distortion were investigated. Throughout the study, gas-nozzle-field quenching of SAE52100 long shafts were simulated. Simulations were performed by commercial finite element analysis software, SYSWELD®. Conceptual results indicate that the most important material properties and dimensionless numbers are the ones that govern volume change.

Moreover, those that determine plasticity of austenite significantly affect isotropy of the dimensional changes. When unimportant dimensionless numbers are eliminated, there remain 14 dimensionless combinations that govern the problem.

In experimental part of the study; effect of microstructure on distortion behavior of SAE52100 long cylinders with various diameters was investigated. In addition to gas-nozzle-field quenching, salt bath and high speed quenching experiments were performed. In regards to experimental findings, there is a correlation between distortions of long cylinders and machining position with respect to billet.

Keywords: Dimensional Analysis, Distortion, SAE5100, Sensitivity Analysis, Through hardening

ÖZ

ÇELİK ŞAFTLARIN SERTLEŞTİRİLMESİ SIRASINDA OLUŞAN ÇARPILMALARIN ANALİTİK, NUMERİK VE DENEYSEL OLARAK İNCELENMESİ

Maradit, Betül Pelin

Yüksek Lisans, Metalurji ve Malzeme Mühendisliği Bölümü
Tez Yöneticisi: Prof. Dr. C. Hakan Gür
Ortak Tez Yöneticisi: Dr. Thomas Lübben

Eylül 2010, 164 sayfa

Çarpılma (istenmeyen boyut ve şekil değişimleri) çeliklerin sertleştirilmesi sırasında meydana gelen en önemli problemlerden biridir. Sertleştirme esnasında meydana gelen klasik plastisite ve dönüşüm plastisitesi kaçınılmaz anizotropik boyut değişimlerine neden olmaktadır. Ayrıca, üretimin farklı aşamalarında "çarpılma potansiyeli taşıyıcıları" parçada yer etmektedir.

Bu çalışmada, sertleştirme işlemi süresince meydana gelen çarpılmalar, analitik, numerik ve deneysel olarak incelenmiştir. Numerik ve analitik kısımda, sertleştirme benzetimlerinin hassasiyet analizi yapılmış, parça çarpılmaları boyut analizi ile incelenmiştir. Analizler deneysel olarak desteklenmiş benzetimler yardımıyla yapılmıştır. Hassasiyet analizindeki amaç, benzetim girdilerindeki belirsizliklerin, benzetim sonuçlarına olan etkisini ortaya koymaktır. Boyut analizindeki amaç ise önceki çalışmalarda belirlenmiş boyutsuz sayıların sertleştirme işleminden kaynaklanan boyut değişimlerine olan etkisini incelemektir. Çalışma boyunca, SAE52100 çelik şaftların gazla hızlı soğutulması modellenmiştir. Benzetimlerde ticari

sonlu eleman programı SYSWELD® kullanılmıştır. Teorik kısımdaki sonuçlar, hacim değişimini etkileyen malzeme özelliklerinin ve boyutsuz sayırın yüksek önem teşkil ettiğini göstermiştir. Ayrıca, östenit fazının plastisitesini etkileyen parametrelerin, boyut değişimlerinin izotropisini önemli ölçüde etkiledikleri gözlemlenmiştir. Önemsiz boyutsuz sayılar çıkarıldığında, geriye sistemi tanımlayan 14 boyutsuz sayı kalmaktadır.

Çalışmanın deneysel kısmında ise, mikroyapının SAE52100 uzun silindirlerin çarpılma davranışına olan etkisi incelenmiştir. Burada, gazla hızlı soğutma deneylerine ek olarak, tuz banyosu ve yüksek hızlı sertleştirme deneyleri yapılmıştır. Sonuçlar, SAE52100 uzun silindirlerinin çarpılma davranışının, ilk kütükten işlendikleri pozisyona bağlı olduğunu göstermiştir.

Anahtar Kelimeler: Boyut Analizi, Çarpılma, Hassasiyet Analizi, SAE52100, Sertleştirme

To My Family & Emre

ACKNOWLEDGEMENTS

TABLE OF CONTENT

LIST OF TABLES

LIST OF FIGURES

FIGURES

LIST OF SYMBOLS AND ABBREVATIONS

Abbreviations

ADS	Averaged data set
ATS	Anisotropic transformation strain
AR	Aspect ratio
CFD	Computational fluid dynamics
CP	Classical plasticity
DA	Dimensional analysis
DN	Dimensionless numbers
FEA	Finite element analysis
FEM	Finite element method
GSM	Global sensitivity method
GQ	Gas nozzle field quenching
HSQ	High speed quenching
LSM	Local sensitivity method
MEEL	Minimum element edge length
SA	Sensitivity analysis
SBQ	Salt bath quenching
TDDS	Temperature dependent data set
TRIP	Transformation induced plasticity

Common Indices

P_k property related to k^{th} microstructural constituent

P_{mix} the overall property of the phase mixture.

P_a, P_m property of austenite, and martensite, respectively

$\tilde{P}$ average value of P

P^o, P_o initial value of P

Operators

$\bullet$ scalar product

$\cdot$ time derivative

$\cdot\cdot$ second time derivative

Δ increment operator

∇ gradient operator

$\nabla\bullet$ divergence operator

Vectors and Tensors

α_{ij} backstress tensor due to kinematic hardening

δ_{ij} Kronecker's delta

ε_{ij} total strain tensor

ε_{ij}^{e} elastic strain tensor

ε_{ij}^{p} plastic strain rate tensor

$\dot{\varepsilon}_{ij}^{th}$ thermal strain tensor

ε_{ij}^{pt} phase transformation dilatational strain tensor

ε_{ij}^{tr} transformation plasticity (TRIP) rate tensor

σ_{ij}	Cauchy stress tensor
σ'_{ij}	stress deviator

Matrices and Vectors

b	bending vector
f	force vector
S	stress tensor
u	nodal displacement vector
u̇	nodal velocity vector
ü	nodal acceleration vector

Latin Letters

c	specific heat capacity, [J/kg°C]
D	diameter, [mm]
E	elastic modulus, [MPa]
h	convective heat transfer coefficient, [W/m²°C]
K	Ramberg-Osgood coefficient, [MPa]
L	length, [mm]
M_s	martensite start temperature, [°C]
M_o	Koistinen-Marburger constant, [°C]
n	Ramberg-Osgood exponent
t	time, [s]
T	temperature, [°C]
T_a	austenitization temperature, [°C]
T_o	ambient temperature, [°C]
V	volume, [mm³]

X	weight fraction of phases
$\bar{x}$	temperature average material property

Greek Letters

α	thermal expansion coefficient, [˚C]
Δ	structural dilatation due to phase transformation
ΔH^{tr}	latent heat of transformation from austenite to martensite, [J/g]
θ	dimensionless temperature
κ	TRIP constant, [MPa]
λ	thermal conductivity, [W/m˚C]
ξ	sensitivity
ρ	density, [kg/mm^3]
σ^o	yield strength, [MPa]
τ	dimensionless time
ν	Poisson's ratio
Ψ	heat flux, [W/m^2]
Ω_Π	dimensionless number set determined by π theorem
Ω_W	dimensionless number set determined by weak formulation

CHAPTER 1

INTRODUCTION

Today, with advancing technology, dimensional precision of the engineering components gains great importance, even for moderate applications. Any deviation from required dimensions may significantly alter service life and performance. Undesired change in dimensions and shapes of the components is referred as *distortion*. In most of the cases, there are various sources of distortion in production chains. During production, any deviation from required precision necessitates expensive machining operations or even leads to product rejections. As a result; simulations of different manufacturing processes, such as; metal forming, machining or heat treatment, gains great importance for the purpose of predicting dimensions of the final products and compensate undesirable dimensional and shape changes.

Distortion is a common problem of most of the manufacturing processes. Compensation of distortion is a hard task which requires detailed investigation of the process, material and its production history. It is a well known fact that heat treatment distortion is a system attribute [1]. That is to say; it depends on the whole manufacturing chain. Certain distortion potential carriers (DPC) such as distributions of alloying elements, segregations, residual stresses and microstructure are brought into material during manufacturing [1, 2]. These carriers may cause distortion in later steps of manufacturing.

In a manufacturing chain, may be the most important process that affects the precision of final dimensions is heat treatment. Even if a component is perfectly machined to tolerances before heat treatment, its dimensions are inevitably changed by thermal, metallurgical and mechanical processes occurring within the component. Also, DPC's which were invisible in previous processes, cause distortion at this stage.

1

Hardening is one of the most frequently used heat treatments that are used to improve mechanical properties of engineering components. Majority of the important engineering parts are hardened before they are used in service. Achievement of high dimensional precision after this process is vital, since machinability of the part is generally worse after hardening. In some cases, machining may result in hardness drop which may even cause product losses. Product losses after hardening stage are more expensive than any other production steps, since it is usually the last step of the production chains. As a result; simulation of hardening is getting more and more important for the purpose of predicting defects in the final products in order to compensate distortion.

Hardening consists of two steps: austenitizing and quenching. Both of these steps have significant effects on distortion and distortion can be predicted better by simulating combination of them. However, conventionally hardening is simulated by modeling only quenching step. In this study, conventional method of hardening modelling was performed.

Quenching is a multi-physics process during which different physical phenomena occur simultaneously and interact with each other. Therefore, prediction of quench distortion is considerably hard since it necessitates complex mathematical model. *"Because of the complexity, coupled and nonlinear nature of the problem, no analytical solution exists for the problem"*[3]. Solution involves numerical methods such as finite difference method (FDM), finite volume method (FVM) and, finite element method (FEM).

Today, various commercial FEM software are available for simulation of quenching. Although these are successful in predicting distortion and residual stresses, there are several difficulties and limitations in their use. Since, quenching process has multi-physics nature, large number of thermal, mechanical and metallurgical material data is needed [4-12]. During quenching temperature continuously evolves and therefore; material data need to be temperature dependent. Thus, vast number of experiments such as; calorimetery, stress-free/stressed dilatometery and mechanical tests at a wide range of temperature are required. Furthermore, a common problem of mathematical models is uncertainties in the input data. These uncertainties might be due to experimental errors or lack of knowledge. The quality of the results depends on the quality of the input data. Accuracy of experimental data might be increased by increasing the number of experiments or by using more reliable and expensive

instruments, however; these lead to a more expensive and time consuming data acquisition process. It should be emphasized that success of the simulations also depends on the quality of the models. It is very important to utilize material models that successfully describe actual material behavior. For instance, choice of plasticity model significantly affects dimensional changes and stress evolution. But, there are also uncertainties in plasticity model. It is not possible to determine properties of super-cooled austenite below martensite start temperature and therefore, it is not possible to determine whether there exists Bauchinger effect in this phase or not. Another limitation of FEM usage is that, it requires certain level of user knowledge. The quality of the simulation results also depends on the success of pre-processing and post-processing which requires considerable knowledge and experience. Moreover; FEM simulations are not suitable for making instant decisions. Performing simulations necessitate intermediate steps such as, gathering input data, preparation and optimization of the model, which are quite time consuming. Even if, there is a pre-prepared and reliable model, performing simulations and post-processing requires considerable time.

This study deals with aforementioned problems; namely distortion and its prediction. It is a comprehensive investigation of distortion of steel shafts and consists of analytical, numerical and experimental investigations. This study can be divided into two major parts (Figure 1); first part is numerical and analytical investigations of quenching, whereas; second part is experimental investigation of distortion of steel shafts. In the first part, which will be referred as "simulation", sensitivity analysis of through hardening model problem and dimensional analysis of through hardening of steel shafts were performed. In simulations, gas quenching of SAE52100 steel shafts were modeled. In the experimental part, on the other hand, the main aim is to verify numerical simulations. SAE52100 long cylinders with various diameters are quenched with gas nozzle field quenching at various heat transfer coefficients. As an additional work; effect of segregation distribution on distortion behavior (dimensional change and bending) of long cylinders was investigated. In addition to gas quenching experiments, salt bath and high speed quenching experiments were performed. Outline of this study is illustrated in Figure 1.

1.1. Aim and contribution of the thesis

1.1.1. Experimental

Experimental part of this study can be divided into two subsections. First one is experimental verification of dimensional changes that are predicted by simulations, and second one is determination of the effect of microstructure on distortion. During experiments, three different types of quenching techniques were used in order to investigate effects of cooling rate and phenomena occurring during quenching on distortion. These techniques are gas nozzle field quenching, salt bath quenching and high speed water quenching. All of three were used to determine the bending behavior, whereas; simulations were verified only by gas nozzle field quenching experiments. (Figure 1)

1.1.1.1. Verification of the simulations

The major aim of experimental part is to verify simulations. Gas quenching experiments at various heat transfer coefficients were performed and length and diameter changes are compared with simulations. Bending behavior was not used for validation since it was not modeled.

Gas quenching experiments were also used for calibration of the hardening model for SAE52100 steel. Although, hardening model can be determined by Bauschinger tests, in the case of quenching, experimental determination of properties of super-cooled austenite below martensite start temperature is not possible. Therefore, hardening model should be optimized by comparing simulations with various hardening rules and quenching experiments. In this study, two hardening model was investigated; namely isotropic and kinematic hardening rules. This is because; in SYSWELD®, only kinematic, isotropic and combined hardening models can be used with phase transformations. Combined hardening is not investigated since it drastically increase the number of required simulations and results of kinematic and isotropic models give hints about combined hardening results.
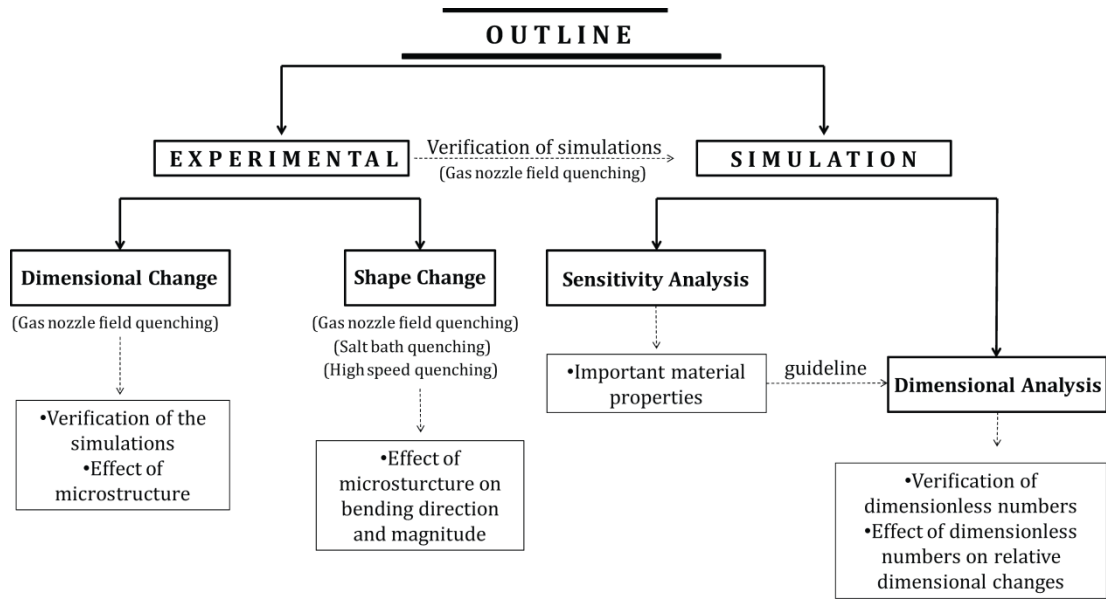
Figure 1:Outline of the study

1.1.1.2. Influence of microstructure on distortion

As it was previously discussed, certain distortion potential carriers (DPC) such as distributions of alloying elements, segregations, residual stresses and microstructure are brought into material during manufacturing [1, 2], which results in different distortion behavior even for samples from the same billet. Amongst these carriers, microstructure and alloying elements attract special interest since they may significantly affect transformation thermodynamics and kinetics. For instance, in certain cases, such as low carbon steels with Mn, the change of local carbon activity due to segregations may introduce development of insistent banded microstructures which cause preferred bending behavior [13].

During through-hardening process;

- isotropic dimensional changes due to volume change,

- anisotropic dimensional changes and shape changes due to transformation plasticity (TRIP) and classical plasticity (CP)

can be predicted by various physical models with the help of standard material data sets [14]. However, the quality of prediction is degraded due to the asymmetry which is brought into material because of the inhomogeneous distributions of DPCs [15, 16] . Therefore; a thorough understanding of their effect on distortion is of vital importance both for the justification of the results from current models and for the development of new models incorporating additional effects.

This study aims to reveal the effect of alloying element distribution and segregation structure on distortion of SAE52100 cylinders. For this purpose, specimens with varying diameters were cut from distinct positions in the cross section of a 45mm diameter billet. Samples were through-hardened in a gas nozzle field in order to investigate dimensional and shape changes.

1.1.2. Simulation

In simulation part, analytical investigations (dimensional and sensitivity analysis) were conducted with the help of numerical simulations. Simulations were performed by commercial FEM software SYSWELD®. In simulations gas nozzle field quenching of long cylinders was modeled. Gas nozzle field quenching was chosen due to its advantages such as, well-defined symmetric cooling and ease of control. By this means, it is ensured that, heat transfer coefficients at the experiments are equal to the simulations. In experiments heat transfer coefficients were determined by CFD calculations [17].

1.1.2.1. Sensitivity analysis

In any mathematical model of a physical process there are several sources of uncertainties in input data, such as experimental errors and lack of knowledge. Quality of input data is very important to obtain reliable results from simulations. It can be improved by increasing number of experiments by using expensive instruments, but these drastically increase expense and required time. In the case of quenching, this is more pronounced since a vast number of material and process parameters are needed to be determined experimentally. These difficulties can partly be solved by determining the effect of each material property on simulation results. Therefore, sensitivity analysis is done in order to;

- build a guideline on the design of experiments for generating input data,

- estimate the magnitude of inevitable experimental errors on simulation results,

- determine model accuracy when certain level of experimental error exists,

- gain preliminary knowledge for building data sets depending on the precision required.

The benefits of conducting sensitivity analysis are not necessarily limited to those stated. The results may be used in many different applications. For example, in this study these results were utilized to describe the effects of dimensionless numbers on dimensional changes. For further utility of sensitivity analysis please refer Section 2.4.

In addition to its practical value, this study fills the gap in literature about the sensitivity analysis of through hardening of steel components. In this study a direct dimensionless index is utilized to grade material properties according to their relative effect on simulation results. Although, Nalltahambi et. al. [18] conducted a related study on distortion of L shaped components, they did not proposed a direct sensitivity index for comparison. At best of author's knowledge, there is not such kind of report in literature.

1.1.2.2. Dimensional analysis

Quenching is a multi-physics process during which different physical phenomena occur simultaneously and interact with each other. Prediction of quench distortion is considerably hard since it necessitates complex mathematical model, solution of which involves numerical methods such as FDM, FVM, FEM. Distortion can be predicted by utilizing commercial FEM software (e.g. MSC.MARC®, SYSWELD®, ABAQUS®, DANTE®)or user subroutines that are implemented on these software. Although, these programs are fairly successful, they are relatively expensive and necessitate certain level of knowledge about the process. Moreover, they are not suitable for making instant decisions, since preparing models and running simulations are time consuming.

Previous studies showed that dimensional analysis can be an alternative to numerical methods. Many aspects of dimensional analysis in transformation-free cooling were clarified [19-21]. This study extends previous approach to the case with martensitic transformation.

Dimensional analysis (DA) is a simple tool that is utilized to understand various physical phenomena or simplify well known expressions that govern a physical system. Although applications of dimensional analysis can be extended to a wide range of physical and social sciences, in theory; the major target of it is to generate a dimensionless number set which completely describes similar systems. Generated dimensionless numbers can be used to deduce occurrences of one system from another similar system (scaling) or they can be used for obtaining expressions with the help of empirical information. Utility of dimensional analysis and dimensionless numbers are not limited to those stated. Please refer to Section 2.5. for detailed information about dimensional analysis and its applications.

In this study, dimensionless number sets that were derived in previous studies [22, 23] were investigated. First of all, validity of these sets were justified and later dimensionless numbers given in the reference [23] were altered one by one in order to investigate their effect on dimensional changes. This study fills the gap in literature and provides knowledge about dimensional analysis of quenching with martensitic transformation, namely:

1. It justifies previously determined dimensionless numbers;

2. It reveals important dimensionless numbers that govern quench distortion;

3. It reveals the effect of dimensionless numbers on dimensional changes;

4. It uncovers several aspects of the system behavior;

5. It provides information about scaling parameters of through hardening.

This knowledge can be used in experimental and theoretical applications to

- decrease the number of quenching experiments in a scientific study;

- predict distortion with the help of scaling;

- set the assumptions for simplification of mathematical model and analytical approaches;

- check validity of proposed mathematical models.

Benefits of provided knowledge are not limited to those stated. It may be used innovatively in many different applications.

CHAPTER 2

THEORY AND LITERATURE SURVEY

2.1. Quenching

2.1.1. In general

"Quenching", in its most general sense, refers to rapid cooling. During quenching, cooling rate is so high that high temperature, diffusion controlled phase transformations are suppressed and instead kinetically accessible and thermodynamically favorable phase transformations occur. Quenching is used to inhibit formation of certain phases and control amount and morphology of the micro-constituents.

Quenching is applied to a wide variety of metallic components (e.g. steel, aluminum and titanium) to improve mechanical properties and service performance. In industry, quenching process is most commonly applied for hardening of steels. Rapid cooling of steels inhibits the formation of ferrite, cementite and bainite, and instead; more hard and strong phase called "martensite" forms. In addition to through hardening, quenching is also used in most of the surface and thermo-chemical treatment of steels such as, laser and induction hardening, carburizing, and carbonitriding.

Although quenching is a vital production step, it causes several problems such as distortion, cracking, undesirable distribution of residual stresses, microstructure and properties such as hardness. Distortion can be defined as undesirable dimension and shape changes that are caused by distortion potential carriers. Distortion may lead to expensive hard-machining or even product rejection. Another severe quenching problem is cracking. Cracking occurs due to large stresses that occur in the component and it results in product loss. Distribution of residual stresses is another factor that

affects quality of the components. Compressive residual stresses at the surface are desirable since it improves mechanical properties such as fatigue life. In some cases, stress evolution may cause accumulation of large tensile stresses at the surface which may significantly destroy service performance of the component. Therefore, optimization of quench process is very important to improve quality of the product and minimize quench problems.

2.1.2. Phenomena occurring during quenching

2.1.3. Physical fields and couplings

Quenching is a multi-physical phenomenon during which different physical fields interact with each other by sharing state variables or couplings. In Figure 2 these physical fields and interactions between them are summarized.
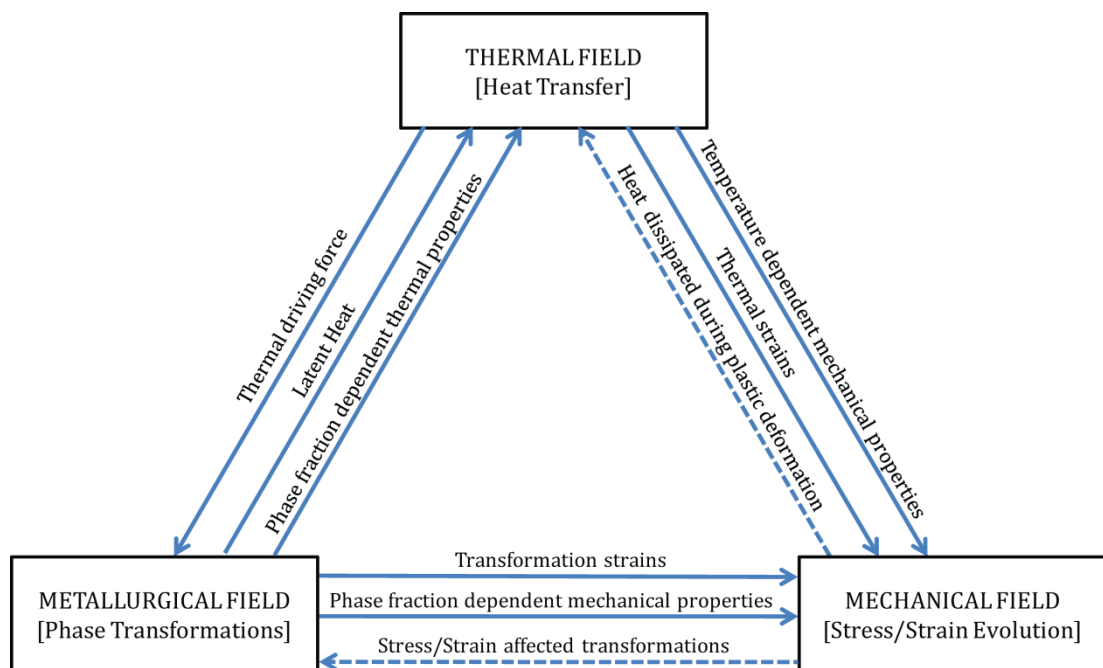
Figure 2: Physical interactions and couplings

During quenching all the physical events are triggered and altered by heat transfer. "*Heat transfer from the surface highly depends on fluid flow, thermo-physical and thermo-chemical processes occurring on the interface*" [3]. *Leidenfrost effect* in immersion quenching is an example of thermo-physical processes occurring in the interface [24, 25].

Temperature evolution within the component triggers phase transformations. Kinetics of the transformations depends on cooling rate and temperature. On the other hand, phase transformations alter temperature by heat release due to latent heat of transformation. It has been previously shown that dissipated heat due to phase transformations has strong effect on temperature evolution [26].

Temperature gradient in the component also causes thermal stresses and hence plastic deformation when yield criterion is met. Thermal field alters mechanical field by changing mechanical properties. Although mechanical field also has contribution to thermal field by heat generation due to plastic deformation and temperature drop due to adiabatic expansion, these are usually neglected since they are quite small.

During phase transformations, volume change due to density differences of parent and product phases causes internal stresses. These stresses together with thermal stresses and transformation induced plasticity (TRIP) determine the stress evolution in the component. Stress state and prior plastic deformation, on the other hand; alters critical temperatures and times in transformation diagrams [27-31]. In some cases, transformation might be induced or totally inhibited by stress.

2.1.4. Thermal field

During quenching, all of the physical events are triggered by temperature evolution. It directly affects thermal stress evolution and mechanical properties of the material. Also, phase transformations start when thermodynamic stability of austenite is altered upon cooling. Moreover, phase fractions and transformation rate is determined by temperature evolution. Therefore, heat transfer from component to quenchant and surrounding is very important. Accurate determination of distortion depends on the accurate prediction of heat transfer. From engineering point of view it is the sole event that can be adjusted.

During quenching, heat transfer occurs all three heat transfer mechanisms; namely conduction, convection and radiation. Simply, heat is transferred to quenchant and surrounding by convection and radiation. This causes thermal gradient in the component which results in conduction within the component.

For simulation purposes, it is very important to predict thermal history and heat transfer phenomenon accurately. However, it is not easy since complex nature of cooling regime due to thermo-physical events occurring between component and the quenchant. *Leidenfrost phenomenon* is one of the examples of the complexity of the heat transfer:

During immersion quenching in an evaporating media, cooling process can be divided into three stages (1) vapor blanket stage, (2) boiling stage, (3) convective cooling stage [24, 25]. This is also known as Leidenfrost phenomenon. In vapor blanket stage, component is surrounded by vapor. In this stage, heat transfer is relatively small since heat capacity of vapor is low, and at high temperatures; heat transfer occurs mainly by radiation. If vapor blanket exists at low temperatures then radiation is neglected and there is conduction through the film. Boiling stage starts when vapor blanket collapses. Heat transfer coefficient reaches its highest value in this stage. This is because, heat is removed from the surface and transferred away while, heated up liquid is replaced with the colder liquid. When temperature of the component decreases below the boiling point of the quenchant, boiling stage ends, and convective cooling stage starts. In this stage, heat transfer coefficient significantly depends on viscosity and heat capacity of the liquid. Leidenfrost effect is undesirable phenomenon during quenching since it causes inhomogeneous cooling which leads to increase in distortion.

2.1.5. Mechanical field

During quenching stress state continually change due to temperature and phase evolutions. Prediction of the stress state is very important since it alters dimensional changes considerably by causing anisotropic plastic flow within the material. Moreover, residual stress state at the end of the quenching process affects the service performance of the components. Stress evolution during quenching (Figure 3) can be summarized as following:

STAGE 1: There is no martensitic transformation within the material. Stress state is determined by thermal stresses. Surface cools down faster than the core. Surface tries to expand whereas, core resists this expansion. Hence, tensile stresses are generated at the surface and this is balanced by compressive stresses at the core.

STAGE 2: Temperature at the surface drops below martensite start temperature, hence; martensitic transformation initiated at the surface. Transformation strains and transformation plasticity unloads tensile stresses that are accumulated at the surface. As a result stress state at the core and surface reversals, namely stress state at the surface becomes compressive whereas, it becomes tensile at the core.

STAGE 3: After surface is completely transformed and it cools down, martensitic transformation is initiated and continuing at the core. This reverses the stresses that are accumulated in the previous stage.

STAGE 4: When quenching finishes, tensile stresses are accumulated at the surface and it is balanced with compressive stresses at the core.

These stages are illustrated in Figure 3.
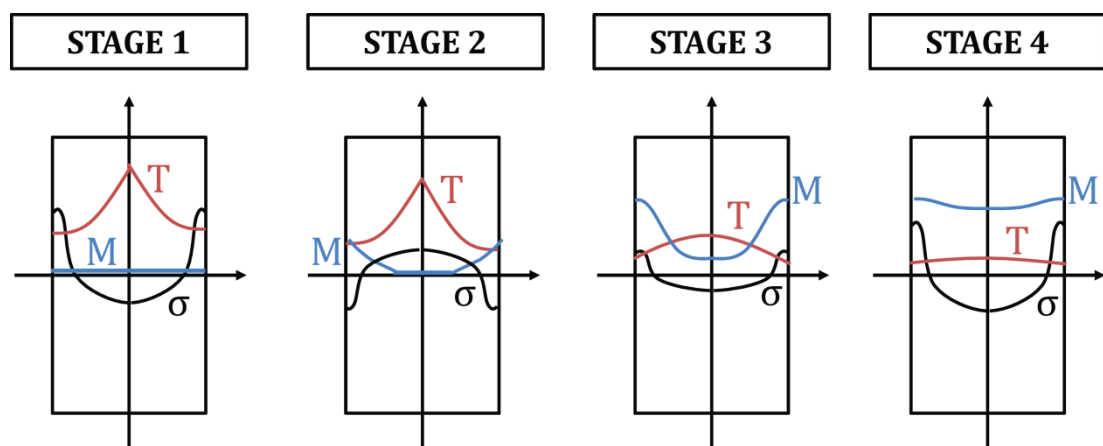
Figure 3: Stress evolution during quenching (σ-axial stress, T-temperature, M-martensite fraction)

2.1.6. Metallurgical field

The most important consequence of quenching of steel components is phase transformations. The mechanical properties of the final product depend on the phase proportions after quenching. Phase transformations have substantial effects on other fields. They directly and indirectly alter final dimensions of the product, the magnitude of distortion, and residual stresses.

In the case of steel, phase transformations can be categorized into two parts, namely; *reconstructive* and *displacive* phase transformations. Reconstructive phase transformations require re-arrangement of the lattice via diffusion process whereas; displacive phase transformations occur via a deformation causing change of lattice [3]. Formation of allotriomorphic ferrite and pearlite are examples of reconstructive phase transformations. Martensite, bainite and Widmanstatten ferrite, on the other hand, are formed by displacive phase transformations.

This study focuses on martensitic transformation. This is because; during through hardening of SAE 52100 steel, the major phase transformation is austenite to martensite transformation. There also forms low amount of bainite at low cooling rates, but in this study it wasn't taken into consideration since it is in negligible amount. For the sake of brevity; phase transformations other than martensitic transformation are not mentioned here. Details about these can be found in elsewhere [3, 14, 32-39].

"*Martensitic transformation is the sole transformation that occurs just by displacive mechanism*" [3]. It is time independent due to the fact that martensite/austenite interface rapidly grows once martensite nucleated. In fact the speed of the interface is almost equal to the speed of sound. Martensitic transformation starts at martensite start temperature (M_s) and proceeds depending on the temperature evolution. M_s is a thermodynamic quantity at which free energy of austenite is equal to free energy of martensite. M_s changes from steel to steel depending on the alloying elements and austenitizing conditions. Also, stress state and prior plastic deformation deviates M_s distribution within the material [40-44]. Here it should be noted that, in the case of consideration, effect of stress state on martensite start temperature is excluded from the model. In utilized quenching model mechanical field and thermo-metallurgical field are not fully coupled. Although, this decrease the quality of the results, it is advantageous in decreasing the computation time.

2.2. Quenching techniques

During hardening process, components are heated up to a uniform temperature and then rapidly cooled with the help of a liquid or gas. From engineering point of view, the sole parameter that can be altered in the quenching process is cooling rate which can be adjusted by changing quenchant type, composition, temperature and flow. Because of its vital importance, quenching techniques are named by referring to the type of the quenchant and method of its application. For instance, in the case of immersion quenching, component is immersed into a liquid, or in gas quenching component is cooled down by blowing gas. Some of the quenching methods are summarized in the following sections.

2.2.1. Immersion quenching

In this method, components are immersed into a liquid. This method can be divided into two categories; (1) Quenching with evaporating media and (2) Quenching with non-evaporating media. This categorization is due to the differences in cooling regimes. In the case of evaporating media Leidenfrost phenomena occurs which might have detrimental effects on distortion. On the other hand, during quenching with non-evaporating media (e.g. salts) there are no different stages of cooling. These show only convective cooling. Therefore; quenching with these lead to less distortion compared to quenching with evaporating media.

2.2.1.1. Quenching with evaporating media

Water, oil and polymers can be used in immersion quenching. Water provides high cooling rates due to its low viscosity and high heat capacity. In some cases, usage of water as quenchant may result in cracking due to accumulation of large stresses within the component. As an alternative, oil quenching is widely used. In oil quenching heat transfer coefficients are lower due to higher viscosity and lower heat capacity. Moreover, a wide range of properties can be attained by adjusting formulation of the oil or blending. Various types of oils are used in quenching process such as; animal oils, vegetable oils, fish oils, or petroleum-based oils. Compared to petroleum-based oils, natural oils are more environmentally friendly, but their oxidative stability is lower and their viscosity range is more narrow [45]. Another quenchant that is widely used is water-polymer solution. There are various polymers that are used in quenching such

as; polyvinyl pyrolidone (PVP), polyethyl oxazoline (PEO), sodium polyacrylate (ACR) and polyalkylene glycol (PAG)[45]. Very flexible quenching conditions can be attained with polymers by changing type and concentration of the polymer.

The major disadvantage of immersion quenching in an evaporating fluid is that Leidenfrost effect causes inhomogeneous cooling which results in an increase in distortion. Furthermore, in oil and polymer quenching, an additional washing step is needed in order to remove quenchant residue. Contaminated wash water and quenchant wastes (oil or polymer) leads to environmental problems.

2.2.1.2. Quenching with non-evaporating media

2.2.1.2.1. Salt bath quenching

In salt bath quenching, austenitized components are quenched in a molten salt bath. Since minimum temperature that can be used is the melting point of the salt, salt bath quenching is followed by a subsequent air or water cooling step. As quenchant salt, nitrates and nitrites of potassium and sodium are usually used [46].

Molten salts have several advantages in quenching of steel components. First of all, a wide temperature range can be attained. Salts can be used as quenchant between their melting and boiling points which can be adjusted by blending or changing the type of salt. Furthermore, in contrast to other quenching mediums (water, oil, polymer solutions), heat transfer occurs by means of single mechanism, namely convection. There are no different stages of cooling as it is in other quenchants [46]. Therefore, more uniform cooling is attained which reduces distortion. Another advantage of salt bath quenching is that; it is possible to perform interrupted quenching methods such as martempering and austempering. For instance, in the case of martempering, austenitization is followed by an intermediate salt bath treatment above martensite start temperature in order to reduce thermal stresses and therefore distortion and cracking.

Salt bath quenching technique also has several limitations. Some of these limitations are as following;

- Salt bath cannot be used below the melting point of salt.

- Since salts are oxidative they should be handled with extra care [46].

- Disposal of contaminated wash water should be carried out carefully due to the environmental issues.

2.2.2. Gas quenching

In gas quenching, components are cooled down by blowing inert gasses (N, H, He or mixtures of these gasses). It can be performed either in a vacuum chamber (high pressure gas quenching), or by gas nozzles in open atmosphere (gas nozzle field quenching). During gas quenching, heat is transferred by radiation and forced convection. Heat transfer coefficients that can be attained are relatively low due to low heat capacity of gasses. Therefore, this method is usually applied to thin sections or materials with high hardenability. The advantages of gas quenching are as following:

- Since there is no Leidenfrost phenomenon, reproducibility is improved;

- It is environmentally friendly since components are not contaminated with oil, salt or other chemicals;

- Heat transfer coefficient can be controlled easily by changing various process parameters such as flow rate, pressure and type of the gas.

During gas quenching, heat is transferred by radiation and forced convection. Heat transfer coefficients that can be attained are relatively low due to low heat capacity of gasses. Therefore, this method is usually applied to thin sections or materials with high hardenability.

2.2.2.1. High pressure gas quenching

Components are austenitized in a vacuum chamber and later pressure of the chamber is increased to a certain value by filling quenchant gas. By this means, a gas flow is attained in the chamber. Cooling rate is adjusted by pressure, flow rate, and type of the gas. In high pressure gas quenching, layout of the batch should be arranged carefully in order to ensure that each component has equal access to pressurized flow [45]. Also, chamber design is very important to avoid non uniform flow and pressure drop [47].

2.2.2.2. Gas nozzle field quenching

The major difference between high pressure gas quenching and gas nozzle field quenching is that the main control parameter in the former is gas pressure whereas, it is gas velocity in the latter. Gas nozzle field quenching is more controllable compared to high pressure quenching, since each component has its own nozzle field. Moreover, it is possible to arrange positions of the nozzle field depending on the component. As a result, highly symmetric and controllable cooling can be attained.

In gas nozzle field quenching, cooling rates are adjusted by geometric configuration of the nozzle field, gas velocity, temperature and type. In a nozzle array there are three parameters for the design of the nozzle arrangement, namely; distance from the component (h), distance from each other (l) and nozzle diameter (Figure 4).
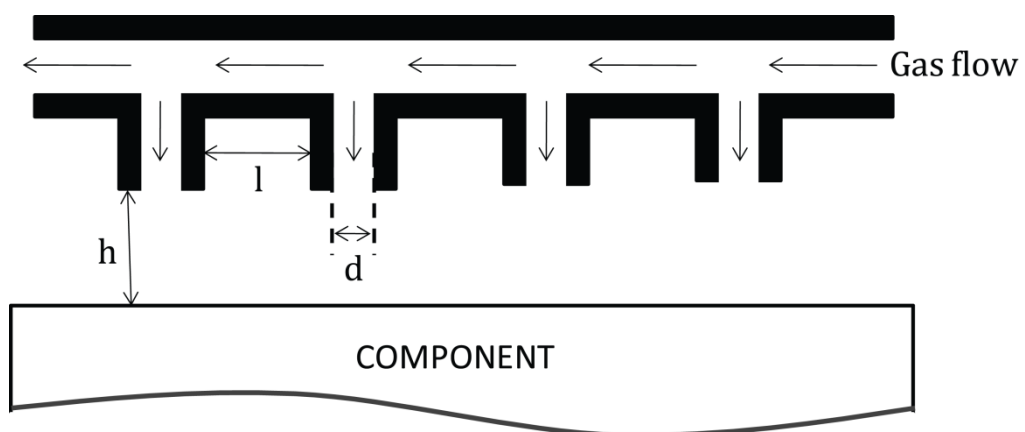
Figure 4: Parameters of a nozzle field

Gas nozzle field quenching does not provide perfectly homogeneous cooling. As getting further from the nozzle, cooling rates decrease within the component. Since thermal conductivity of steel is quite high, this variation is compensated by conduction. At this point, design of the nozzles is very important. If distances between the nozzles (l) are too large, cooling rate variation might not be compensated by conduction and this may cause large hardness variations throughout the component. On the other hand, if they are too close, gas flow at the nozzles might interact and annihilate each other. It should also be noted that, gas nozzle field quenching provides perfectly symmetric cooling. Therefore, it causes only very small avoidable distortion by itself.

2.2.3. High speed quenching

It is a well known fact that the probability of crack formation increases with increasing cooling rate. In 1964, Kobasko [48] showed that, although this is correct up to a certain cooling rate, crack formation probability starts to decrease above this critical point. High speed quenching can be defined as the quenching technique during which cooling rates are well above this critical quench rate.

High speed quenching technique can be characterized by two major factors: (1) high cooling rates (2) compressive residual stresses at the surface of the component. High cooling rates are attained by continuous agitation of the liquid (water or oil) around the component. Agitation is so violent that vapor blanket and nucleate boiling stages do not occur. Heat is instantaneously exchanged between the liquid and the component and carried away by the liquid. In this type of quenching, internal stress evolution and residual stresses are different from conventional quenching. High speed quenching causes compressive residual stresses at the surface which improves mechanical properties such as fatigue life [49-53]. Stress evolution during high speed quenching can be summarized as following:

Once quenching starts, surface cools down very fast and outer layer of the component quickly drops below martensite start temperature. As a result; a martensitic shell forms and compressive stresses are accumulated at this layer due to volumetric expansion. At this stage, temperature at the core is very high (almost at austenitization temperature). During further cooling, austenitic core contracts, whereas; surface maintains its initial size with low distortion. Therefore, magnitudes of compressive stresses at the surface increase. When temperature of the core drops below martensite start temperature,

core expands due to martensitic transformation. Compressive stresses at the surface start to unload but its sign does not change. This is because, shrinkage before the transformation offsets expansion due to the transformation. On the other hand, high speed quenching technique has several disadvantages such as;

- Capital cost is relatively high since large reservoirs and pumps are needed;

- It is suitable for hardening of symmetrical geometries;

- Usage of high speed quenching is generally limited to low production rates since large volumes of liquid is required;

- Existence of a critical Biot number leads to a critical dimension for a given quenching device. This critical value must be exceeded. Consequently, small parts are not suitable for high speed quenching.

2.3. Modeling of quenching

Modeling of quenching is a multi-physics problem during which thermal, mechanical and metallurgical fields interact with each other. No analytical solution exists for the problem due to its complexity, coupled and non-linear nature. However; many algorithms are purposed for staggered numerical solution which involves application of finite difference method, finite volume method and finite element method [3].

In this study, quenching was modeled by commercial finite element analysis software; SYSWELD®. In this framework, utilized quenching model is not fully coupled. Mechanical field is computed by using the information from thermo-metallurgical field but thermo-metallurgical field does not gather information from mechanical field. Therefore; couplings that are shown in Figure 2 with dashed lines are not taken into consideration. This approach considerably decreases duration of simulations. On the other hand; consequences of this are as following:

1. Heat dissipated due to plastic deformation, and temperature drop due to adiabatic expansion are not modeled. These do not have any significant consequence on simulation results since evolved heat due to these mechanisms is very small and negligible [54].

2. Effect of stress field on critical temperatures is neglected. Since stress field has significant effects on martensitic transformation [40-44] and hence volume change of the component, this negligence might have significant affects on dimensional changes.

2.3.1. Prediction of properties of phase mixture

During quenching, microstructure continuously evolves. Therefore, determination of material properties of the phase mixture should be mentioned before discussing governing equations.

SYSWELD® uses linear rule of mixture to determine the properties of austenite-martensite phase mixture.

$$P_{mix} = \sum_{k=1}^{n} X_n P_n \qquad (2.1)$$

where P_{mix}, X_n and P_n are property of mixture, fraction of the nth phase, and property of the nth phase, respectively.

However, for yield strength situation is different. Linear phase mixture can be used for yield strength only when constituents have comparable harnesses [55]. Otherwise; plastic strains tend to accumulate in the soft phase (austenite) and real yield strength lie below the yield strength that is predicted by linear rule of mixture [56]. In the case of consideration hardness of martensite is well above the hardness of austenite. Thus, linear rule of mixture does not give reliable results. SYSWELD® approximates yield strength of phase mixture by a non-linear rule of mixture (Eq. 2.2).

$$\sigma^o = \left(1 - f(X_m)\right)\sigma_a^o + f(X_m)\sigma_m^o \qquad (2.2)$$

In the equation $f(X_m)$ is a non-linear function of fraction of martensite (X_m).

2.3.2. Governing equations

Quenching can be described by three governing equations;

1. Fourier heat conduction equation (Thermal field),

2. Phase transformation equations (Metallurgical field),

3. Impulse equation (Mechanical field).

These are discussed in more detail in following chapters.

2.3.3. Modeling heat transfer and heat conduction (Thermal field)

Heat conduction within the component can be determined by using Fourier's equation $\left(\psi = -\lambda \nabla T\right)$ relating heat flux (ψ) to temperature gradient (∇T). Considering the law of conservation of energy, heat equation for a transient case can be expressed as;

$$\rho c \dot{T} = \nabla \cdot \left(\nabla\left(\lambda T\right)\right) + Q \tag{2.3}$$

where ρ, c and λ are density, specific heat under constant pressure, and thermal conductivity of the phase mixture as a function of temperature. In the right side of the expression, "ρc" term indicates the heat storage capacity of the material. The additional term Q represents internal heat source and it stems from latent heat of transformation:

$$\dot{Q} = \rho \Delta H_i^{tr} \dot{X}_i \tag{2.4}$$

where ΔH_i^{tr} and $\dot{X}_i$ are transformation enthalpy and rate of phase transformation. Temperature drop due to adiabatic expansion and heat dissipated due to plastic deformation are neglected since their contribution to the temperature field is very low [54].

Latent heat can be incorporated into the heat equation by using enthalpy based formulation or by defining a fictitious specific heat (c*). In the case of former method, heat equation reformulated as:

$$\rho \dot{H} = \nabla \cdot \left(\nabla\left(\lambda T\right)\right) + \rho \Delta H_i^{tr} \dot{X}_i \tag{2.5}$$

where H is enthalpy of formation of the phase mixture. This method is computationally more efficient than defining c* due to sharp variations in c. Since SYSWELD® uses enthalpic approach, c* will not be discussed here for the sake of brevity. Details about this method can be found in elsewhere [3].

Specific heat, density, thermal conductivity and transformation enthalpy are temperature and phase fraction dependent. Properties of phase mixture are approximated by utilizing linear rule of mixture;

$$P(T, X_i) = \sum_{i=1}^{n} X_i P_i \tag{2.6}$$

where P, X_i and P_i represents, property of the mixture, fraction and thermal property of ith phase, respectively. Although, in the case of quenching, pressure is not constant due to the stress evolution, dependence of specific heat on pressure is neglected since pressure dependency of c is low in solids.

Boundary condition that is used to introduce heat flux to the side wall is

$$\lambda \frac{\partial T}{\partial n} = -\psi_S(T_c) \tag{2.7}$$

where n, ψ_S, and T_c are external normal to the side wall, heat flux imposed on the side wall and temperature of the component, respectively. Heat flux on the side wall can be expressed as;

$$\psi_S(T_c) = -h(T_c)(T_c - T_o) \tag{2.8}$$

where T_o represents the temperature of the quenchant.

2.3.4. Modeling martensitic transformation (Metallurgical field)

Kinetics of martensitic transformation can be described by Koistinen-Marburger equation [57];

$$X_m = X_a \left(1 - \exp\left(-M_o\left(M_s - T\right)\right)\right) \tag{2.9}$$

when $T \leq M_s$. Here X_a and X_m represents fraction of austenite and martensite where X_a is time dependent. M_o is Koistinen-Marburger constant and M_o is a kinetic parameter that governs the evolution of the transformation. It can be determined by dilatometer tests and X-Ray-retained austenite measurements.

Here it should be noted that, in this study only martensitic transformation is modeled. Therefore, reconstructive phase transformations and other displacive transformations are not discussed here for the sake of brevity.

2.3.5. Modeling mechanical interactions (Mechanical field)

2.3.5.1. Impulse equation

In the case of small deformations, the equation of conservation of linear momentum is expressed as;

$$\rho \ddot{\mathbf{u}} - \nabla \cdot \mathbf{S} = \mathbf{f} \tag{2.10}$$

where ρ - denstiy, $\ddot{\mathbf{u}}$ - second order time derivative of displacement vector, $\nabla \cdot$ - divergence operator, $\mathbf{S}$ – stress tensor and $\mathbf{f}$ – force vector. The term $\rho \ddot{u}$ is inertial term and in the case of consideration it is neglected since it is very small.

2.3.5.2. Constitutive model

In this study *elasto-plastic constitutive model* was used. SYSWELD® formulates constitutive equations based on additive decomposition of the strain tensor. The assumptions behind additive decomposition can be found in reference [58].

In simulation of quenching, total strain rate $(\dot{\varepsilon}_{ij})$ tensor can be decomposed to strain rates from different fields namely;

- elastic strain ($\dot{\varepsilon}_{ij}^{e}$)

- plastic strain ($\dot{\varepsilon}_{ij}^{p}$)

- thermal strain ($\dot{\varepsilon}_{ij}^{th}$)

- phase transformation strain ($\dot{\varepsilon}_{ij}^{pt}$)

- transformation plasticity strain ($\dot{\varepsilon}_{ij}^{trip}$)

Thus, total strain increment can be expressed as;

$$\dot{\varepsilon}_{ij} = \dot{\varepsilon}_{ij}^{e} + \dot{\varepsilon}_{ij}^{p} + \dot{\varepsilon}_{ij}^{th} + \dot{\varepsilon}_{ij}^{pt} + \dot{\varepsilon}_{ij}^{trip} \qquad (2.11)$$

2.3.5.2.2. Plastic strain

Elasto plastic behaviors of the materials are determined by three rules;

1. Yield criterion,

2. Flow rule,

3. Hardening rule.

Yield criteria determines the stress state at which yielding occurs, flow rule governs the stress-strain relationship during flow and hardening rule determines the evolution of yield surface.

Yield criterion can be expressed in terms of a surface lying in the stress space; ($F(\sigma_{ij})$). Any stress state (σ_{ij}) in the surface implies elastic deformation. Therefore, this surface is also referred as *elasticity domain*. Yielding occurs only when stress state is on the surface, and σ_{ij} can never lie outside the surface. In this study, von Mises type of yield surface was used. This surface is a cylinder in the stress space. According to von Mises yield criterion, material yields when stress state exceeds effective stress $\bar{\sigma}$;

$$\bar{\sigma} = \sqrt{\frac{3}{2}\left(\sigma_{ij}^{'} - \alpha_{ij}\right)\left(\sigma_{ij}^{'} - \alpha_{ij}\right)} \qquad (2.12)$$

26

In the expression S_{ij} is the stress deviator;

$$S_{ij} = \sigma_{ij} - \frac{1}{3}\delta_{ij}\sigma_{mm} \qquad (2.13)$$

and α_{ij} is back stress tensor that exists in the case of kinematic hardening.

According to plastic potential theory, materials have a plastic potential (Q) and plastic strain is proportional to the change in plastic potential function with stress state (2.14).

$$\dot{\varepsilon}^p = \dot{\lambda}\frac{\partial Q(\sigma_{ij})}{\partial \sigma_{ij}} \qquad (2.14)$$

Equation 2.11 is the most general form of flow rule. A geometrical consequence of this rule is that, elastic strain rate is always perpendicular to the yield surface. Therefore, Equation 2.11 is also called as *normality principal*. When plastic potential function assumed to be equal to the yield criteria ($Q(\sigma_{ij})=F(\sigma_{ij})$), the resultant flow rule is named as associated flow rule. In this study *Prandtl-Reuss flow rule,* which is a special case of associated flow rule, was used. In Prandtl-Reuss flow rule potential function is equal to the von Mises yield criteria.

Final parameter that determines the elasto-plastic behavior of the materials is hardening rule. In SYSWELD®, three kinds of hardening rules are available, namely; isotropic, kinematic and combined hardening. As it is illustrated in Figure 5, in the case of isotropic hardening yield surface expands, whereas; in the case of kinematic hardening it translates. Kinematic hardening model can be utilized to model Baushinger effect that cause yield stress drop during stress reversal. Combined hardening rule, as its name implies, is the combination of isotropic and kinematic hardening rules. Yield surface both expands and translates. In this study, simulations are performed with both isotropic and kinematic hardening rules.

Isotropic and kinematic hardening model can be applied to the model in terms of the equations (2.12) and (2.13) respectively.

$$\sigma^f(T,\varepsilon_{eq}^p) = \sigma^o + K(T)\left(\varepsilon_{eq}^p\right)^{n(T)} \qquad (2.15)$$

$$\alpha_{ij} = C(T)\varepsilon_{ij}^p \qquad (2.16)$$

In the equations σ^f and σ^o are final and initial yield strengths, whereas; K(T), n(T) and C(T) are temperature dependent material parameters. ε_{eq}^p, on the other hand, is equivalent plastic strain which is formulated as;

$$\varepsilon_{eq}^p = \int_0^t \dot{\varepsilon}_{eq}^p dt \; ; \; \dot{\varepsilon}_{eq}^p = \sqrt{\frac{2}{3}\dot{\varepsilon}_{ij}^p \dot{\varepsilon}_{ij}^p} \qquad (2.17)$$

(a) Isotropic Hardening   (b) Kinematic Hardening
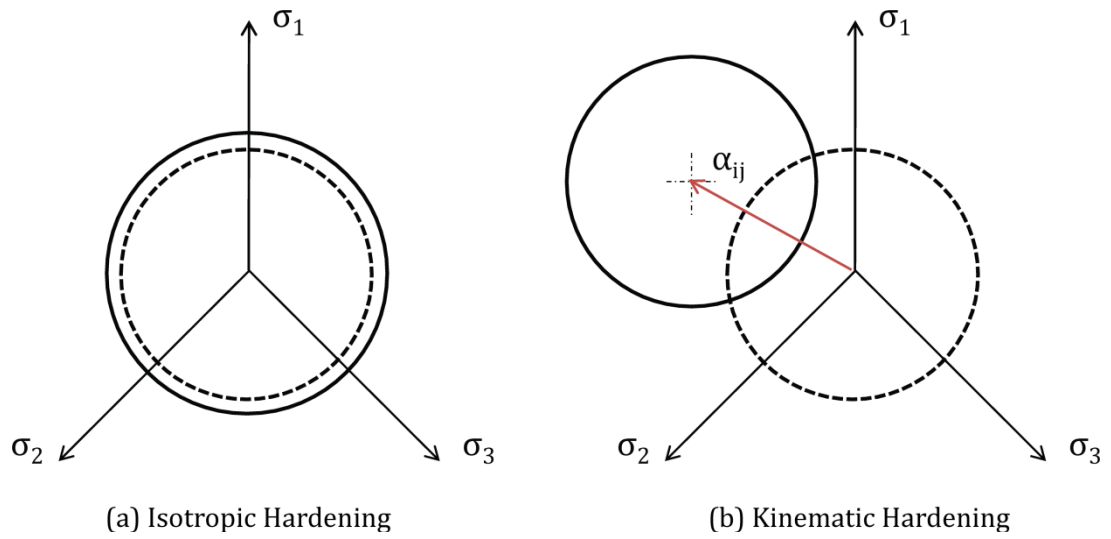
Figure 5: Changes in yield surface in the cases of isotropic and kinematic hardening rules

2.3.5.2.3. Elastic strain

If the material is considered as linearly elastic, elastic strains are related to the stress state by Hooke's law;

$$\varepsilon_{ij}^e = \frac{1}{E}\left[(1+v)\sigma_{ij} - \delta_{ij}v\sigma_{ij}\right] \qquad (2.18)$$

where E and υ are elastic modulus and Poison's ratio as a function of temperature.

2.3.5.2.4. Thermal strain

Thermal strains are formulated as;

$$\varepsilon_{ij}^{th} = \sum_{i=1}^{p} X_i \int_0^T \alpha_i dT \qquad (2.19)$$

where α is thermal expansion coefficient.

2.3.5.2.5. Transformation strain

Volume change due to the transformation of austenite to the phase *i* is expressed as;

$$\varepsilon_{ij}^{pt} = \sum_{i=1}^{p} \frac{1}{3} \frac{\rho_a - \rho_i}{\rho_i} X_i \qquad (2.20)$$

where ρ and X are density and fraction, respectively.

2.3.5.2.6. Transformation plasticity (TRIP) strain

Transformation induced plasticity (TRIP) can be defined as increased plasticity during phase tranformations. Material plastically deforms even at a stress state that does not met yield criteria. Formation of TRIP is attributed to the formation of irreversible strains that are caused by phase transformations under stress. During phase transformations, there occur misfit between parent phase and transformed microregion due to volume and shape change. This misfit is compensated by an eigenstress state which is influenced by applied stress. Superpositon of applied stresses and this stressing-straining causes plastification of the material. TRIP can be explained by competition of two mechanisms which are

> **Greenwood and Johnson mechanism:** Volume difference of parent and product phase cause microscopic internal stresses, which interacts with applied stress. And this cause irreversible strain in the direction of applied loading.

> **Magee effect:** When there is an external force, martensite platelets form in preferential direction.

For the sake of brevity details of these mechanisms will not be discussed here. Please refer references [42, 59-86] for detailed information.

Generally, a phenomenological approach is used to derive expressions for evolution of TRIP [3]. Under uniaxial stress, transformation strain can be expressed as;

$$\varepsilon^{trip} = \kappa\sigma'\phi(X_m) \tag{2.21}$$

where σ' is the deviatoric component of stress state. TRIP constant κ and saturation function $\phi(X_m)$ can be determined either experimentally or by calculation [84, 87-89]. Saturation function changes from model to model. In this study $\phi(X_m)$ that is proposed by Leblond [90] was used. In this model $\phi(X_m)$ is expressed as

$$\phi(X_m) = p\left(1 - \ln(X_m)\right) \tag{2.22}$$

In the current framework, TRIP strains rate is formulated as;

$$\dot{\varepsilon}_{ij}^{trip} = \frac{3}{2}\kappa\sigma'\frac{d\phi}{dX}(X_m)\dot{X}_m \tag{2.23}$$

2.4. Sensitivity analysis

As an indispensible part of scientific methods, mathematical models (numerical or otherwise) are used to interpret real world by utilizing input variables (data), governing equations and boundary conditions. Mathematical model can be considered as a function; f(.) in which user enter experimentally or theoretically determined input data and gather output. It is a well known fact that, quality of the output depends on the quality of the input data. Unfortunately; in any case, there are inevitable uncertainties in input data due to experimental errors or lack of knowledge. Besides, every single input data influences output in different magnitude and direction. Therefore, whichever model is used one should always consider the effect of uncertainties on input in order to

1. build a guideline on the design of experiments for generating input data;

2. estimate the magnitude of inevitable experimental errors on the results;

3. determine model accuracy when certain level of experimental error exists;

4. gain preliminary knowledge for building data sets depending on the precision required.

The preliminary knowledge about the influence of these uncertainties is not only useful in the application of the mathematical model but also it is useful for;

1. setting the assumptions for simplification of mathematical model and analytical approaches,

2. model verification and development,

3. determining the reliability of the models during decision making.

In most of the cases, it is not straight forward to reveal the effect of uncertainties on the output and, therefore; *sensitivity analysis* should be performed. Sensitivity analysis can be defined as; "*the study of how uncertainty in the output of a model (numerical or otherwise) can be apportioned to different sources of uncertainty in the model input*"[91]. There are various sensitivity analysis methods such as; direct analytical differentiation [92-94], Fourier amplitude sensitivity test [95-99], fractional factorial design method [100], regression method [101, 102], sampling base method [92, 103, 104] and Sobol's method [105].

Shortly, in sensitivity analysis, input variables are varied and the changes in output are quantified with respect to the modifications in the input data. Sensitivity analysis methods are distinguished from one another by their strategy in varying input and processing output. Comparison of sensitivity analysis methods and review of the topic can be found in [91, 93, 94, 100, 105-111].

Sensitivity methods can be categorized into two groups, namely; local and global sensitivity analysis methods [94]. Local sensitivity analysis methods (LSM) determine the behavior around a single input data whereas global sensitivity analysis methods (GSM) investigate the system throughout the domain of the model. Compared to GSM's methods, LSM's are not efficient in revealing the nonlinear behavior of the system. However, when there is large number of input variable, it becomes impractical to use GSM's since it necessitates more reference and perturbed points hence more computer simulations .

2.5. Dimensional analysis

Dimensional analysis (DA), also called *"Principal of Similitude"*, is a general and simple tool to understand various physical phenomena. It is utilized to gather information about the relations that govern a phenomenon by using the units of the quantities that are associated with the system. In other words; it employs units as a tool for grouping physical quantities to obtain dimensionless products that define a physical system. Dimensional analysis does not give any expression that describes physical phenomena. It is only a tool for;

1. reducing the number of variables of a well known expression or partly understood complex physical phenomena,

2. determining a dimensionless number set describing physical phenomena without destroying generality.

Today, dimensional analysis is used in a wide range of fields such as; physics, aerodynamics, fluid mechanics , chemistry, mechanics, dynamics, electronics, surface science, biology, engineering applications, economy, environmental sciences, social sciences and so on (e.g. [112-126]). In order to explain the procedure of dimensional analysis, definitions of *quantity*, *dimension*, *unit* and *dimensional homogeneity* should be clarified.

2.5.1. Quantity, dimension, unit and dimensional homogeneity

All physical quantities are properties of physical things or events. Addition and comparison operations are invalid between quantities of different kinds. For instance; length and force are different quantities, and they cannot be added together or compared to each other.

There are two types of quantities:

1. Base (primary or fundamental) quantities,

2. Derived (secondary) quantities.

Base quantities are independent of other quantities. These quantities can be measured by comparison and addition with the quantities of the same kind. In physics; most commonly acknowledged base quantities are mass (M), length (L), and time (t). However; number of base quantities is not limited and they can be extended according to the problem in consideration. For instance, temperature (T) can be used in thermal problems. Derived quantities, on the other hand, are obtained by physical expressions of the other quantities. For example; velocity (V) is determined by the division of length (L) by time (t). However; it should be noted that, there is not a strict distinction between base and derived quantities.

Physical quantities are defined with their dimensions. If X is the numerical value of the length of a pencil, then the dimension of X is length. By definition, base quantities have their own dimensions, whereas; dimensions of derived quantities are determined by physical expressions. For instance; the dimension of velocity is; $[V] = Lt^{-1}$, or the dimension of force is; $[F] = MLt^{-2}$. Whether it is base or derived; the dimension of a quantity (Q) must have a power law form;

$$[Q] = (A)^a (B)^b (C)^c \ldots \tag{2.24}$$

where A, B, C are base quantities and a, b, c are exponents.

Although units and dimensions are related concepts, they are, by definition, different. Units are reference magnitudes of dimensions which are used to describe the magnitudes of physical quantities. In other words; magnitude of a quantity is expressed relative to a unit. Certain units imply certain dimensions, regardless of the magnitude of the quantity.

It is a well-known fact that the magnitudes of the physical quantities are independent of the choice of units that are used to define them. For instance; area of a room does not change whether it is indicated in terms of cm^2 or $inch^2$. Therefore; equations that describe any physical quantity must also be independent of the system of units (e.g. SI system of units (Table 1)), namely; physical equations should give same results for every unit system. For example, Newton's second law, F=ma, gives similar results regardless of the unit system. This fundamental and obligatory property of physical relations is called *dimensional homogeneity*. Dimensional homogeneity, which is the basis of dimensional analysis, was first expressed by French scientist Joseph Fourier in the first quarter of the nineteenth century [127-129]. A physical equation can be meaningful, only if it is dimensionally homogeneous and this is possible only when;

1. both sides of the equation have the same dimensions,

2. summation operation is done between the quantities of the same kind,

3. special functions, such as; exponential, logarithmic or trigonometric, are dimensionless.

Table 1:SI system of units

Quantity	SI name	SI symbol
Length (L)	Meter	m
Mass (M)	Kilogram	kg
Time (t)	Second	s
Temperature (T)	Kelvin	K
Current (I)	Ampere	A
Number of elementary particles	Mole	mol
Luminous intensity	Candela	cd

2.5.2. Buckhingam π Theorem

In the light of Fourier's work, Buckingham [127] made a very significant contribution to dimensional analysis with his famous article; "*On Physically Similar Systems*" in 1914. He revealed that when a *complete* set of variables defining a physical phenomenon is expressed in dimensionless form, number of variables, k, decrease to (k-r), where; r is the number of *dimensionally independent variabl*es. A variable set is *complete* if there is no other quantity that affects the physical phenomena and *dimensionally independent* if variables cannot be written as products of powers of each other. In π theorem, utilized *dimensionally independent* subset of a *complete* set should include minimum number of reference variables that can describe the dimensions of quantities; those are not in the subset.

Let $(Q_1, Q_2,...,Q_k)$ be the complete set of variables that describe quantity Q_o, and function f is a dimensionally homogeneous physical expression describing Q_o;

$$Q_o = f(Q_1, Q_2,...,Q_r, Q_{r+1},...Q_k) \tag{2.25}$$

where; Q_1 Q_2,...,Q_r are independent variables. Buckingham π theorem states that function f can be written in terms of (k-r) dimensionless products of the form;

$$\frac{Q_o}{Q_1^{x_{0,1}} Q_2^{x_{0,2}} ... Q_r^{x_{0,r}}} = F\left(\frac{Q_1}{Q_1^{x_{1,1}} Q_2^{x_{1,2}} ... Q_r^{x_{1,r}}}, \frac{Q_2}{Q_1^{x_{2,1}} Q_2^{x_{2,2}} ... Q_r^{x_{2,r}}}, ..., \frac{Q_{k-r}}{Q_1^{x_{k-r,r}} Q_2^{x_{k-r,r}} ... Q_r^{x_{k-r,r}}} \right) \tag{2.26}$$

where x represents exponent of the quantities.

There is not a unique dimensionless number set for a system and all gathered dimensionless numbers need not to be important or relevant. However; the theorem guarantees that the system can completely be described with these dimensionless numbers. For two different systems, if all of the DN's in the complete dimensionless number set are equal, dimensionless behaviors of the systems are equivalent.

2.5.3. Procedures of dimensional analysis

2.5.3.1. Utilizing π Theorem

Buckingham suggested a procedure for determining dimensionless numbers, which can be divided into three steps;

Step 1: Problem set up; determining complete set of variables

First and may be the most important step of the analysis is determining the complete set of variables. The success of dimensional analysis depends on this step. Any missing variable may cause inaccurate dimensionless numbers. Moreover, selected variables should be independent, namely; it should be possible to change any of the parameters without affecting the other.

Step 2: Selecting dimensionally independent variables

A dimensionally independent subset of variables is chosen from the variable set. These variables are used to express the dimensions of remaining variables.

Step 3: Determining dimensionless numbers

In this step, dimensionless numbers in the dimensionally independent set are divided by the products of powers of the variables that are out of the subset. These products should have the same dimension of the variable taken from the subset. Resultant numbers are dimensionless and a member of dimensionless number set.

Here it should be noted that, dimensionless number set derived by Buckingham π theorem is user dependent. There is infinite number of dimensionless numbers that describe a physical system. This is because; the problem of determining dimensionless numbers is over-determined. Therefore, in some cases, physical relevance of the dimensionless numbers may not be clear.

2.5.3.2. Nondimensionalization (or scaling) of physical expressions

Dimensional analysis is also beneficial for understanding or simplifying the physical phenomena that are fairly well known. In addition to the procedure that Buckingham suggested, dimensional analysis can also be performed via reformulation of the full system by normalizing all of the governing equations and boundary conditions with respect to physical quantities in the expressions. In contrast to π theorem, this method produces a relevant set off dimensionless numbers which give important information about the similarities between two different physical systems.

Let us illustrate this procedure by nondimensionalization of Navier-Stokes equation which describes conservation of momentum in a fluid (or in any non-relativistic continuum):

Step1: Write down governing equations, (and initial and boundary conditions, if exist)

$$\rho\left[\frac{\partial \boldsymbol{v}}{\partial t} + (\boldsymbol{v}\cdot\nabla)\boldsymbol{v}\right] = -\nabla p + \mu\nabla^2\boldsymbol{v} + \rho\boldsymbol{g} \tag{2.27}$$

where ρ, v, p, μ and g are density, velocity, pressure, viscosity and gravitational acceleration, respectively.

Step2: Introduce reference or scale factor for the variables to nondimensionalize them

$$t^* \equiv f_c t; \quad \boldsymbol{v}^* \equiv \frac{\boldsymbol{v}}{v_c}; \quad \nabla^* \equiv L_c\nabla; \quad p^* = \frac{p-p_\infty}{p_o-p_\infty}; \quad \boldsymbol{g}^* = \frac{\boldsymbol{g}}{g} \tag{2.28}$$

Where, f_c, v_c, L_c, g and p_o-p_∞ are characteristic frequency, characteristic velocity, characteristic length, gravitational acceleration and reference pressure difference.

Step3: Substitute scaled factors into the governing equations (and initial and boundary conditions, if existing)

$$\rho V f \frac{\partial \boldsymbol{v}^*}{\partial t^*} + \frac{\rho V^2}{L}(\boldsymbol{v}^*\cdot\nabla^*)\boldsymbol{v}^* = -\frac{p_o-p_\infty}{L}\nabla^* p^* + \frac{\mu V}{L^2}\nabla^{*2}\boldsymbol{v}^* + \rho g\boldsymbol{g}^* \tag{2.29}$$

Step4: Multiply each side of the equation by a factor (in this case $L_c/\rho v_c^2$) to obtain dimensionless version of the equation and distinguish dimensionless numbers form the resultant equation

$$\left[\frac{fL}{V}\right]\frac{\partial \boldsymbol{v}^*}{\partial t^*}+\left(\boldsymbol{v}^*\cdot\nabla^*\right)\boldsymbol{v}^* = -\left[\frac{p_o-p_\infty}{\rho V^2}\right]\nabla^* p^* + \left[\frac{\mu}{\rho VL}\right]\nabla^{*2}\boldsymbol{v}^* + \left[\frac{gL}{V^2}\right]\boldsymbol{g}^* \qquad (2.30)$$

Here square brackets are dimensionless numbers which are Strouhal number (St), Euler number (Eu), inverse of Reynolds number (Re) and inverse of Froude number squared (Fr) respectively. When Navier-Stokes equation is rewritten in terms of these numbers, it becomes;

$$[St]\frac{\partial \boldsymbol{v}^*}{\partial t^*}+\left(\boldsymbol{v}^*\cdot\nabla^*\right)\boldsymbol{v}^* = -[Eu]\nabla^* p^* + \left[\frac{1}{\mathrm{Re}}\right]\nabla^{*2}\boldsymbol{v}^* + \left[\frac{1}{Fr^2}\right]\boldsymbol{g}^* \qquad (2.31)$$

It should be noted that there is not a unique procedure for deriving dimensionless numbers by nondimensionalization of the governing equations. The procedure might change from equation to equation. Even different dimensionless numbers might be obtained from the same equation depending on the procedure or choice of scale and reference factors.

Nondimensionalization can also be done by scaling weak form of the governing equations. Constants of the nondimensionalized weak form are also dimensionless and they are potential candidates for being dimensionless numbers. In this study, utilizing weak form of the equations is advantageous since they are also used in the finite element model of the problem. By this means, obtained dimensionless numbers are totally consistent with the simulation framework.

2.5.4. On the utility of dimensional analysis

DA is only a tool for generating all of the governing dimensionless products from related physical quantities. It cannot directly be employed to generate law-like statements itself, but still it is an important tool for;

1. reducing the number of variables that are needed for describing a physical phenomenon,

2. checking whether developed equations are reasonable or not,

3. gathering information about the similarities between different physical phenomena,

4. out-of-scale-modeling,

5. optimization of experiments.

2.5.5. State of art about dimensional analysis of quenching

In former studies, many aspects of dimensional analysis of transformation-free heating and cooling are clarified. Frerichs et al. [19, 20] has previously shown that Biot number is an important dimensionless number that determines dimensional changes when there is no phase transformation. They revealed that $\Delta L/L_o$ increases until a certain Biot number and then start to decrease. Also they showed that after a critical Biot number cylindrical work pieces approach spherical shape which is parallel to the Ameen rule [130]. But below this Biot number, this is not correct [19]. Later Frerichs et al performed dimensional analysis and derived 8 more dimensionless numbers that describes transformation-free cooling [131]. They investigated the effect of these numbers on dimensional changes and eliminated those that have negligible or no influence on dimensional changes. After the elimination there remain 6 dimensionless numbers (F_n);

$$F_1 = Bi = \frac{hV}{\lambda S}, \ F_2 = \alpha(T_a - T_o), \ F_3 = \nu, \ F_4 = \frac{E}{\sigma^o}, \ F_5 = \frac{E}{K}, \ F_6 = n \qquad (2.32)$$

where Bi - Biot number, h - heat transfer coefficient, λ - thermal conductivity, V/S – volume to surface ratio, α - thermal expansion coefficient, T_a - austenitization temperature, T_o - temperature of the quenching medium, ν - Poisson's ratio, E - elastic modulus, σ° - yield strength, K - Ramberg-Osgood coefficient, n - Ramberg-Osgood exponent

As a continuation of this study, Landek et. al. [21], used a non-linear regression analysis to determine correlation between proposed dimensionless numbers and relative length change;

$$\frac{\Delta L}{L_o} = \begin{cases} \left(0.008410 - 0.011136p - 0.009914p^2\right)pF_1^3 \\ \left(-0.030270 - 0.174116p + 0.015132p^2\right)pF_1^2 \\ \left(-0.040149 - 0.0285998p + 0.0320051p^2\right)pF_1 \\ \left(0.006319 + 0.262553p + 0.023156p^2\right)pF_1 \\ \left(0.000532 + 0.002315F_1 + 0.000792F_1^2\right)F_1 \\ 0.000100 \end{cases} \qquad (2.33)$$

$$p = \frac{0.59284F_2}{(1-F_3)F_4} + \left(\frac{F_2F_5}{1-F_3}\right)^{F_6} - \frac{0.03492}{F_4} \qquad (2.34)$$

Later, Wolff et. al. [132] derived a new dimensionless number set for transformation free cooling by nondimensionalization of weak form of the governing equations. Advantage of this dimensionless number set is that it directly stems from governing equations and therefore, validity of dimensionless numbers in this set are more clear.

Aforementioned studies are followed by the studies on dimensional analysis of quenching with martensitic transformation. Wolff et. al. [133] derived a dimensionless number set for this case by using Buckingham's π theorem (Section 4.2.2.2.). They also included Biot number in this set. Şimşir et. al. [134] investigated the effect of Biot number on dimensional changes and introduced the "*Biot number of austenite*" definition. In [23], Şimşir et. al. introduced another dimensionless number set which is derived by non-dimensionalization of the weak form of the governing equations (Section 4.2.2.3.). They investigated the influence of dimensionless numbers that are related with dilatation and transformation on dimensional changes. They illustrated the importance of these numbers.

Dimensional analysis part of this study can be considered as the continuation and verification of the aforementioned studies. It fills the gap in literature about the dimensional analysis of quenching with martensitic transformation. In this study, the validity and completeness of dimensionless number sets that are proposed in [133] and [23] are verified. Furthermore, influence of the dimensionless numbers that are proposed in [23] on relative dimensional change are investigated.

CHAPTER 3

EXPERIMENTAL AND NUMERICAL PROCEDURE

3.1. Experimental procedure

Target of experimental framework is to verify simulation results and reveal the effect of microstructure on dimensional and shape changes. For these purposes, long cylinders with various diameters (D=10-25 mm, L=200 mm) were through hardened by quenching in a gas nozzle field, salt bath and by high speed water quenching. The majority of the experiments were performed by gas quenching technique and simulations were verified by these experiments. Salt bath and high speed quenching experiments were employed to investigate the effects of quenching methods on distortion behavior. Moreover, high speed quenching experiments provide hints about distortion at high Biot numbers. In this thesis, 93 gas quenching, 10 salt bath quenching and 10 high speed quenching experiments' results are presented.

Two data were gathered from the experiments:

- Changes of length and diameter,

- Shape change (bending).

These were determined by coordinate measurements.

3.1.1. Material; SAE 52100 steel

In the experiments, a high-carbon steel SAE 52100 (100Cr6) that is widely used in ball bearings (Table 2) was used. In Table 2 chemical composition of this steel is presented.

Table 2: Chemical compositions of the steel that are used in the experiments (melt analysis)

Element	C	Si	Mn	P	S	Cr	Mo	Cu	Al
Wt%	0.97	0.21	0.44	0.011	0.007	1.51	0.05	0.11	0.006

In the initial stage of production, steel was continuous casted into 265x265mm^2 billets. It is followed by a spheroidizing heat treatment. Subsequently, billets were shape-rolled to obtain 45mm diameter bars. After rolling process, a second spheroidizing was done. Microstructures before and after this treatment are shown in Figure 6. Main advantage of the second spheroidizing is the improvement in machinability due to spheroidized carbides (Fe_3C and Cr_3C) in ferrite matrix (Figure 6).
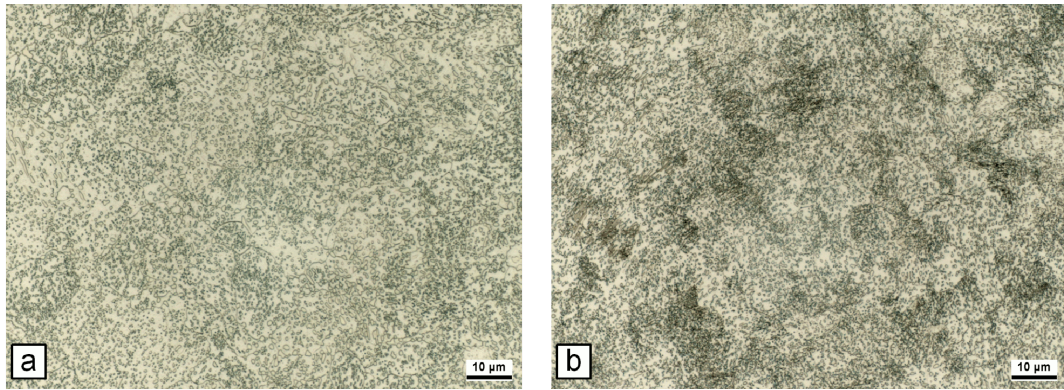
Figure 6: Optical micrograph of SAE 52100 steel (a) in semi-finished condition and (b)after second spheroidizing treatment [135]

Since Cr is the main alloying element, one problem of this steel is Cr_3C segregations at the core. In Figure 7, microprobe photographs of 45mm diameter billet are shown. Measurements were done with Electron Probe Micro Analysis (JEOL). From figure, it can be seen that there is significant core segregation in the material.

In a former study, Epp et. al. [135] determined the carbide fractions in this steel by X-Ray diffraction, and compared with simulation results. They observed that carbide fractions at room temperature are 16.3%. Figure 8 shows the dissolved carbide fractions at different temperatures and times [135].
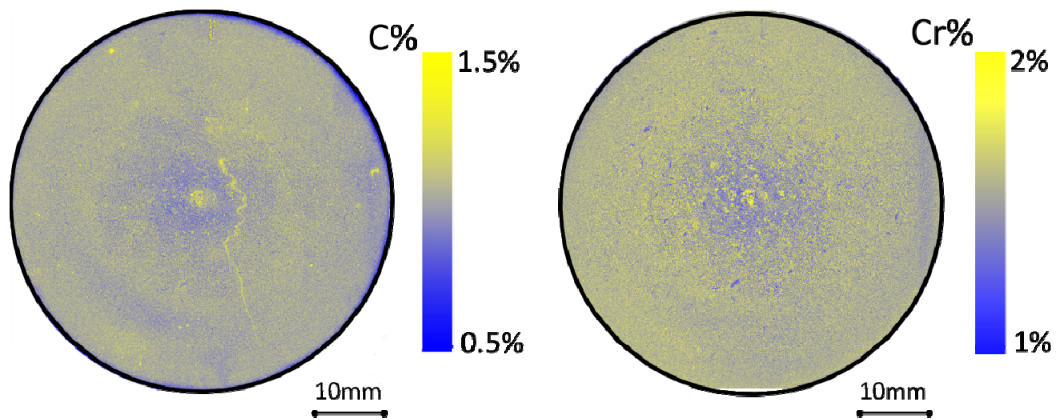
Figure 7: Cr and C concentrations in the cross-section of the 45mm diameter billet
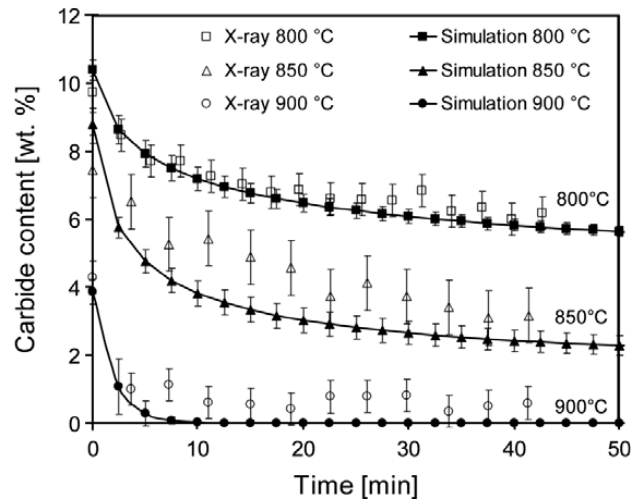
Figure 8: Carbide dissolution kinetics obtained by simulation (from dilatometry) and by in situ X-ray diffraction. (Reproduced from [135])

Various properties of SAE52100 steel are listed in Table 3 as a function of temperature;

$$P(T) = \sum_{i=0}^{4} k_i T^i \tag{3.1}$$

where P, k and T are the property, coefficient, and temperature respectively. Also, CCT diagram of the steel is presented in Figure 9.

Table 3: Properties of SAE52100 steel [12]

Property	Phase	k_0	k_1	k_2	k_3	k_4
Thermal Conductivity [W/mm²°C]	M*	$4.355 \cdot 10^{-2}$	$-1.6 \cdot 10^{-6}$	$-4.8 \cdot 10^{-8}$	$1.82 \cdot 10^{-11}$	
	A**	$1.46 \cdot 10^{-2}$	$1.27 \cdot 10^{-5}$			
Specific Heat [J/kg°C]	M	$4.22 \cdot 10^{2}$	$9.31 \cdot 10^{-1}$	$-2.14 \cdot 10^{-3}$	$2.64 \cdot 10^{-6}$	
	A	$4.54 \cdot 10^{-2}$	$3.88 \cdot 10^{-1}$	$-3.22 \cdot 10^{-4}$	$1.1 \cdot 10^{-7}$	
Enthalpy [J/kg]	M	$3.82 \cdot 10^{3}$	$4.22 \cdot 10^{2}$	$4.66 \cdot 10^{-1}$	$-7.13 \cdot 10^{-4}$	$6.6 \cdot 10^{-7}$
	A	$8.18 \cdot 10^{4}$	$4.54 \cdot 10^{2}$	$7.13 \cdot 10^{-4}$		
Density [kg/m³]	M	7770	$-2.53 \cdot 10^{-1}$			
	A	8041.4	$-5.74 \cdot 10^{-1}$	$2.6 \cdot 10^{-5}$		
Elastic Modulus [MPa]	M	214240	-82.85			
	A	266930	-221.3			
Ramberg-Osgood Exp. [-]	M	0.1278	$8.449 \cdot 10^{-5}$			
	A	0.1092				
Ramberg-Osgood Coeff. [MPa]	M	5724.1	-6.76			
	A	1007.2	-1.155			
Poisson's Ratio [-]	M	0.344	$1.0 \cdot 10^{-4}$			
	A	0.233	$2.5 \cdot 10^{-4}$			
TRIP constant [MPa]	-	$7 \cdot 10^{-5}$				
Martensite start temp. [°C]	-	211				
Koistinenen-Marburger C. [°C]	-	93				

*Martensite, **Austenite*

Figure 9: CCT diagram of SAE52100 steel (Reproduced from [136])
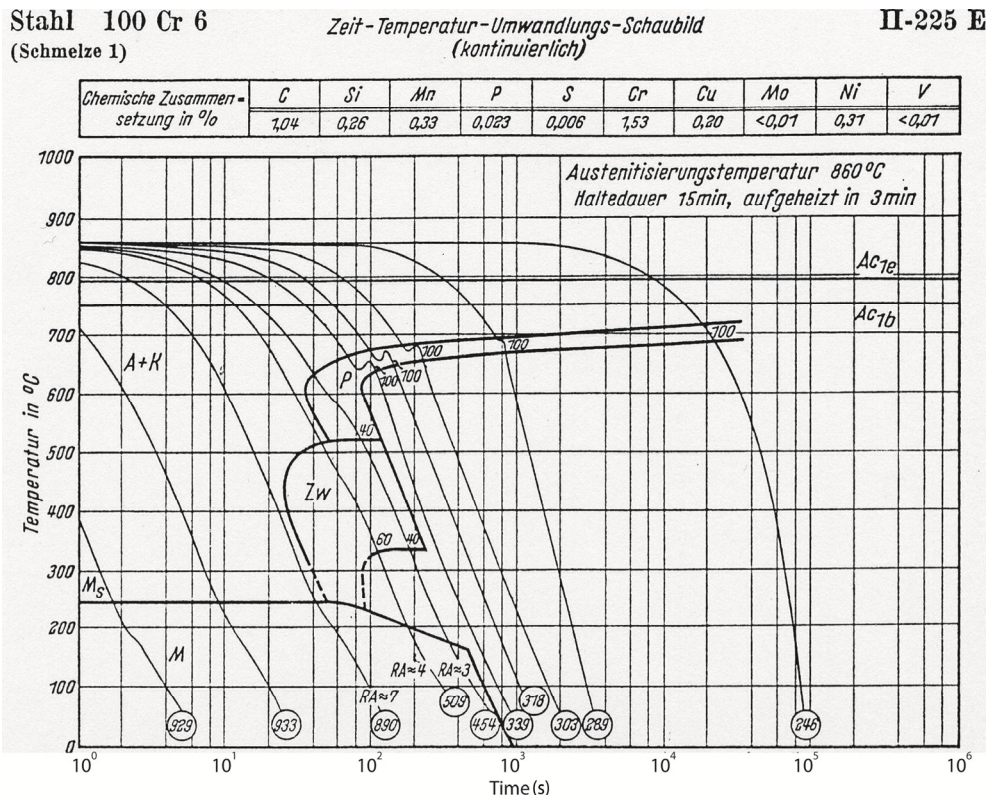
3.1.2. Production of the specimens

All cylinders were machined from 45mm diameter billet according to Figure 10. Distance between center of the billet and centers of the outer most cylinders are 13.5mm. It should be noted that the specimen centers were chosen such that they all coincide. This consideration is useful in investigation of the probable bending due to asymmetrical distribution of microstructure throughout the billet. The specimens of the diameters 20 and 25mm are going to be directly machined from the center of the billets.

The specimens' radial directions were marked with small indentations in order to investigate bending directions with respect to billets axis. Small dots in Figure 10 represent these indentations. On the same surface, M5 screw threads were opened in order to connect cylinders into the quenching system. A photograph including 20, 15 and 10mm diameter specimens is presented in Figure 11. From magnified picture at bottom left, indentation and M5 screw thread can clearly be seen.
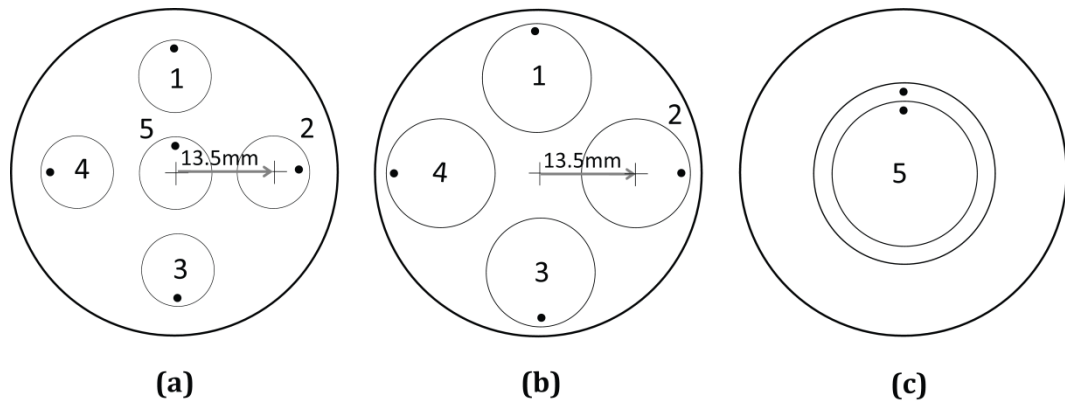
Figure 10: Machining positions for (a) 10mm, (b) 15mm, (c) 20 and 25mm diameter cylinders
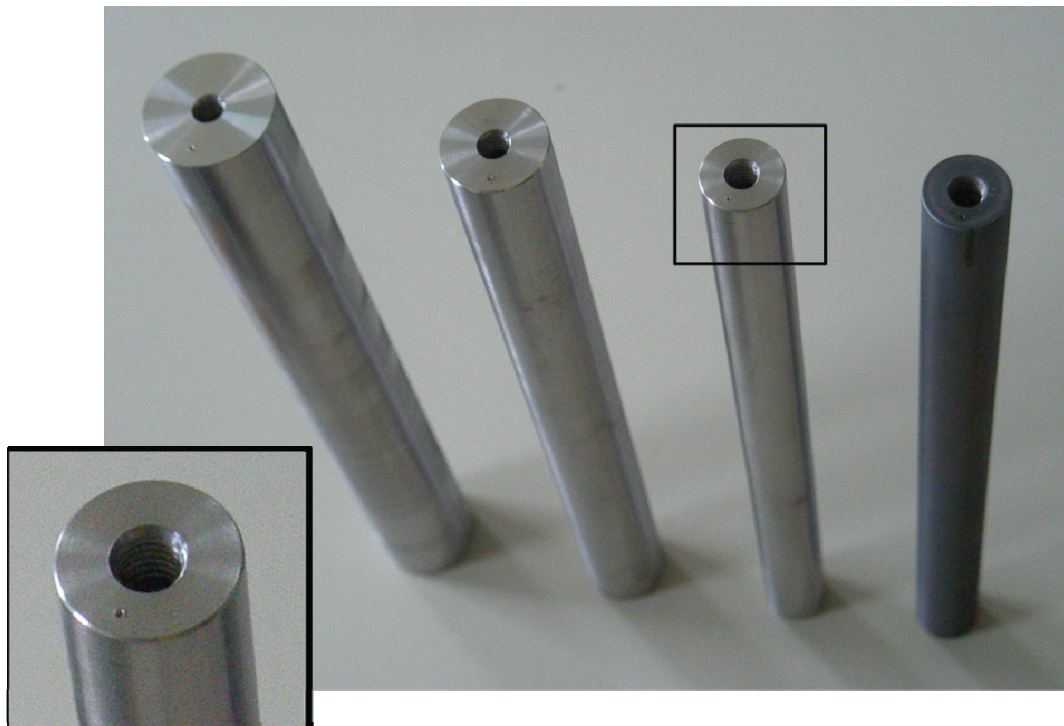
Figure 11: Cylinders with D=20, 15 and 10mm, respectively (from left to right). The right most cylinders is darkened due to the thin oxide layer which occurred after quenching

3.1.3. Gas quenching experiments

3.1.3.1. Experiment setup

Experimental setup consists of a vertical furnace with nitrogen atmosphere and an optically-triggered gas nozzle field (Figure 12). The nozzle field is made up of four nozzle arrays that are located 90 degrees to each other. Each array has 12 nozzles for nitrogen ejection. Each nozzle array is fed with four feeding pipes. Three mass flow controllers with capacities of 8000, 4000 and 3000 l/min are connected to the pipes for feeding the nozzles. It has been recently proven that such a setup provides a very symmetric and controllable quenching [137]. In Figure 13 and Figure 14 pictures of experimental set up and nozzle field are presented, respectively.
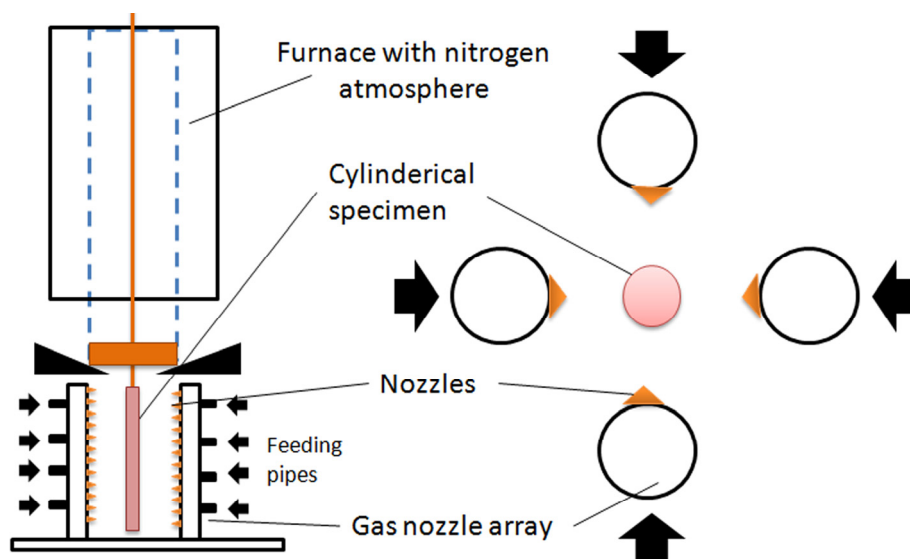
Figure 12: Experimental set up; whole system (left) and distribution of gas nozzle arrays (right)

As it can be seen in Figure 14 the cylinders are connected to the system by screws. Specimens can be moved freely along the nitrogen chamber. During quenching, in order to prevent specimen fluctuations due to gas flow, cylinders are restrained by the fixtures.

Maximum capacity of the quenching system is 333.3l/min per nozzle. By adjusting gas flow rate, a certain range of heat transfer coefficients (h) (Figure 15) can be attained. Heat transfer coefficients for 10 and 20mm diameter cylinders are determined approximately by CFD calculations [17], whereas; h of 15mm diameter cylinders is determined by the interpolation of the results of the other two diameters.
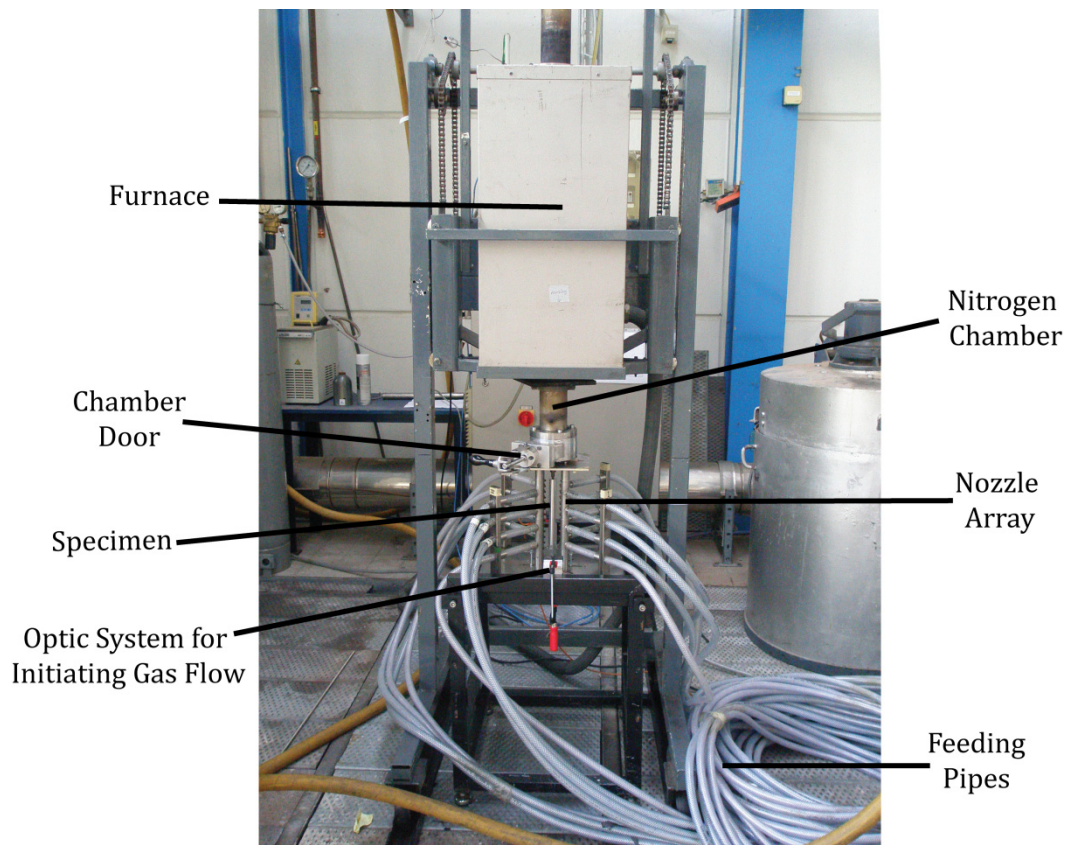
Figure 13: Quenching system
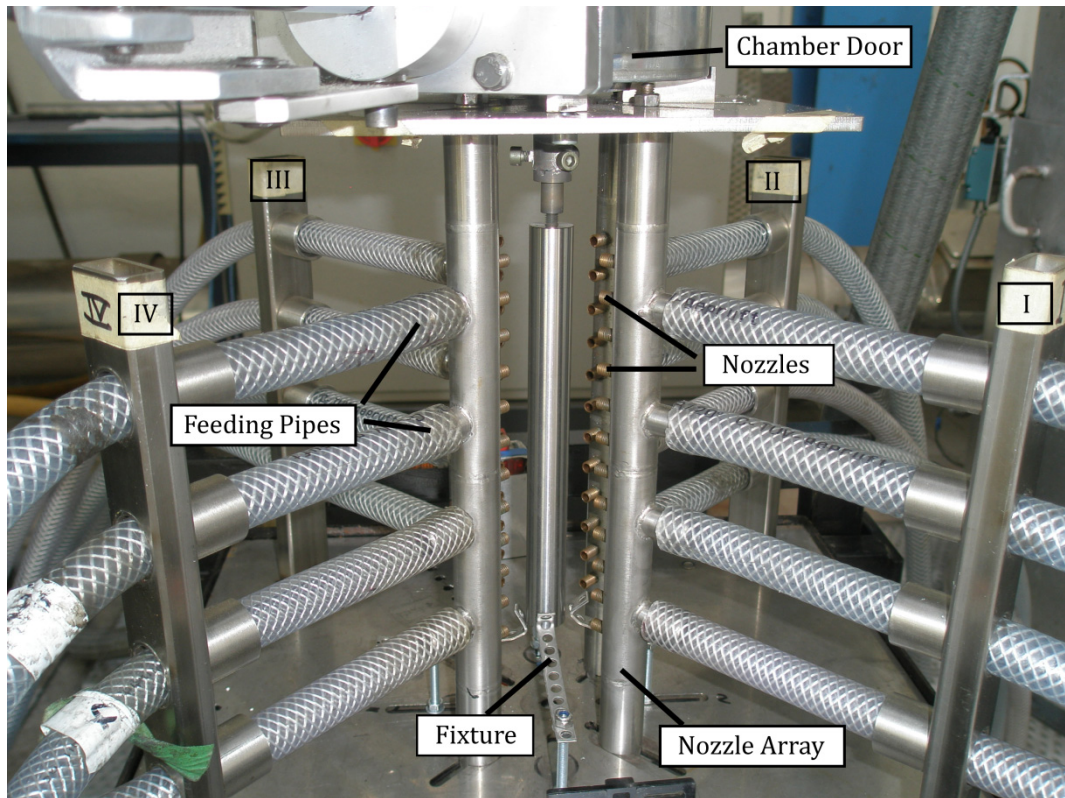
Figure 14: Arrangement of gas nozzle arrays
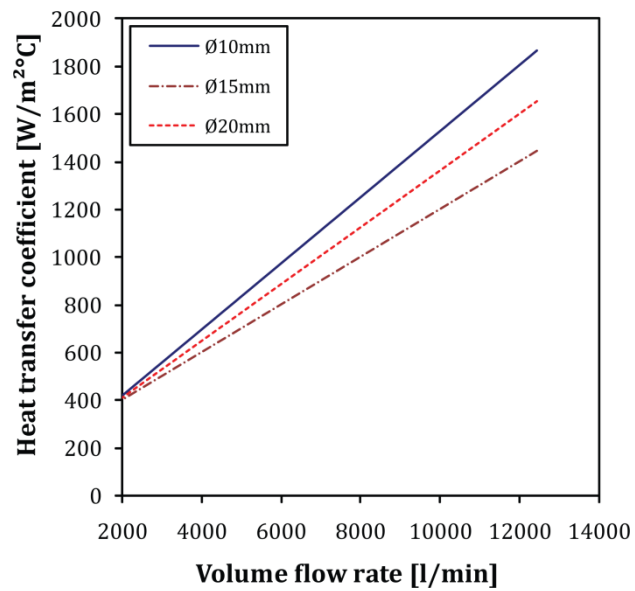
Figure 15: Heat transfer coefficients corresponding to the volume flow rates [17].

3.1.3.2. Experimental procedure

During the experiments, cylinders were first heated at $850°C$ in a preheated furnace under nitrogen atmosphere. Total time in furnace was the sum of heating up and austenitization durations, ($t_{tot} = t_{heating} + t_{aust.}$). Isothermal holding time for all specimens was 25 minutes in order to have equal fraction of solutionized carbides, which is very important for validation of simulations. It is known that material properties such as martensite start temperature deviate significantly with carbide precipitates. Material data set that is used in the simulations is valid for this austenitization condition.

In order to achieve equivalent austenitization, heating up times were calculated as a function of diameter by using Fourier number (Table 13). Heating up times and total times in furnace are listed in Table 4.

Table 4: Heating up and total time in the furnace

		10mm	15mm	20mm
Heating up time	[min]	15	33	60
Total time in furnace	[min]	40	58	85

After heating and austenitization, the specimens were transferred to the nozzle field where Nitrogen gas at room temperature was immediately released when the sample has passed a light barrier. Quenching duration was 3 minutes in order to ensure complete cooling. After quenching, positions of the gas nozzle arrays were marked on to the specimen. This provided a base to check the symmetry of cooling after measuring the bending of the specimens.

3.1.3.3. Experimental window

The philosophy behind the experiments was to obtain a rough experimental window which will yield a spectrum of Biot numbers. Therefore, different heat transfer coefficients were imposed to each specimen in combination with different diameters.

Before deciding experimental window, a pre-screening was done to eliminate the conditions which will not result in through hardening. Moreover, presence of bainite is not desirable in ball bearings since it results in considerable decrease in impact toughness. In ball bearing industry maximum tolerable amount of bainite is determined as approximately 2%. The pre-screening of the results can be performed either by simulations or by use of approximate analytical solution. Since the evaluation by FEM simulations is a time consuming task, it has been decided to perform the pre-screening by approximate analytical solution. This approach relies on the following concepts and approximations.

Gas quenching of steel cylinders can be considered as a Newtonian cooling process since the process window is confined in considerably small Biot numbers due to small dimensions and heat transfer coefficients. A lemma of Newtonian cooling states that processes having the same value of τ will have similar thermal histories that can be expressed by:

$$T(t) = (T_a - T_o) . \exp\left(\frac{-t}{\tau}\right) + T_o \qquad (3.2)$$

where T_a, T_o are the initial (austenitization) and ambient temperature, respectively. τ is the thermal time constant defined as :

$$\tau = \frac{t}{Bi.Fo} = \frac{h}{\rho_a c_a D} \qquad (3.3)$$

where h is heat transfer coefficient. Using these concepts in combination with a few simulations, pre-screening of the experiments was performed to avoid bainite formation above critical amount. For this purpose, Biot and Fourier numbers were calculated using the geometry, heat transfer coefficient and temperature independent average thermal conductivity and specific heat of austenite phase. The integrated average densitiy ($\tilde{\rho}_a$) and specific heat ($\tilde{c}_a$) of the austenite phase were calculated using the following equations;

$$\tilde{\rho}_a = \frac{\int_{T_o}^{T_a} \rho_a(T).dT}{T_a - T_o} \quad , \quad \tilde{c}_a = \frac{\int_{T_o}^{T_a} c_a(T)dT}{T_a - T_o} \tag{3.4}$$

where T_i and T_a are the initial and ambient temperatures, respectively. In Table 5 material and process sets used for calculation of Biot and Fourier numbers are listed. The choice of time does not affect the results of pre-screening. It is required that cooling condition yields $T(t)$ curve below the critical $T(t)$ curve at any instant of time.

Table 5: Material and process parameters used for calculation of Biot and Fourier numbers

L	[mm]	200
D	[mm]	10 to 20
h	[W/m²°C]	300 to 1200
$\tilde{\rho}_a$	[kg/m³]	7798
$\tilde{c}_a$	[J/kg°C]	560.66

After the calculation of Biot and Fourier numbers, a few simulations have been conducted using SYSWELD® to determine the critical value of the product of $B_i.F_o$, at which 2% bainite limit is exceeded. These simulations indicate that 2% critical bainite limit had been exceeded when $B_i.F_o$ value becomes smaller than 0,011. Table 6 illustrates the results of pre-screening. Grey boxes show cooling conditions that cannot be applied due to excessive bainite formation. After the pre-screening, exact number of specimens and number of simulations to be performed have been determined. Details of this approach can be found elsewhere [23] .

Table 6: Pre-screening of the experimental window

h	Bi × Fo		
[W/m²°C]	**Ø10mm**	**Ø15mm**	**Ø20mm**
300	0,005	0,004	0,003
400	0,007	0,005	0,004
500	0,009	0,006	0,004
600	0,011	0,007	0,005
700	0,012	0,008	0,006
800	0,014	0,010	0,007
900	0,016	0,011	0,008
1000	0,018	0,012	0,009
1100	0,020	0,013	0,010
1200	0,021	0,014	0,011

Experimental window that was built according to prescreening is presented in Table 7. Specimens with 25mm diameter were excluded and they were only quenched by salt bath and high speed water quenching due to formation of excessive amount of bainite under gas quenching conditions.

Each experiment was repeated several times for checking the repeatability and reliability of the procedure. For various heat transfer coefficient-diameter combinations, the experiments were repeated several times at every position in order to investigate bending behavior with respect to machining position. In Table 7 these experiments are marked with "*". Remaining experiments were done only for investigating the dimensional changes.

Table 7: Experimental window

D	Vol. flow rate	h	Machining positions					Total
[mm]	[l/s]	[W/m²°C]	1	2	3	4	5	
10	5600	885	1	-	1	1	2	5
	7200	1131	1	-	1	1	-	3
	8000*	1254	5	4	4	5	4	22
	12000*	1800	6	3	5	5	5	24
15	4000**	663	1	2	1	1	-	5
	8000	1128	1	2	1	1	-	5
	9040*	1250	6	5	5	5	-	21
20	10400*	1250	-	-	-	-	5	5
	12000*	1400	-	-	-	-	3	3

these experiments were performed to investigate bending behavior.
**there is excessive bainite

3.1.4. High speed quenching experiments (HSQ)

High speed quenching experiments were performed with the instrument shown in Figure 16a. The instrument consists of a vertical furnace with nitrogen atmosphere and a quenching-chamber. In the quenching chamber, high speed cooling is attained by circulating water. Details of the cooling chamber and direction of the water flow are presented in Figure 16b. A certain range of heat transfer coefficients can be attained by manipulating the water velocity. The maximum flow rate of the instrument is 18l/s.

Similar to the gas quenching set up, specimens are attached to the system by screws and they can be moved vertically. Specimens are transferred from furnace to the quenching system by an automatic system which is initiated by the user.

High speed quenching experiments were applied to 20 and 25mm diameter specimens. Austenitization temperature and time were similar to the gas quenching experiments which are 850°C and 25min, respectively. Total holding time in furnace was 40min. Water velocity that was imposed to the specimens was 18l/s [138]. Corresponding heat transfer coefficients for 20mm and 25mm diameter specimens are approximately 19kW/m²°C and 21kW/m²°C. Experiments were repeated 5 times.
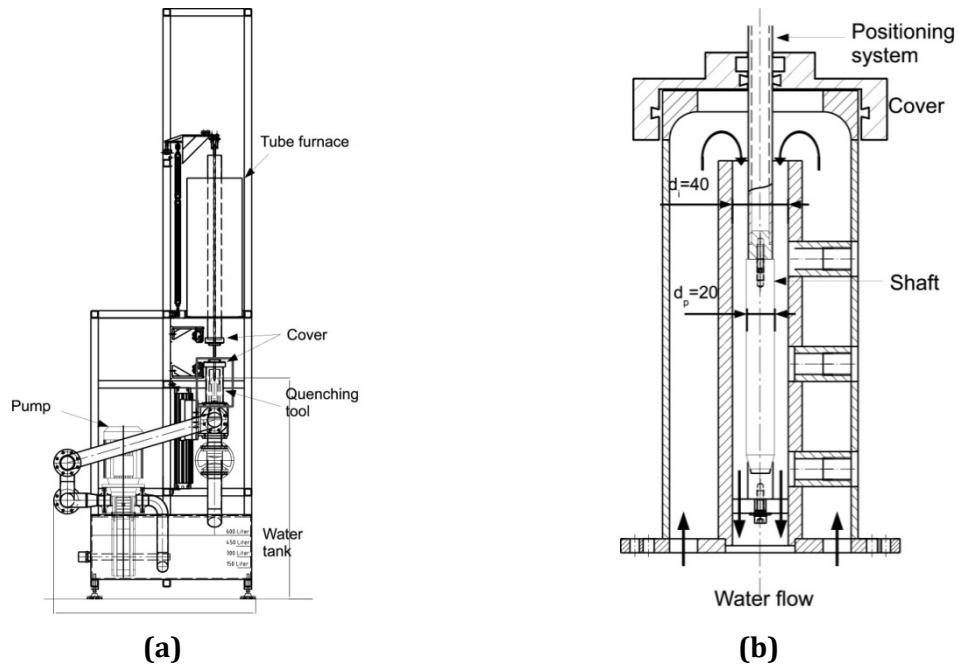
Figure 16: (a) High speed quenching instrument, (b) Quenching tool for shafts

3.1.5. Salt bath quenching experiments (SBQ)

Salt bath quenching experiments were done in three different baths (Figure 17). First bath is filled with GS540 (Degussa) at 850°C. 20 and 25mm diameter specimens were held here for austenitization and heating up during 27 and 28 minutes, respectively. Second bath was filled with AS140 (Degussa) at 230°C which is slightly above martensite start temperature. Specimens were held here 5min in order to reduce thermal stresses before martensitic transformation started. And finally, specimens were transferred to the last bath which was filled with water at 25°C. In Figure 18 this procedure was presented.

Figure 17: Salt bath quenching set up
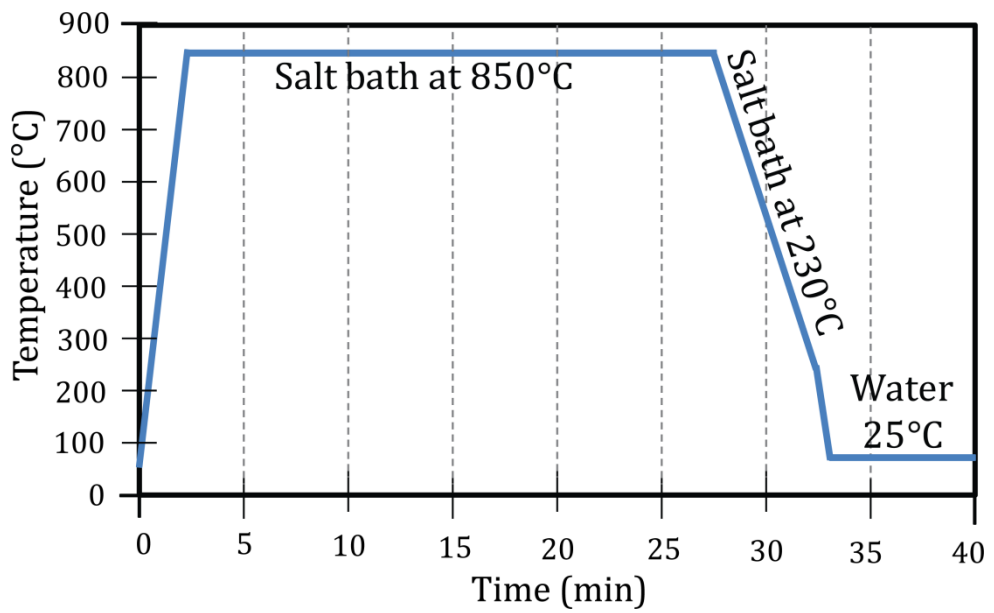
Figure 18: Salt bath quenching procedure

3.1.6. Measurement procedures

3.1.6.1. Coordinate measurement

Coordinate measurements were performed before and after the heat treatment to determine dimensional changes using a contact based instrument PRIMAR MX 4 (Figure 19). The error bound of the instrument is

$$E = \pm \left[1.2 + \frac{L(mm)}{300(mm)} \right] \mu m \qquad (3.5)$$

Figure 20 illustrates the coordinate measurement strategy for calculation of dimensional changes. Twelve roundness plots at specified longitudinal positions (Figure 20a) were measured and circles were fitted to measured data in order to calculate the diameter change as function of length. The length changes at specified radial position were computed by calculating the distance between fitted circles at the top and bottom surfaces.

Initial and final bending vectors were calculated from the projections of center of the fitted circles to the x-y plane (Figure 20a). Bending vector during heat treatment was determined by the subtraction of initial bending vector from the bending vector after the heat treatment (Figure 20b).
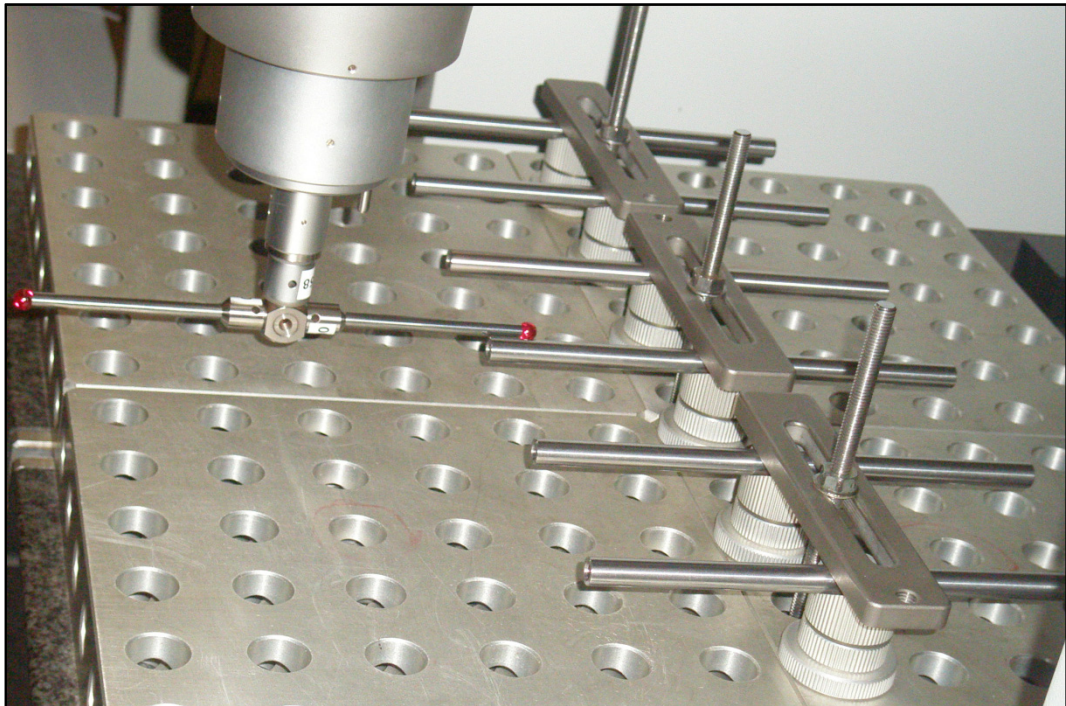
Figure 19: Coordinate measurement instrument

(a)

(b)
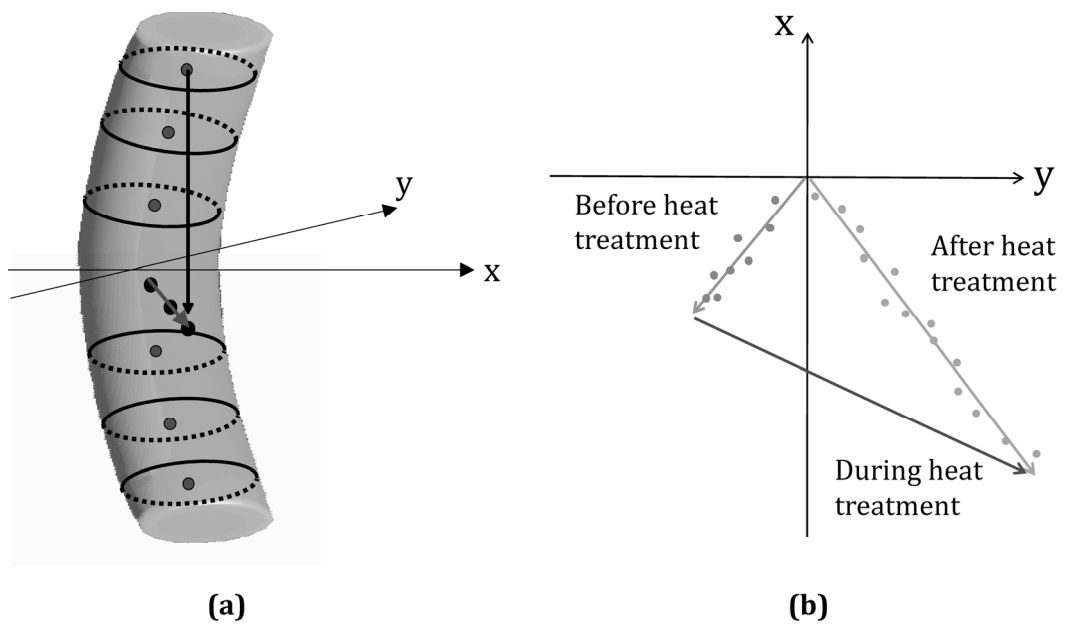
Figure 20: (a) Positions of the roundness plots and projection of circle centers, (b) Calculation of the bending vector

3.2. Numerical Procedure

Simulations were performed by using commercial FEA software SYSWELD® using the material data published in [11, 12] was used. Simulations were performed using axisymmetric models with boundary conditions shown in Figure 21. Using symmetry ¼ of the cylinder was modeled. Heat transfer coefficient at the top (h_T) was taken as ⅛ of the surface heat transfer coefficient (h_S) [137]. All elements have been assumed to be 100% austenite. Initial temperatures of cylinder and gas have been set to 850°C and 20°C respectively. Automatic time step algorithm was used to ensure convergence, obtain conservative results in numerically critical stages such as beginning martensitic transformation and to save time in less critical stages. Numerical parameters of the simulations are listed in Table 8. After performing the simulations, mean dimensional changes were calculated from the extracted contour displacements, as it is illustrated in Figure 21. Details of the mesh that were used and optimization of the model are presented in Section5.1.

Table 8: Numerical parameters

Solution of the linear systems: *Direct method*

Numerical solution algorithm: Quasi-Newtonian method
     Implicit/explicit: Pure implicit algorithm
     Maximum number of iterations at each increment: 100

Convergence criteria (Precision):
     Temperature: 10^{-2}°C
     Displacement: 10^{-8}mm
     Force: 10^{-30}N

Time step algorithm: *Automatic*
     Maximum time step: 1sec
     Minimum time step: 0.001sec
     Factor to increase time step: 1.1
     Factor to decrease time step: 0.8
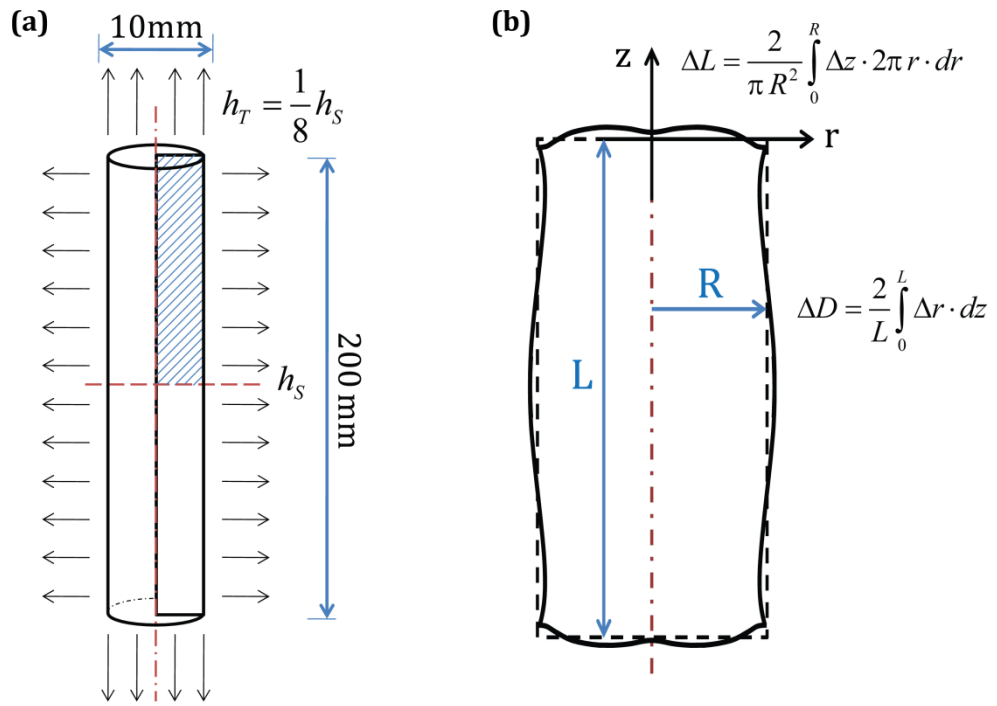
Figure 21: (a) Boundary conditions and geometry of long cylinders, (b) Extraction of the contour displacements

CHAPTER 4

MATHEMATICAL FRAMEWORK

4.1. Sensitivity analysis

In this part of the study, a *local sensitivity analysis method (LSM)* was utilized to reveal the effects of deviations in input parameters on simulation results. As its name implies, LSM focuses on a reference input data (x) and reveals the effects of perturbations of this reference data on output (y). An alternative to the LSM is global sensitivity methods (GSM). In contrast to LSM's, global sensitivity methods utilize more than one reference point (x,y), therefore they are effective tools to obtain information about the complete behavior of nonlinear systems. However; in the case of consideration, it is practically not possible to make use of GSM's. This is because, quench problem has large number of input parameters (24), and therefore, extremely large number of simulations are necessary to investigate global behavior of the system. As a result, choice of LSM in sensitivity analysis of quenching problem is inevitable. Local sensitivity analysis procedure, which was utilized in this study, is as following:

4.1.1. Procedure

Input data that is generated from material data set published in [11, 12] together with specified quenching conditions (h=1200W/m²°C) and geometry (L=200mm) are denoted as reference state (x_j^o). Later, all the material and process parameters except the geometry are perturbed one by one around this state and the magnitude of the disturbance in results are quantified by defining a non-dimensional measure 'sensitivity' (ξ). It should be noted that higher order interactions between parameters are not taken into consideration, that is to say; input parameters are changed one at a time. Otherwise, it becomes necessary to perform vast number of simulations, which is

practically impossible. For instance, to be able to investigate second order interactions, required number of simulations increases to 1152. Since sensitivity analysis was performed for both kinematic and isotropic hardening models, this number increases to 2304. On the other hand, currently used approach necessitates only 96 simulations which is applicable and considerably lower.

4.1.2. Sensitivity definition

The mathematical model of distortion after quenching is considered as a black-box function $f_i(x_1, x_2, ..., x_j) = y_i$, where x_j and y_i are input (material properties) and output (relative dimensional and shape changes) parameters, respectively. When the partial derivative of f with respect to x_j at x_o is approximated by using central difference formula;

$$\left. \frac{\partial f_i}{\partial x_j} \right|_{x_j^o} \approx \frac{y_i^+ - y_i^-}{x_j^+ - x_j^-} \tag{4.1}$$

the local sensitivity of output y_i on input parameter x_i ($\xi_{y_i}^{x_j}$) is defined as;

$$\xi_{y_i}^{x_j} = \frac{x_j^o}{y_i^o} \left. \frac{\partial f}{\partial x_j} \right|_{x_j^o} \approx \frac{x_j^o}{y_i^o} \left(\frac{y_i^+ - y_i^-}{x_j^+ - x_j^-} \right) \tag{4.2}$$

where x_j^+ and x_j^- are perturbed inputs, whereas; y_i^+ and y_i^- are corresponding outputs. From equation (4.2) one can see that ξ can equivalently be defined as the first coefficient of Taylor series expansion of the function f(x):

$$f_i(x_j) = f_i(x_j^o) + \frac{f(x_j^o)}{x_j^o} \xi_{y_i}^{x_j} (x_j - x_j^o) \tag{4.3}$$

where higher order terms are neglected.

Graphical interpretation of ξ is shown in Figure 22 where mathematical model of quenching is represented as a function $f(x_j)$ when input parameters other than x_j are kept constant. Accordingly, ξ is the slope of $f(x_i)$ multiplied by $x_j^o \big/ y_i^o$.
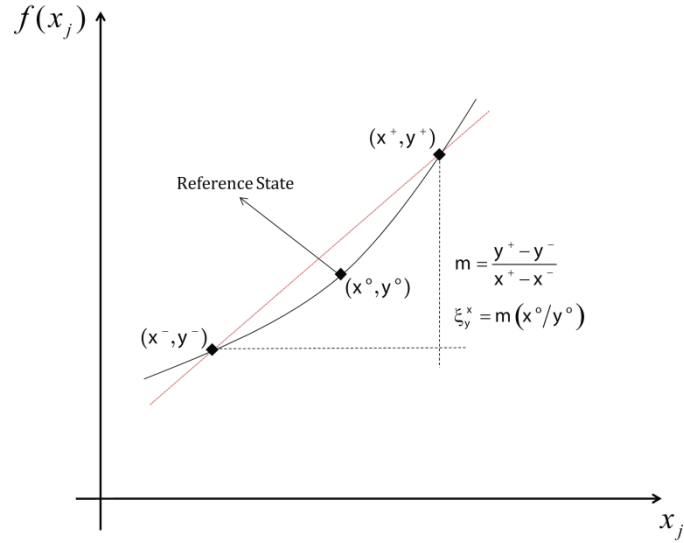
Figure 22: Graphical interpretation of the sensitivity

4.1.3. Perturbation of temperature dependent properties

Quenching is a thermal process during which material properties continuously change with respect to temperature. Therefore, a problem arises in interpreting material properties in the sensitivity definition and determining amount of perturbation. To deal with these problems, temperature independent (averaged) material properties were used in the definition of sensitivity. Average material property $\overline{x}_j$ is defined as

$$\overline{x}_j = \frac{\displaystyle\int_{T_o}^{T_f} x_j(T)dT}{T_o - T_f}$$

(4.4)

64

where T_o and T_f are the minimum and maximum temperatures at which considered phase exists in the process window. For instance, these are M_s and quenching medium temperature for martensite, respectively. By this means, averaging window is confined to obtain more representative values. Averaged material properties are listed in Table 9.

Averaged material properties were also used for interpreting properties in dimensionless numbers. Since it is out of the scope of this section it will not be mentioned in detail here. Details are discussed in "dimensional analysis" section.

The magnitude of perturbation ($x_j(T)$) was determined by using standard deviation of the experimental data or 5% of the property if calculation of error bound is not possible. However, two questions arise due to temperature dependent nature of the material properties. Firstly; temperature dependency brings a problem in determining Δx_j, when perturbation is required to be made in a certain percentage of the property. Secondly, a strategy should be developed to make perturbations on material property function; $x_j(T)$. These problems were also considered by Rajhi et al. and they solved these by calculating perturbation for each temperature and modifying material property function accordingly [139]. In this case, however; another question arise in defining Δx_j in ξ due to temperature dependency of Δx_j. As an alternative, in this study; Δx_j was taken as 5% of the integrated average material properties ($\bar{x}_j$) if calculation of error bound is not possible. Later, perturbation is made by shifting $x_j(T)$ with an amount of Δx_j, which is illustrated in Figure 23. This procedure is advantageous in defining Δx_j in ξ, since it becomes a constant value. The averaged and perturbed inputs are listed in Table 9.
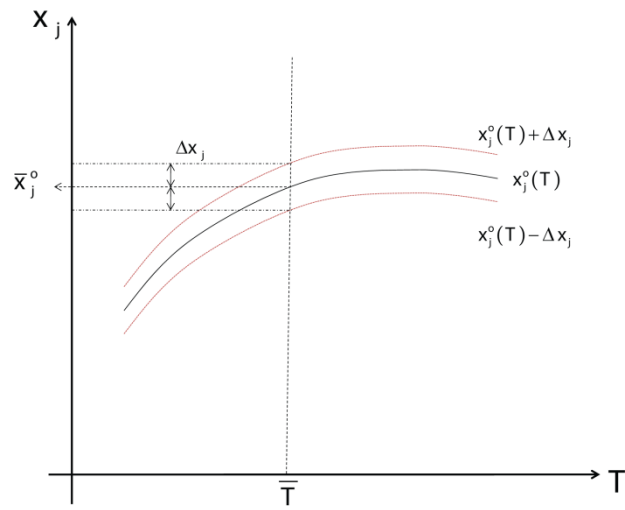
Figure 23: Perturbation procedure

Table 9: Integral average material properties (reference state), perturbation amounts and perturbed material properties

	Unit	Reference State $\bar{x}_j^o$	Perturbation amount $\Delta x/x_o$	Positive Perturbation x_j^+	Negative Perturbation x_j^-
h	[W/m²ᵒC]	1200	0.083	1300	1100
ρ_a	[kg/m³]	7798	0.050	8185	7411
ρ_m	[kg/m³]	7741	0.050	8131	7351
c_a	[J/kgᵒC]	560.7	0.021	572.7	548.7
c_m	[J/kgᵒC]	501.3	0.028	515.3	487.3
λ_a	[W/m ᵒC]	20.12	0.015	20.42	19.82
λ_m	[W/mm ᵒC]	42.73	0.019	43.53	41.93
M_s	[ᵒC]	211.0	0.007	212.4	209.6
M_o	[ᵒC⁻¹]	0.01071	0.040	0.01115	0.01027
$\Delta H_{a \to m}^{tr}$	[J/kg]	78520	0.0013	78620	78420
ε^{tr}	[-]	0.356	0.079	0.384	0.328
κ	[MPa·10⁻⁵]	7.0	0.286	8.9	5.0
α_a	[10⁻⁶ ᵒC]	23.80	0.050	24.99	22.61
α_m	[ᵒC 10⁻⁶]	10.90	0.050	11.45	10.34
E_a	[MPa]	170665	0.050	179198	162132
E_m	[MPa]	204671	0.050	214905	194437
ν_a	[-]	0.332	0.050	0.315	0.349
ν_m	[-]	0.356	0.050	0.338	0.374
K_a	[MPa]	449	0.050	472	427
K_m	[MPa]	4819	0.050	5060	4578
n_a	[-]	0.264	0.050	0.277	0.250
n_m	[-]	0.279	0.050	0.293	0.265
σ_a^o	[MPa]	173.3	0.050	181.9	164.6
σ_m^o	[MPa]	1278.4	0.050	1214.4	1342.3

The rows are grouped into three categories: **Thermal** (h through λ_m), **Transformation** (M_s through κ), and **Thermomechanical** (α_a through σ_m^o).

4.1.4. Ranking

Although ξ gives an idea about the importance of input parameters, it is not easy to make a classification at first glance. The questions of "*which value of ξ is large?*" and "*at which value of ξ, the parameter should be considered as unimportant?*" need to be answered in order to evaluate sensitivity results. To clarify these questions and simplify evaluation of the results, a sensitivity ranking system (Table 10) was developed. Ranking system was arranged such that it divides the range between maximum and minimum ξ into meaningful parts. For instance; if a parameter with grade 3 is perturbed with a certain percentage ($d\%$), the deviation in input will approximately cause a relative deviation of the same magnitude ($d\%$) in the output. When grade is 2, output deviates approximately $\frac{1}{2}d\%$ and when grade is 4 deviation in the output is $2d\%$. Therefore; parameters of ranking smaller than 3 can be considered as relatively unimportant, whereas, ones with larger rankings are significant.

Table 10: Sensitivity ranking system

Sensitivity Range	Ranking
ξ<0.1	0
0.1≤ξ<0.5	1
0.5≤ξ<0.8	2
0.8≤ξ<1.1	3
1.1≤ξ<2.0	4
2.0≤ξ	5

4.2. Dimensional analysis

As it is mentioned in Chapter 2.5. , dimensional analysis provides a set of dimensionless numbers that describes a system. Although; this section is named as "dimensional analysis", it does not focus on the derivation of the dimensionless numbers that describe the quenching problem. Basically, it includes the validation and an application of the dimensionless number sets that are determined in former studies. That is to say; this study aims to;

1. justify dimensionless number sets that were derived in [23, 133],

2. determine the effects of the dimensionless numbers in these sets on dimensional changes,

3. derive an expression of dimensionless numbers to approximate dimensional changes after quenching.

The rest of this section has the following outline: The variables of quenching problem are introduced in Section 4.2.1. Dimensionless number sets that were derived from these variables were presented in 4.2.2. and finally; procedure for 1, 2 and 3 were explained in Section 4.2.3.

4.2.1. Parameters of quenching

Quenching of long cylinders can be described in terms of 27 variables which can be classified as geometric parameters, process parameters, and material properties (thermal, transformation and mechanical). Four base quantities of the SI unit system; [L], [M], [t] and [T], are enough to describe the units of these variables. These variables and their dimensions in terms of SI system of units are listed in Table 11. For the sake of brevity, thermal and mechanical properties for austenite and martensite were not designated separately.

Table 11: List of variables and their dimensions in terms of SI base units

			[L]	[M]	[t]	[T]
Geometry	L	Length	1	0	0	0
	D	Diameter	1	0	0	0
Process	T_a	Austenitization Temperature	0	0	0	1
	T_o	Ambient Temperature	0	0	0	1
	h	Heat Transfer Coefficient	3	-1	-3	-1
Thermal	$\rho*$	Density	-3	1	0	0
	$c*$	Specific Heat	-2	0	-2	-1
	$\lambda*$	Thermal Conductivity	2	-1	-3	-1
Mechanical	$\alpha*$	Thermal Expansion Coefficient	0	0	0	-1
	$E*$	Elastic Modulus	1	1	-2	0
	$\nu*$	Poisson's Ratio	0	0	0	0
	$K*$	Ramberg-Osgood Coefficient	1	1	-2	0
	$n*$	Ramberg-Osgood Exponent	0	0	0	0
	$\sigma^{o}*$	Yield Strength	1	1	-2	0
Transformation	ΔH^{tr}	Transformation Enthalpy	2	0	-2	0
	M_s	Martensite Start Temperature	0	0	0	1
	M_o	Koistinen-Marburger Constant	0	0	0	1
	κ	TRIP Constant	0	-1	2	0

*Properties of austenite and martensite are not designated separately for the sake of brevity.

4.2.2. Dimensionless number sets

According to the π theorem, number of variables (n) of a physical system can be decreased to n-k dimensionless numbers where k is the quantity of independent variables. Quenching of cylinders can be described 28 variables including time (t). Therefore, the system can be described by a dimensionless number set consisting of 24 DN's. Since Fourier number has no effect on final state of the system, distortion of the cylinders is governed by 23DN's. In other words, at equilibrium, Fourier number (or dimensionless time) can be considered as infinite at any case because theoretically infinite time is needed for the equilibrium. Time is an additional process parameter which is related to progress not the final state.

In this study; two different dimensionless number sets were investigated. One of these was determined by utilizing π theorem (Ω_Π) whereas; the other was derived from the constants of the non-dimensionalized weak form of the governing equations (Ω_W). Although both of these sets were validated and discussed, this study is mostly focuses on the latter. This is because; the latter was directly derived from governing equations that describe the quenching system. Consequently, their physical relevance is more probable and their effect on the system is more predictable. On the contrary, physical meaning and relevance of the dimensionless set derived by π theorem is not clear. It directly depends on the choice of the user. Before getting in to detail of DN sets, assumptions that were made during their derivations should be mentioned.

4.2.2.1. Assumptions in the dimensional analysis of the problem

Quenching is a complex phenomenon during which temperature evolves continuously and various physical events occur simultaneously. Therefore; while performing dimensional analysis of quenching, several assumptions need to be done to simplify the problem. Both of the dimensionless number sets that were mentioned in the previous section were derived based on the same assumptions [23, 133]:

o System solely consisted of austenite and martensite phases. Quenching is fast enough to obtain through hardening, therefore; there is no bainite formation. This assumption eliminates constraints due to bainitic phase. Therefore, during this study, bainitic transformation is eliminated from the simulations

o   Material properties were assumed to be independent of temperature, and in the definitions of dimensionless numbers their integrated average over temperature ($\bar{x}$) were used. Simulations were also done by using averaged material data set instead of temperature dependent set. This simplification was needed since temperature dependence of material properties causes problem in defining dimensionless numbers. By this means; inconvenient temperature dependent dimensionless numbers were avoided. The consequences of this assumption are discussed in the "Results and Discussion" section.

o   For the sake of simplicity, E, ν, α, c, λ and n of the austenite and martensite phases were assumed to be equal. However, this assumption neglects large differences between the two phases which might significantly affect the results. Furthermore, it brings difficulty in defining these material properties in dimensionless numbers. Therefore; six dimensionless numbers of these dimensionless number sets were defined as;

$$\Pi_{18} = \frac{\lambda_m}{\lambda_a}, \ \Pi_{19} = \frac{c_m}{c_a}, \ \Pi_{20} = \frac{\alpha_m}{\alpha_a}, \ \Pi_{21} = n_m, \ \Pi_{22} = \frac{\nu_m}{1 - 2\nu_m}, \ \Pi_{23} = \frac{E_m}{E_a} \qquad (4.5)$$

where Π_{18} and Π_{19} are related with heat conduction, Π_{20} is related with dilatation, Π_{21} is related with plasticity and finally Π_{22} and Π_{23} are related with elasticity. Moreover, material properties in the DN's in dimensionless number sets were taken as the material property of austenite.

o   Material properties depend on the dissolved carbide fraction during austenitization. In dimensional analysis the effect of austenitization temperature and duration on material properties was neglected.

Although these assumptions damage the precision and generality of the analysis, these were necessary to be able to perform dimensional analysis. The consequences of these assumptions and remedies are discussed in more detail in the "Results and Discussion" part.

4.2.2.2. Dimensionless number set; π theorem (Ω_{Π})

In reference [133], Wolf et. al. performed dimensional analysis for quenching of conical rings by utilizing π theorem. But still resultant DN's can be used for long cylinders when extra parameters coming from the geometry are excluded. These dimensionless numbers are listed in Table 12. It is not easy no name these numbers since physical relevance of them is not clear.

Details of the dimensional analysis procedure can be found in reference [133].

Here, Biot number is defined in terms of diameter of the cylinder. In a former study, Frerichs et al. [19] showed that this Biot number definition was valid for cylinders. However, during this study more general form of the Biot number was used;

$$Bi = \frac{\alpha}{\lambda}\left(\frac{V}{S}\right)$$

(4.6)

where diameter was replaced by volume to surface ratio (V/S). This definition is more general and can be applied to any geometry.

Table 12: Dimensionless number set that is derived by Buckingham π theorem

$F_1 = v$	$F_7 = \dfrac{K_m}{E}$	$F_{13} = \dfrac{\rho_m(T_a)}{\rho_a(T_a)}$
$F_2 = n$	$F_8 = \kappa E$	$F_{14} = \dfrac{\Delta H_{tr}}{cM_s}$
$F_3 = \dfrac{L}{D}$	$F_9 = \alpha T_a$	$F_{15} = Bi = \dfrac{\alpha D}{\lambda}$
$F_4 = \dfrac{\sigma_a}{E}$	$F_{10} = \alpha(T_a - T_o)$	$F_{16} = Fo = \dfrac{t\lambda}{\rho_a(T_a)c_p D^2}$
$F_5 = \dfrac{\sigma_m}{E}$	$F_{11} = \alpha M_s$	$F_{17} = \dfrac{\alpha E}{\rho_a(T_a)c}$
$F_6 = \dfrac{K_a}{E}$	$F_{12} = \alpha M_o$	$F_{18} = \dfrac{E\rho_a(T_a)c^2 D^2}{\lambda^2}$

4.2.2.3. Dimensionless number set; weak formulation(Ω_W)

In reference[23], another dimensionless number set (Table 13) was derived by nondimensionalization of the governing equations. Instead of classical formulations, weak forms of the governing equations were used in order to combine differential equations, initial and boundary conditions. Derivation procedure of the dimensionless numbers [23] can be summarized as follows:

- The mathematical model was transformed to weak form.

- Cylindrical domain (r, z) and time (t) was transformed into dimensionless space $(\bar{r}, \bar{z})$ and time (τ);

$$\bar{r} = \frac{r}{R}, \quad \bar{z} = \frac{z}{L}, \quad \tau = \frac{t}{t^*} \tag{4.7}$$

  where t* is Fourier number at time when equilibrium is reached. In the case of considerations t is time at which temperature of the core reaches 0.1°C above ambient temperature (T=T_o+0.1°C). This is because; theoretically infinite time is needed to reach equilibrium.

- Similarly, displacements and temperature were converted to dimensionless form:

$$\theta = \frac{T - T_a}{T_a - T_o}, \quad \delta r = \frac{dr}{R}, \quad \delta z = \frac{dz}{L} \tag{4.8}$$

- Finally, dimensionless numbers are extracted from constants of the weak form of the governing equations.

Principals and detailed mathematical derivation is in reference [23]. Here, one can also find details about the derivation of the weak formulation of transformationless case. application of this framework for the case with phase transformations can be found in reference [22].

74

Table 13: Dimensionless number set that is determined by nondimensionalization

Geometry	$\prod_0$	$\dfrac{L}{D}$	Aspect Ratio
Thermo-metallurgical	$\prod_1$	$\dfrac{h}{\lambda}\left(\dfrac{V}{S}\right)$	Biot Number
	$\prod_2$	$\dfrac{\lambda t}{\rho_a(T_a)c}\left(\dfrac{S}{V}\right)$	Fourier Number
	$\prod_3$	$\dfrac{\Delta H_{tr}}{c(T_a - T_o)}$	Latent Heat Number
Transformation	$\prod_4$	$\dfrac{M_s - T_o}{T_a - T_o}$	Martensite Start Number
	$\prod_5$	$\dfrac{T_a - T_o}{M_o}$	Koistinen-Marburger Number
Dilatational	$\prod_6$	$\dfrac{(1+\nu)\alpha(T_a - T_o)}{1-2\nu}$	Thermal Strain Number
	$\prod_7$	$\dfrac{(1+\nu)}{3(1-2\nu)}\left(\dfrac{\rho_a(T_a) - \rho_m(T_a)}{\rho_m(T_a)}\right)$	Transformation Strain Number
Thermoelasto-plastic	$\prod_8$	$\dfrac{(1+\nu)\lambda^2}{E\rho_a(T_a)c^2}\left(\dfrac{S}{V}\right)$	Thermoelastic Fourier Number
	$\prod_9$	$\dfrac{E\alpha T_a}{(1-2\nu)\rho_a(T_a)c(T_a - T_o)}$	Thermoelastic Dissipation Number
	$\prod_{10}$	$\dfrac{\sigma_a^o}{\rho_a(T_a)c(T_a - T_o)}$	Plastic Dissipation Number
Elastoplastic	$\prod_{11}$	$\sqrt{\dfrac{2}{3}}\dfrac{(1+\nu)\sigma_a^o}{E}$	Yield Number
	$\prod_{12}$	$\sqrt{\dfrac{2}{3}}\dfrac{(1+\nu)K_a}{E}$	Isotropic Hardening Number
	$\prod_{13}$	$\dfrac{3\kappa E}{2(1+\nu)}$	TRIP Number
Purely Plastic	$\prod_{14}$	n	Ramberg-Osgood Exponent
	$\prod_{15}$	$\dfrac{\sigma_m^o}{\sigma_a^o}$	Yield Strength Ratio
	$\prod_{16}$	$\dfrac{K_m}{K_a}$	Isotropic Hardening Ratio
Purely Elastic	$\prod_{17}$	$\dfrac{\nu}{1-2\nu}$	Poisson Ratio Number

4.2.3. Procedure

Effect of dimensionless numbers on simulation results was investigated in three steps. Firstly, dimensionless number sets were verified. Later, effects of these numbers on dimensional changes were investigated. Finally, the expression is determined from relative dimensional change versus Biot number curves. Details of these steps are mentioned below.

Step 1: Justification of the validity of the dimensionless number sets

The main aim of this part is to determine whether dimensionless number sets are enough to describe the system or not. If dimensionless numbers in a valid and complete set are kept constant, system behavior does not change. The dimensionless number set was checked by utilizing this property. Material properties were manipulated such that all of the dimensionless numbers were kept constant. Later, dimensionless behaviors of the system were investigated. For the case in consideration, dimensionless behaviors of the system were (1) all of the strains, (2) dimensionless stresses (σ/σ°), and (3) dimensional changes ($\Delta D/D_o$, $\Delta L/L_o$, $\Delta V/V_o$).

Step 2: Manipulation of dimensionless numbers

In this part, each dimensionless number was multiplied by various factors while others were kept constant. One of the main problems was that changing some of the material properties affects more than one dimensionless numbers. Therefore, several material properties had to be multiplied by several constants systematically, in order to affect only one dimensionless number.

*Step 3: Investigation of Biot number versus r*elative dimensional change curves ($\Delta D/D_o$, $\Delta L/L_o$, $\Delta V/V_o$)

Simulations were performed at a range of Biot number (Bi_a=0.037 - 2). For each dimensionless number characteristics of these curves were investigated.

4.3. Variation of the correlated properties

In both sensitivity and dimensional analysis, material properties need to be manipulated. This is relatively easy for most of the material properties, such as; thermal conductivity and Poisson's ratio, since they have independent nature. These can directly be multiplied or divided by constants and shifted without any problem. On the contrary, some of the material properties, such as; density and transformation enthalpy, are correlated with other material properties. It is physically impossible to change these properties independently. Thus, these properties should be treated carefully in order to avoid a non-physical system.

Other difficulties in manipulating correlated properties are caused by the strict input requirements of the utilized software; SYSWELD®. First problem due to the software restriction is that several material properties are to be entered in terms of other quantities. For instance; instead of thermal expansion coefficient, software requires densities and thermal strains at different temperatures. Information about α is embedded in those data. Therefore; thermal expansion coefficient has to be changed indirectly by changing these two quantities. Second problem comes from the weakly coupled independent thermal and mechanical simulations. SYSWELD® requires two separate input data for thermal and mechanical simulations. Some of the correlated properties are entered directly or indirectly in both of the input data. Therefore; thermal and mechanical data sets are to be manipulated carefully in order to avoid input mismatch. Correlated material properties and remedies for their manipulation are as following:

Thermal expansion coefficient, density, thermal and transformation strains

Thermal expansion coefficient (α) and density (ρ) are correlated material properties. Manipulating one of these without changing the other will result in a non-physical system. Moreover, SYSWELD® requires only ρ(T). Therefore; thermal expansion coefficient can only be manipulated by changing density data over temperature.

As a remedy, density curve was described by density at a reference temperature ($\rho(T_o)$) and thermal expansion coefficient. Former describes the height of the curve whereas latter determines its slope. This is consistent with the DNs presented in Section 4.2.2. Since in these DNs, density is defined in terms of its value at austenitization temperature; $\rho(T_a)$. As a result, ρ and α were manipulated by changing the slope of the density curve and shifting it, respectively (Figure 24).
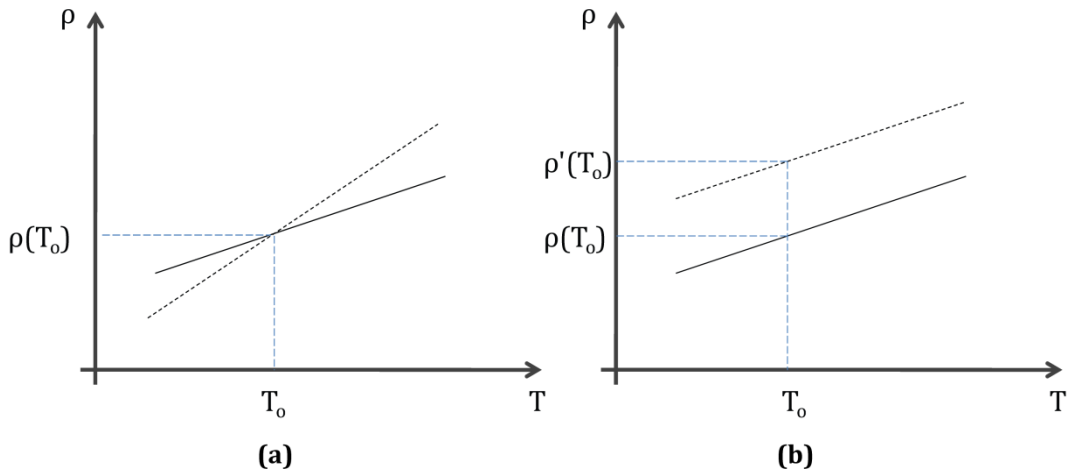
Figure 24: Multiplication procedure of (a) thermal expansion coefficient and (b) density

Density and thermal expansion coefficient data were entered to the simulations in two places. Firstly, they were included into thermal input data as $\rho(T)$. The procedure of manipulation of the function was discussed above. Secondly; α and ρ were entered to the mechanical input data indirectly in terms of dilatation;

$$\Delta = \varepsilon^{th} + \varepsilon^{tr}_{1\rightarrow2}$$

(4.9)

where ε^{th} and ε^{tr} are thermal and transformation strains, respectively. Here, thermal and transformation strains were determined by density and thermal expansion coefficient according to the equations:

$$\varepsilon^{th}(T) = \alpha\left(T - T_o\right), \qquad \varepsilon_{1\rightarrow2}^{tr} = \left(\frac{\rho_1(T_o)}{\rho_2(T_o)}\right)^{1/3} - 1$$

(4.10)

Therefore, dilatation was altered when one of the parameters α or ρ were changed, in order to avoid data mismatch.

Specific heat and latent heat of transformation

Similar to ρ-α couple, in the case of specific heat (c) and transformation enthalpy (ΔH_{tr}) two problems should be considered. Firstly; specific heat (c) and transformation enthalpy (ΔH_{tr}) are correlated properties. ΔH_{tr} is determined by enthalpy of formation of each phase (H_i) according to the equation;

$$\Delta H_{1\rightarrow2}^{tr}(T) = H_2(T) - H_1(T)$$

(4.11)

whereas H_i is related to specific heat;

$$H_i(T) = H_i(T_o) + \int_{T_o}^{T} c_i(T)dT$$

(4.12)

As a result; any modification in specific heat causes an inevitable change in transformation enthalpy. Also, ΔH_{tr} should be changed carefully to avoid any deviation in c. Second problem comes from the restrictions of the software. As an input, SYSWELD® requires enthalpy of formation of each phase. Therefore, ΔH_{tr} and c should be modified indirectly by changing $H_i(T)$.

While considering density, it was possible to make direct modifications in density curve; in this case however, the situation is much harder. First of all; both ΔH_{tr} and c should be changed indirectly. Moreover, it is impossible to use averaged enthalpies of the phases in the input of the simulations; otherwise it would be a thermodynamic mistake. Since, this data need to be temperature dependent, a different multiplication procedure should be applied to transformation enthalpy.

The remedies of these problems are as following:

o   Although, ΔH_{tr} was taken as temperature dependent in the simulation input data, its integral average over temperature are used in dimensionless numbers. This definition is meaningful since integral average transformation enthalpy ($\Delta \bar{H}_{tr}$) gives average dissipated heat during phase transformation.

o   Transformation enthalpy was modified by shifting the curve of enthalpy of formation of martensite ($H_m(T)$). The slope of this curve was not changed in order to keep specific heat of martensite constant. When ΔH_{tr} needed to be multiplied by a factor "m_1", $H_m(T)$ is modified such that integral average of resultant ΔH_{tr} is equal to "$m_1 \Delta \bar{H}_{tr}$".

o   Specific heat of austenite and martensite was modified by changing the slopes of $H_a(T)$ and $H_m(T)$ curves. When $H_i(T)$ was considered as a polynomial;

$$H_i(T) = A_3 T^3 + A_2 T^2 + A_1 T^1 + A_o \tag{4.13}$$

Slope was changed by multiplying A_1, A_2, and A_3 with a factor "C_1". In order to keep $\Delta \bar{H}_{tr}$ constant, another constant "m_2" was added to the polynomial. As a result, a new polynomial such as;

$$H_i(T) = C_1(A_3 T^3 + A_2 T^2 + A_1 T^1) + A_o + m_2 \tag{4.14}$$

was obtained which has a slope of "$m_2 c$" whereas, $\Delta \bar{H}_{tr}$ kept constant.

Yield strength, hardening exponent and coefficient

In the simulations, Ramberg-Osgood (R-O) flow rule;

$$\sigma = K \varepsilon^n \tag{4.15}$$

was used. Yield strength of the material was taken as the stress value corresponding to the 0.00005 strain ($\sigma_{0.005\%}^{R-O}$). Main disadvantage of R-O is that, yield strength (σ) is embedded in hardening exponent (n) and coefficient (K). That is to say, any change in K and n effects yield strength. As a remedy following procedure was used.

(1) Ramberg-Osgood coefficient or exponent was manipulated and stress strain data was gathered.

(2) Ludwig exponent and coefficient corresponding to the flow data were determined via Equation. 4.16. Yield strength was taken as $\sigma_{0.005\%}^{R-O}$.and was not manipulated.

$$\sigma = \sigma^o + K\varepsilon^n \qquad (4.16)$$

With the help of this procedure, only stress strain curve after yield strength was manipulated and yield strength kept constant.

CHAPTER 5

RESULTS AND DISCUSSION

5.1. Optimization of the FE model

In order to optimize finite element model, three parameters – number of elements, hardening rule and element type - were investigated. Test cylinder has diameter of 10mm and length of 200mm. Boundary and initial conditions are similar to those given in Section 3.2. Surface heat transfer coefficient is $1200W/m^2°C$. Three meshes with varying number of elements were generated. With the aid of gradient mesh, finer elements were generated near quench corner (Figure 25). As it is presented in Table 14, for each of the meshes three different hardening rules and element types were used. In the table, Q4 and Q8 refer four and eight node quadrilateral elements respectively. Integ2 denotes reduced integration and x3 refers that the simulations were performed with three hardening rules (isotropic, kinematic and combined hardening. Similar designations are also used in the subsequent tables.

Table 14: FEM parameters that are analyzed

		Mesh (# of elements in radial direction x # of elements in longitudinal direction)		
		5 x 50	10 x 100	20 x 200
Element Parameter	Q4	x 3*	x 3	x 3
	Q8 – Integ 2	x 3	x 3	x 3

* evaluated in combination with different hardening rules (kinematic, isotropic and combined 0.5)

Figure 25: Gradient mesh

Results of the simulations are presented in Figure 26. First observation is that having the same mesh and element type, there is a measureable difference between the dimensional changes in correlation with different hardening rules. This variation can be a useful tool to calibrate material model by employing coordinate measurements. Regardless of other parameters, dimensional changes that are obtained by isotropic hardening rule do not significantly altered by the mesh. However, kinematic hardening results have significant oscillation.

Figure 26: Simulation results for different meshes listed in Table 14.

Table 15: Simulations that were made in order to check stability of kinematic hardening model

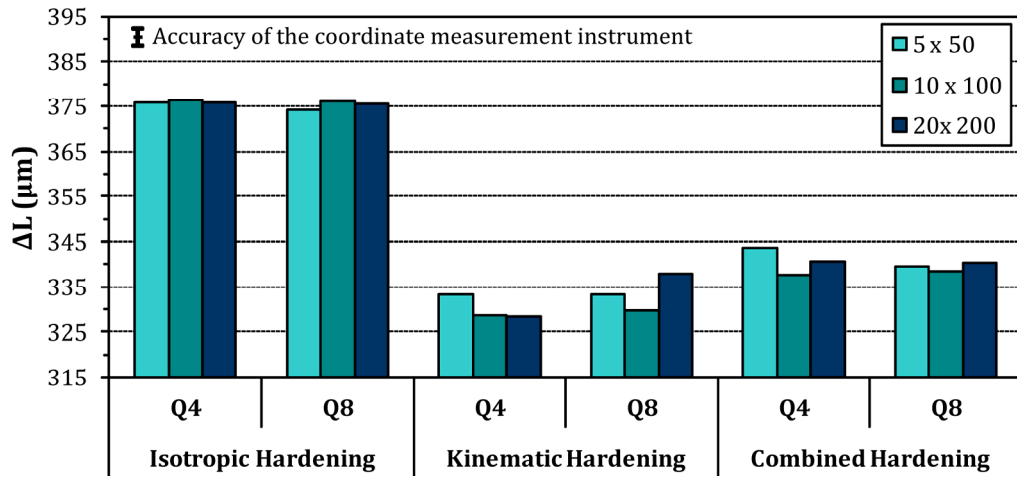|		Mesh (# of elements in radial direction x # of elements in longitidunal direction)				
		5 x 20	**10 x 40**	**20 x 80**	**40x160**	**80x320**
Element Parameter	**Q4**	x 2*	x 2	x 2	x 2	x 2
	Q8 – Integ 2	x 2	x 2	x 2	x 2	x 2

evaluated in combination with kinematic and combined (0.01 isotropic) hardening rules

These results cast doubt on the stability of kinematic hardening algorithm implemented in SYSWELD®. To be sure about the stability of the algorithm, simulations presented in Table 15 were performed. In addition to kinematic hardening, also models obeying combined hardening rule with 0.01% isotropic hardening were used to ensure stability and accuracy of both hardening models. In these simulations a cylinder with dimensions of 10 mm diameter and 40 mm length were modeled. Initial state, boundary conditions and cooling parameters were taken similar to the previous simulations. Here uniform meshes with aspect ratio 1 were used. Finer meshes are obtained by mesh refinement. Results indicate that dimensional changes are rather close which shows kinematic hardening model of SYSWELD® is as stable as combined

hardening when finer mesh and elements with aspect ratio close to 1 are used. That is to say, the quality of the kinematic hardening model of SYSWELD® is mesh dependent in the case of course meshes.
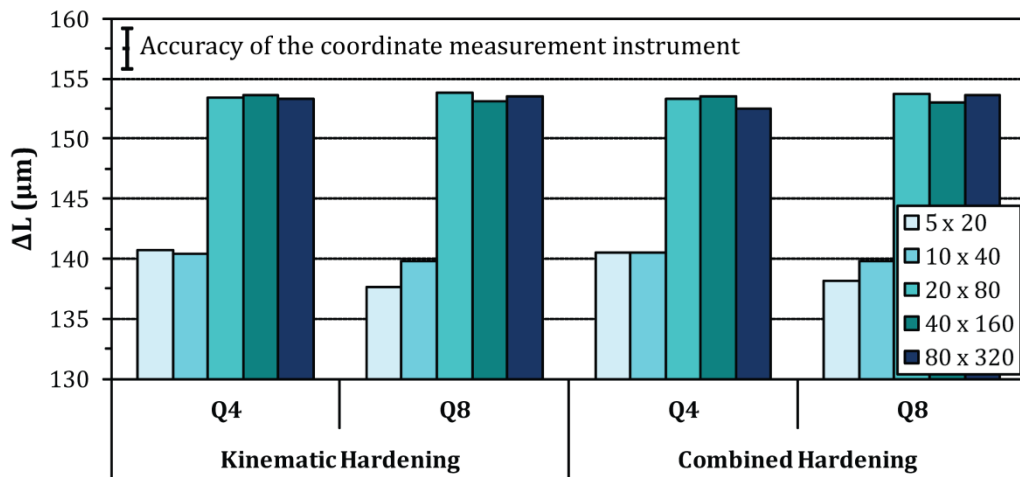
Figure 27: Stability check for kinematic hardening model in SYSWELD®. Kinematic hardening results are compared with combined hardening with 99% kinematic hardening

Another factor that might affect stability of the simulations is aspect ratio (AR) of the elements. For the purpose of checking the effect of AR, simulations with different aspect ratio and minimum element edge length (MEEL) combinations, which are shown in Table 16 , were done. In these simulations; geometry, initial and boundary conditions were the same with previous ones.

Table 16: Simulations that were done to check the effect of AR

				Aspect ratio			
		0.25	0.33	0.50	0.66	0.75	1.00
Minimum edge length (mm)	1.00	x3*	x3	x3	x3	x3	x3
	0.50	x3	x3	x3	x3	x3	x3
	0.25	x3	x3	x3	x3	x3	x3
	0.125	x3	x3	x3	x3	x3	x3

* evaluated in combination with different hardening rules (kinematic, isotropic and combined 0.5)

In Figure 28 results of the simulations that were listed in Table 16 are presented. Knowing that the quality of Gauss integration is highest when AR=1 and MEEL=0.125mm, reliable AR and MEEL combinations are marked with "+". Results indicate that for each element size there is a certain minimum aspect ratio to have accurate results.

In Figure 29, simulated aspect ratio and element size combinations are shown by small diamonds at the coordinates (AR,MEEL). Drawn lines show minimum conditions that need to be attained to have acceptable stability and accuracy for each hardening rule. When aspect ratio goes to zero, minimum element edge length should go to zero. Therefore, lines are drawn such that they pass through (0,0). AR-MEEL curves are approximated to straight lines in order to simplify evaluation. Here it should also be noted that there is a range that the accuracy and stability of simulations are not clarified. This range is the area between the drawn lines and the closest (AR, MEEL) point. In Figure 29a this range is illustrated for Q4-Isotropic hardening with pink color. Real behavior of AR-MEEL curves can be revealed by performing more simulations, but this is out of the scope of this study. Here, the main aim is to find an AR-MEEL region to attain reliable simulation results and current results are enough to attain required information.
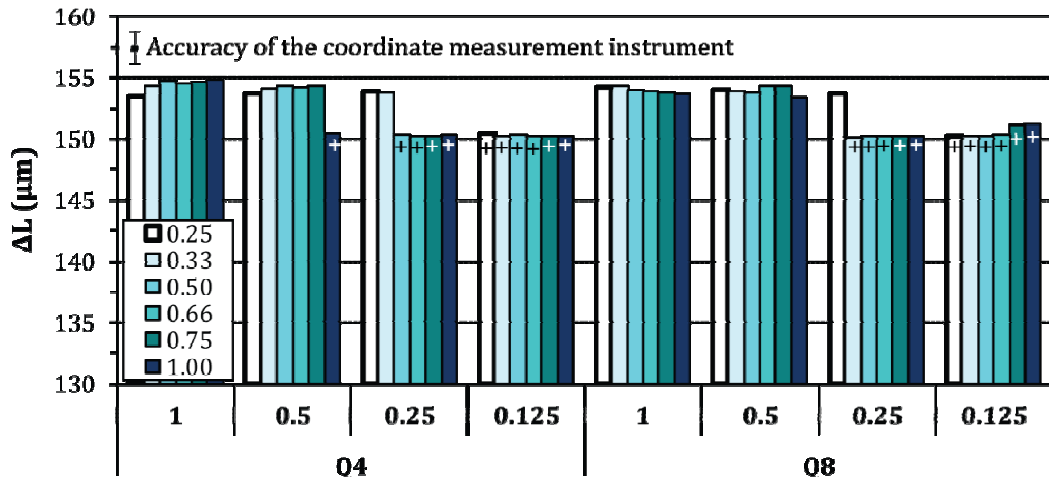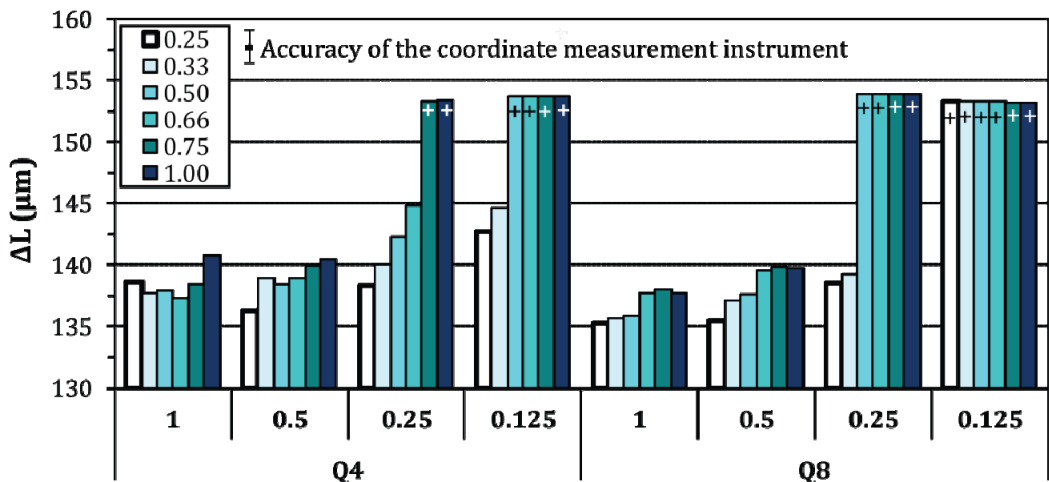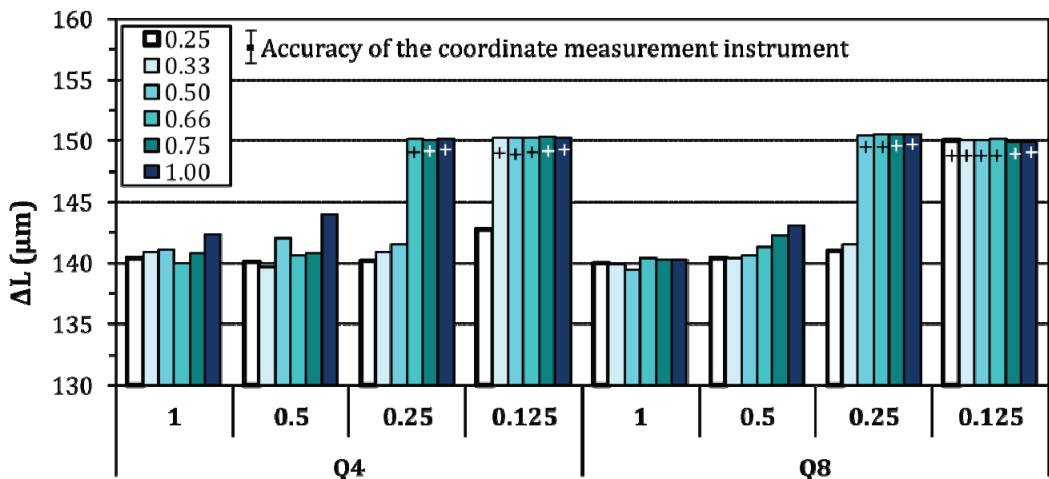
Figure 28: Simulation results for different aspect ratio - minimum element size combinations Here "+" shows reliable AR-MEEL combinations.

Figure 29: Simulated aspect ratio and min element size combinations for (a) Q4 and (b) Q8 (reduced integration)

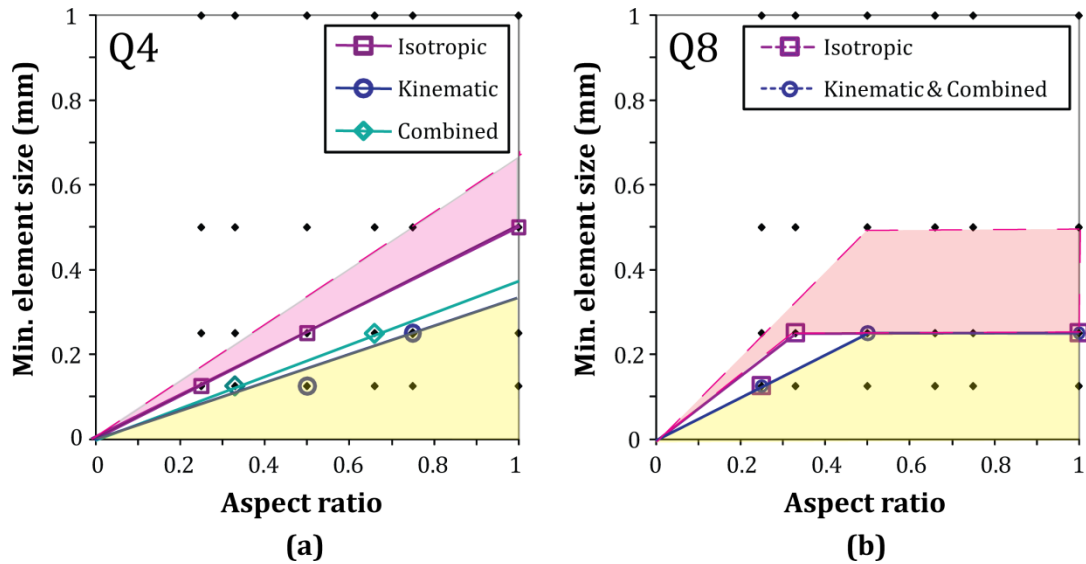In the case of Q4-isotropic hardening; it is possible to use a wide range of AR-MEEL combination. On the other hand, when kinematic hardening rule is used, element edge length should be considerably small at low AR's. Combined hardening line is in between isotropic and kinematic hardening ones. From these results it can be concluded that yellow triangle is a safe region. The situation in Q8 is quite different from Q4. Kinematic and combined hardening have the same results, whereas; isotropic hardening has a slightly wider region. However, with these results, it is not possible to tell the behavior in detail, since unknown region (pink) is quite large. But still it is possible to conclude that, when Q8 is used there is a critical MEEL above which simulation results are not reliable. This critical MEEL is between 0.25 and 0.5mm. In this study, for the sake of safety, MEEL and AR were arranged such that meshes remain in the yellow region.

To add up; all of the simulations relive that SYSWELD® produces reliable results as long as correct mesh is used. Oscillation of results in Figure 26 might be owed to the sensitivity of the material law to the changes in the positions of the nodes and the aspect ratios of the elements, which cannot be avoided with gradient meshes. It should be noted that those meshes in Figure 26 were not the results of mesh refinement. Those were different gradient meshes with increasing number of elements. Thus, this had raised the necessity to use a mesh which produces stable results. This can be achieved

by successive refinement of the gradient mesh. With the help of the simulation results discussed, gradient mesh having aspect ratio between 0.5-0.83 were chosen. For further investigations number of elements was chosen by performing simulations presented in Table 17. Results of these simulations (Figure 30) showed that, mesh with 20 x 400 elements and element type 8-node quadrilateral elements (reduced integration) gives stable and safe results which can be used in succeeding simulations.

Table 17: FEM parameters that are analyzed after stability check of kinematic hardening model

,	Mesh (# of elements in radial direction x # of elements in longitidunal direction)		
		10 x 200	20 x 400	400 x 800
Element Parameter	Q4	x 3*	x 3	x 3
	Q8 – Integ 2	x 3	x 3	x 3

evaluated in combination with different hardening rules (kinematic, isotropic and combined 0.5)
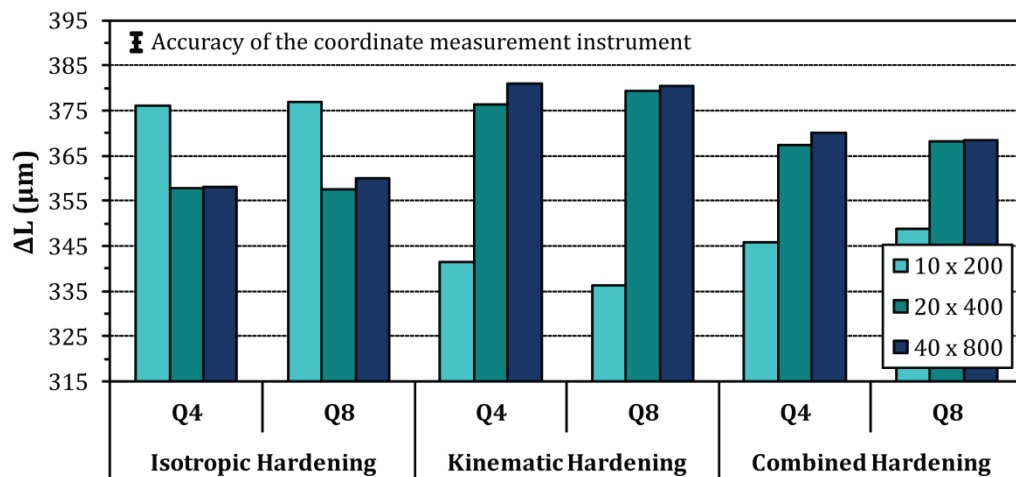

Figure 30 Simulation results for the meshes given in Table 17.

5.2. Experimental results

Distortion was investigated in terms of two aspects which were elaborated with respect to the position of the cylinders in the bar:

- Dimensional changes (length, diameter and volume change),

- Shape changes (bending).

5.2.1. Dimensional change

5.2.1.1. Influence of position

Relative dimensional changes of the samples which are representing different positions of the cross section of the initial billet are shown in Figure 31; namely, length ($\Delta L/L_o$), diameter ($\Delta D/D_o$), and volume change ($\Delta V/3V_o$). It is clearly seen that dimensional changes deviate significantly with machining positions. It might be owed to the inhomogeneous distribution of martensite start temperature (M_s) due to inhomogeneous distribution of Cr and C (Figure 7).

For instance, the fraction of alloying elements for the specimens machined from the center of the billet (position 5) have less alloying elements in the parent phase due to core segregation, which eventually results in a higher average M_s. Consequently, a larger volume change occurs since they have less retained austenite at the room temperature. However, it is not possible to make such deductions for other machining positions 1-4 by referring to Figure 31.

Other reasons for the variation of the dimensional changes with respect to machining position might be the spatially asymmetric variation of material properties and the anisotropy in the transformation strain [15]. However, the justification of these assumptions requires additional dilatometer and mechanical tests.
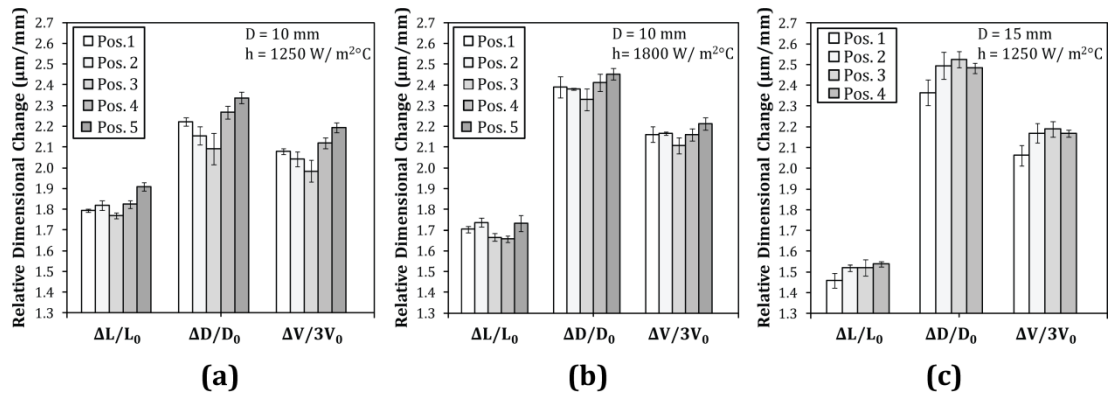
Figure 31: Relative dimensional changes of cylinder samples when (a) D=10mm, h=1250W/m2 K, (b) D=10mm, h=1800W/m2 K, (c) D=15mm, h=1250W/m2 K

5.2.1.2. Influence of Biot number

Summary of relative dimensional changes with respect to Biot number is presented in Figure 32. Maximum standard deviation is 0.1µm/mm. Therefore, standard deviation bars are not visible in the current scale. Diameters of the specimens are given in the top of the bars.

Gas quenching (GQ) results show that relative length change ($\Delta L/L_o$) decreases with increasing Biot number whereas; relative diameter change ($\Delta D/D_o$) increases with Biot number. In regards to relative volume change ($\Delta V/V_o$) results indicate that Biot number does not have significant effect on volume change. This is anticipated since Biot number does not have any influence on the fraction of martensite and transformation strains.

When salt bath quenching results are considered, the situation is quite different. It is observed that $\Delta V/V_o$ is considerably low in this case. This might be because of the bainite formation during quenching of 230℃ bath. It is also seen that volume change in 25mm diameter specimen is lower than that of 20mm diameter specimen. This might be attributed to the lower cooling rate and hence higher bainite fraction. Due to these reasons, it is not safe to consider these results in explaining the dimensional change behavior.
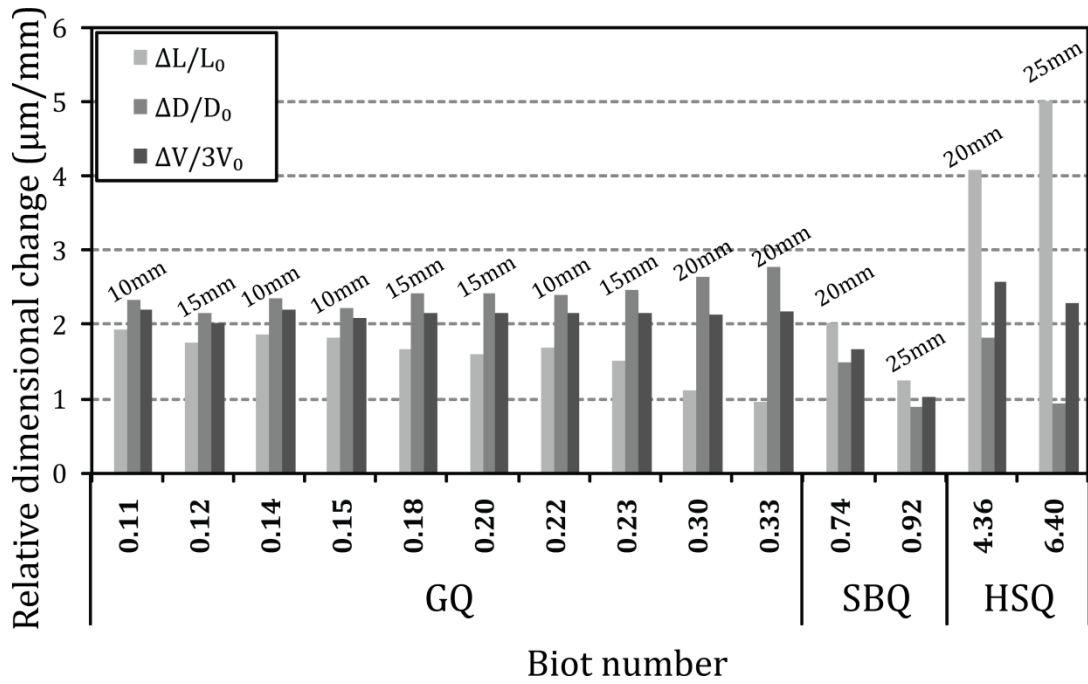
Figure 32: Influence of Biot number on relative dimensional changes. Diameter of the specimens are given on the figure. Standard deviation bars are not visible in the current scale.

In the case of high speed quenching experiments (HQ), volume change is slightly higher than the results of gas quenching experiments. This might be attributed to the differences in undesirable differences in austenitization time. However, these differences do not seem to be detrimental since volume change has not affected significantly. Again difference in $\Delta V/V_o$ of 20mm and 25mm might be due to the austenitization time. This is because furnace holding time of these specimens was equal. Less carbide dissolution and hence higher martensite start temperature is expected in 25mm diameter specimen. This results in lower martensite fraction in 25mm diameter specimen. When results of HSQ are compared to GQ it is observed that $\Delta L/L_o$ is considerably higher and $\Delta D/D_o$ is considerably lower. Moreover, $\Delta L/L_o$ increases and $\Delta D/D_o$ decreases at higher Biot numbers. This shows that trend in low Biot number changes at higher Biot numbers. In low Biot number it was observed that $\Delta L/L_o$ decreases and $\Delta D/D_o$ increases. At higher Biot number, these trends reversal, namely; length change increases and diameter change decreases with increasing Biot numbers.

5.2.2. Shape change (Bending)

5.2.2.1. Bending amplitude

In Figure 33 bending magnitudes ($|\mathbf{b}|$) of the cylinders at different Biot numbers are presented. Also diameters of the specimens are given in the figure. These results indicate that there is no clear dependency of $|\mathbf{b}|$ on diameter due to large scatter in the experimental data. In regards to the dependency of $|\mathbf{b}|$ to the heat transfer coefficient for 20 mm diameter cylinders, the mean magnitude of the bending vector seems to decrease slightly until a certain Biot number (Bi≈0.20) and then increase with increasing heat transfer coefficient. However, it is speculative to generalize this behaviour due to the large scatter in the results. Also, small values of bending vectors at Bi=0.74 and 0.92 might be attributed to the excessive bainite in the structure.
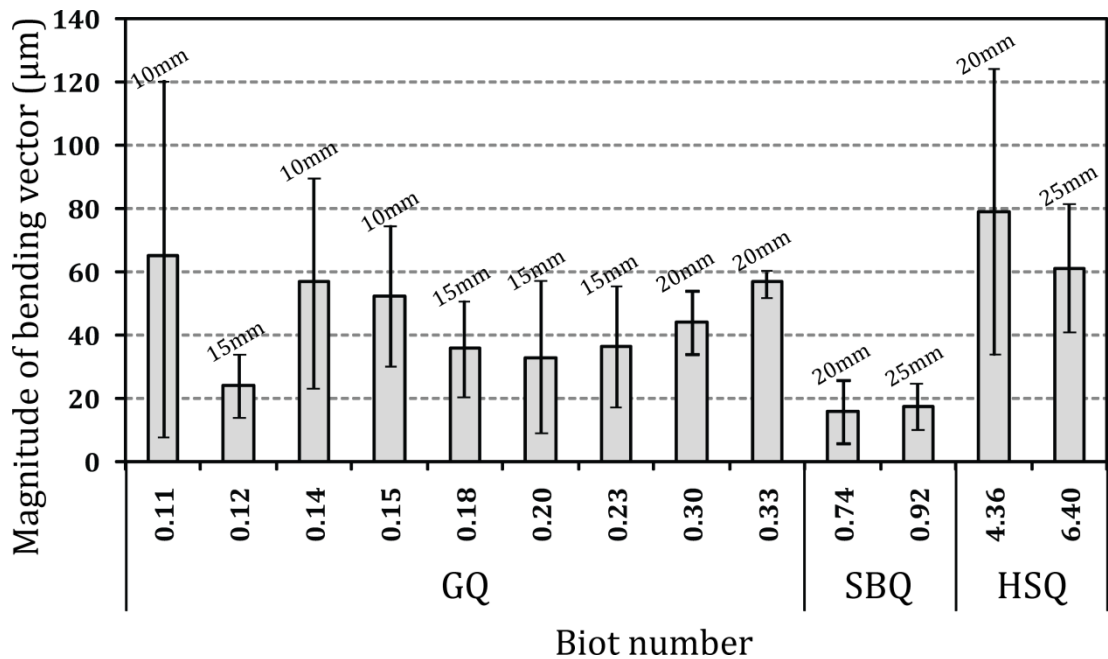
Figure 33: Influence of Biot number on bending magnitude

5.2.2.2. Bending orientation

Summary of the bending directions from gas-nozzle field quenching (GQ) experiments is presented on Figure 34(b-c). In the figure, the magnitudes were magnified (x125) in order to improve visibility. These results show that, bending directions do not exhibit a distinct correlation with respect to machining position.
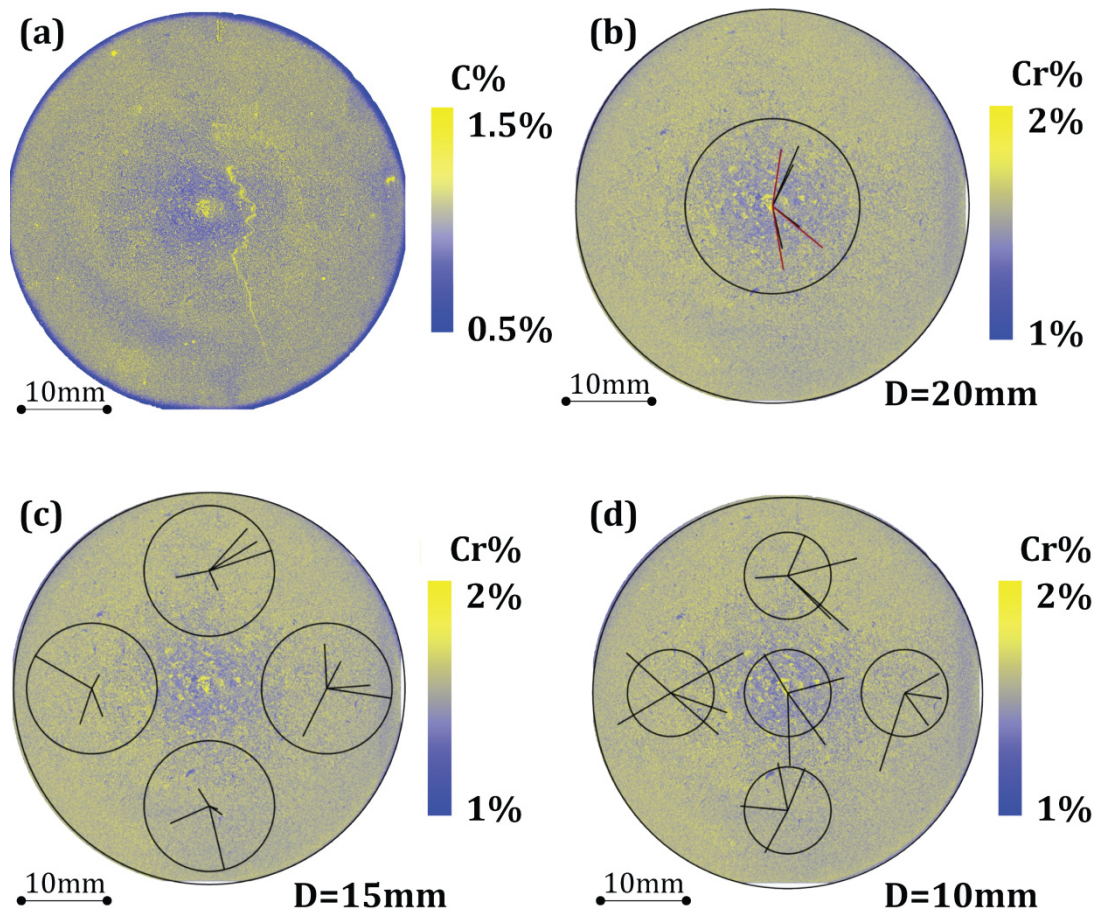
Figure 34: (a) C concentration in the cross-section of the 45mm diameter billet, (b-d) Directions and magnitudes of bending vectors. (Bending magnitudes are magnified by x125)
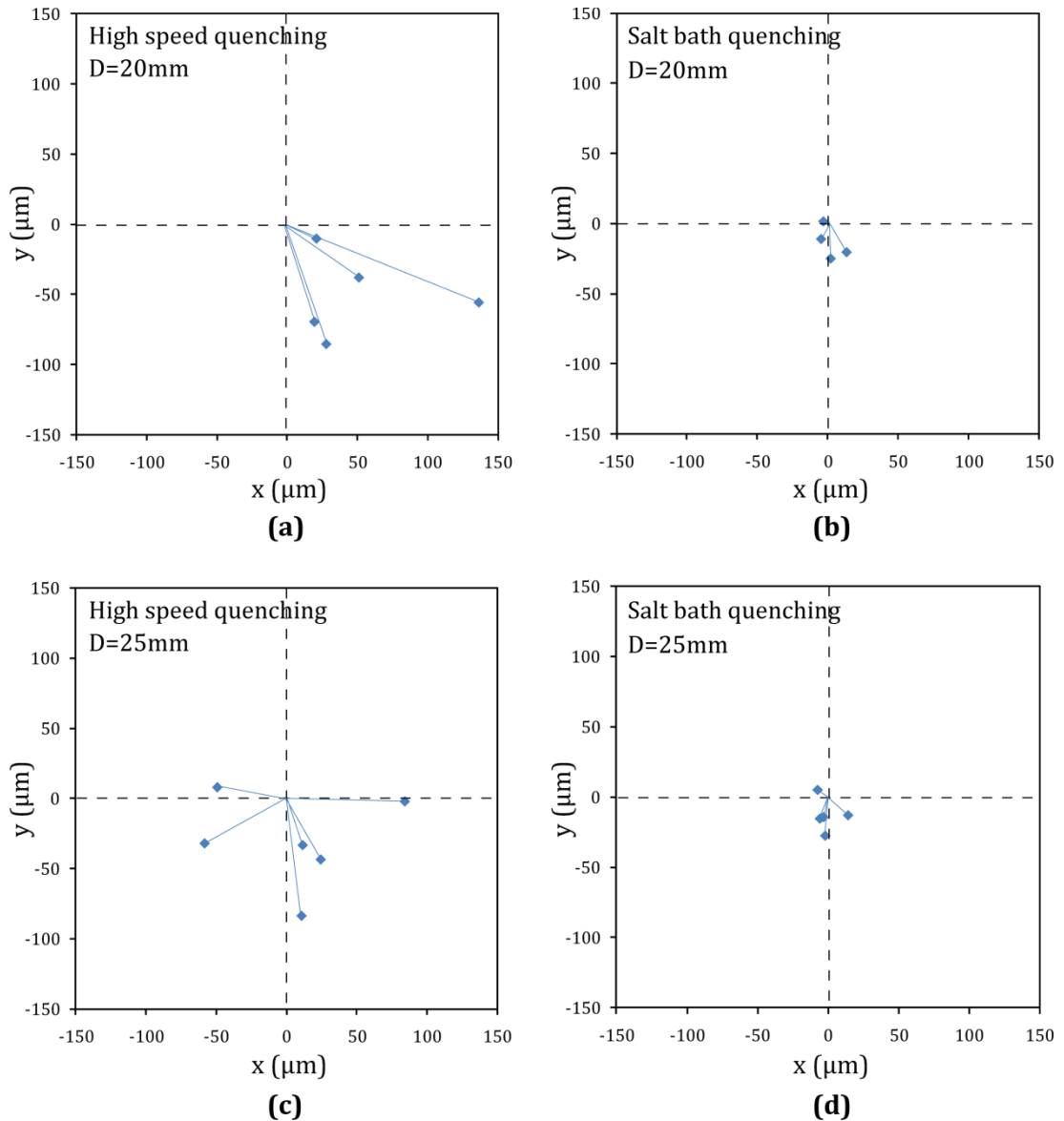
Figure 35: Bending directions and magnitudes of 20 and 25mm diameter cylinders after salt bath and high speed quenching

Bending results of HSQ and SBQ experiments are contradictory to those of GQ. From Figure 35 one can see that at both HSQ and SBQ experiments, there is a tendency towards a particular direction. Bending directions are mainly spread in third and fourth quadrants. In regards to the bending directions of HSQ experiments; **b** of 25mm diameter cylinder, spread over a wide range, whereas; **b** of 20mm diameter cylinders confined to a range of only 45°. On the other hand, SBQ results are consistent in themselves. For both 20 and 25mm diameter cylinders, **b** is confined to a small range

and they tend towards –y direction. Bending vectors of HSQ experiments seem to have a similar trend but it is speculative to make such deduction due to the large scatter in the results.

5.2.2.3. Elaboration of the bending results

During quenching, cylinders are bended due to inhomogeneities and asymmetries in the material and process. If bending happens due to material itself, when homogeneous cooling is attained, similar bending behavior is expected for the same material, regardless of the process. In the case of consideration, bending behavior significantly differ with the process. These discrepancies cast doubt about the reliability of the processes:

As it is mentioned above, the bending directions of cylinders that are quenched with gas nozzle field do not exhibit a distinct correlation with respect to machining position. On the contrary, HSQ and SBQ results show that there is a tendency in the bending behavior. In order to clarify whether the reason for random behavior of **b** in GQ experiments is process or not, a simple strategy was followed:

In each GQ experiment, there is an angle "φ" between cylinder and nozzle field axes (Figure 36a). This angle is random and depends on the screw of each specimen. With the help of φ, angle between bending vector and nozzle field axes (θ) can be determined (Figure 36b). θ is a good measure to investigate the effect of nozzle field on bending behavior. If θ is constant, it can be concluded that the nozzle field is the factor that determined the bending behavior.
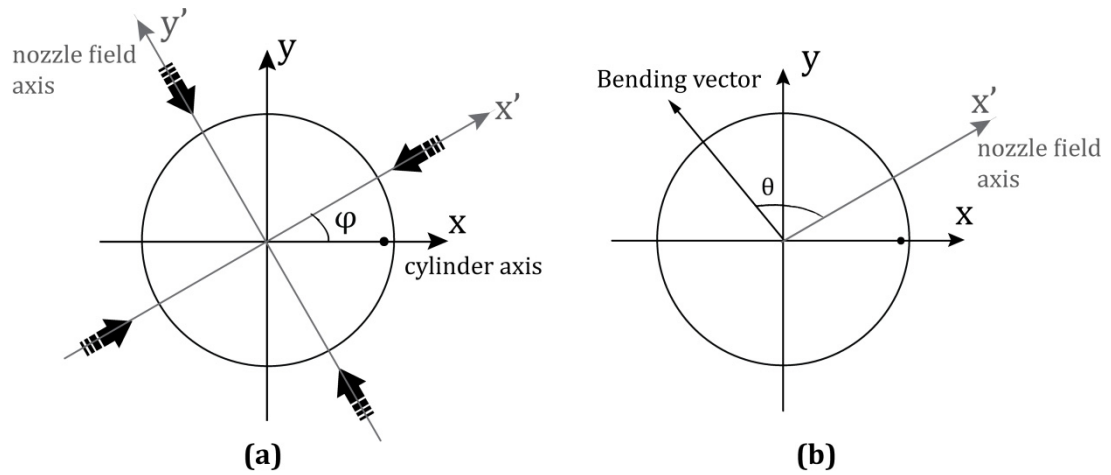
Figure 36: (a) Nozzle field and cylinder axis (b) Angle between nozzle field axis and the bending vector

After each quenching experiment, positions of the nozzle arrays was noted with respect to the cylinder axis (Section 3.1.3.2.), therefore; φ and θ are known. Gas quenching results indicate that, θ is almost constant and it deviates at most 10 degrees. This error bound is most probably due to measurement and marking errors. Therefore, it can be concluded that current bending results owed to the asymmetries in the gas quenching system. Moreover, when total bending ($\mathbf{b}_t$) is considered as the summation of bending due to material ($\mathbf{b}_m$) and bending due to process asymmetry ($\mathbf{b}_{as}$), one can say that bending due to materials inherent effects is too small that it has a negligible effect on total bending and it is lost in 10° error bound. Therefore, it is not possible to determine the magnitude and direction of the material effect from current results.

Since, gas quenching experiments has not provided any information, HSQ and SBQ results are remaining options to reveal the bending behavior of 100Cr6 cylinders. However, there are serious discrepancies between the results of two processes, namely magnitudes and directions of the bending vectors. Amongst these processes, HSQ is prone to error due to the movement and rotation of the specimen during quenching. The success of the quenching depends on the screwing force which might change even with user. Thus, the scatter in the results is most probably due to fastening problems. In spite of this factor, bending directions show a tendency.

In the case of SBQ, there is a problem of excessive bainite. However, results clearly indicate that there is tendency in the bending directions. It is not possible to attribute this tendency to martensitic transformation and correlate bending magnitudes with other cases. But still, it is observed that microstructure affects bending behavior during phase transformations.

As a result; it can be concluded that,

(1) There is a correlation between microstructure and bending directions. This is visible in HSQ even when there is experimental drawbacks which increases scatter of the bending. Similarly, SBQ show that microstructure has an effect on bending behavior. Even if there is excessive bainite, this tendency is observed. These results are parallel to the findings of a similar study [15] on SAE 5120 (EN 20MnCr5) which revealed that the bending were correlated to the distribution of segregations

(2) Since there is a large scatter in the experimental data, it is not possible to correlate bending magnitudes with diameter. On the other hand, when they are compared to the SAE 5120 [15], bending magnitudes are considerably small.

Here it should be noted that in [15] shafts were not machined from the center of the billet. Therefore, it is not possible to make direct comparison between the results of [15] and this study. But still differences between the magnitudes of bending vectors of SAE52100 and SAE5120 might be attributed to the differences *in the type of the inclusions (mainly Fe_3C/Cr_3C for SAE 52100 and $MnS/Fe_3C/Cr_3C$ for SAE 5120) and initial/final microstructures* [140].

"In the former study on SAE 5120, the trend in the bending direction was explained by using the systematic distribution of anisotropic transformation strain (ATS) resulting from the development of banded microstructures during both heating and cooling. However, development of highly banded microstructure is not expected for SAE 52100 because of the following reasons:

- *The initial microstructure consists of more or less randomly distributed spheroidized carbides without ferrite/pearlite, bainite/martensite bands. Consequently, ATS during heating is expected to be considerably low with respect to SAE 5120 for which early transformation of pearlite or bainite which results in rod-like growth of austenite.*

- *The final microstructure of SAE 52100 after quenching is mainly martensite with some retained austenite and negligible amount of bainite (at most 2%), whereas; the quenching results in a banded microstructure of bainite and martensite for SAE 5120. The ATS during quenching is also expected to be lower since the rod-like growth of bainite due to chemically banded microstructure is much likely than the rod-like growth of martensite.*

- *Chemical banding may not always result in strong microstructural banding. Low carbon steels with Mn are known to generate strongly banded microstructures [13]. At best of authors` knowledge, there is no such kind of report in the literature for high carbon steels with Cr as the main alloying element."* [140]

Due to aforementioned reasons, the origin of bending in SAE 52100 steels are expected to be different. The reason of the tendency might be owed to the variation in local hardenability along the crossection due to segregations. This causes differences in volume change along the crossection which might result in bending. Another reason for this bending behaviour might be asymmetric distribution of material properties in the cylinder. But justification of these assumptions requires additional dilatometer and mechanical tests.

5.2.3. Verification of the simulations

5.2.3.1. Dimensional Changes

In Figure 37 comparison of experimental and simulation results are presented. It can be seen that results of isotropic hardening model and experiments with 10 and 15mm diameter specimens are consistent. Since bainite was observed at Bi_a=0.125, dimensional changes are lower for that data point. Also 20mm diameter results are quite different from experiments. This might be because of the shift in M_s due to long heating times.

These results show that utilized model is successful enough in predicting dimensional changes during gas nozzle field quenching of SAE52100 steel.
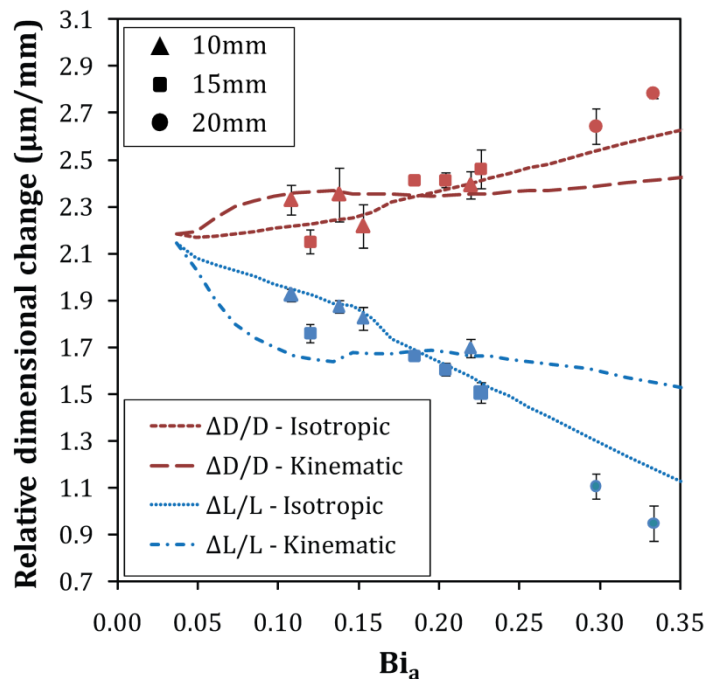

Figure 37: Comparison of experimental and simulation results. Here markers show experimental results and lines show simulation results for 10mm diameter cylinder

5.3. Sensitivity analysis

In this part of the study, long cylinders with dimensions D=10mm and L=200mm were used. Input data that is generated from material data set published in [11, 12] together with h=1200W/m²°C are denoted as reference state (x_j^o). Initial and boundary conditions that were given in Section 3.2. were used. In following chapters results of sensitivity analysis are presented.

5.3.1. General overview of the results

Results of the sensitivity analysis are summarized in Table 18 and Table 19. It can be seen that regardless of the hardening rule the most important material properties are;

- Martensite start temperature (M_s),

- Koistinen-Marburger equation constant (M_o),

- Transformation strain (ε^{tr}),

- Thermal expansion coefficients of austenite (α_a) and martensite (α_m),

- Yield strength of austenite (σ_a^o)

Table 18: Sensitivity rankings when isotropic hardening rule is used

		$\Delta L/L_o$	$\Delta D/D_o$	$\Delta V/V_o$			$\Delta L/L_o$	$\Delta D/D_o$	$\Delta V/V_o$
Thermal	h	-1	0	0	**Thermomechanical**	α_a	**-4**	**-3**	**-4**
	ρ_a	-1	1	0		α_m	**-5**	**-5**	**-5**
	ρ_m	1	0	0		E_a	-1	1	0
	c_a	2	-1	0		E_m	0	0	0
	c_m	0	0	0		ν_a	-1	0	0
	λ_a	1	-1	0		ν_m	0	0	0
	λ_m	0	0	0		K_a	1	0	0
Transformation	M_s	**4**	**4**	**4**		K_m	0	0	0
	M_o	**4**	**4**	**4**		n_a	0	0	0
	ΔH^{tr}	0	0	0		n_m	0	0	0
	ε^{tr}	**4**	**4**	**4**		$\sigma_a°$	2	-1	0
	κ	1	0	0		$\sigma_m°$	0	0	0

Table 19: Sensitivity rankings when kinematic hardening rule is used

		$\Delta L/L_o$	$\Delta D/D_o$	$\Delta V/V_o$			$\Delta L/L_o$	$\Delta D/D_o$	$\Delta V/V_o$
Thermal	h	0	0	0	**Thermomechanical**	α_a	**-4**	**-3**	**-4**
	ρ_a	-1	0	0		α_m	**-5**	**-5**	**-5**
	ρ_m	0	0	0		E_a	2	-1	0
	c_a	-1	1	0		E_m	-1	0	0
	c_m	1	0	0		ν_a	0	-1	0
	λ_a	1	-1	0		ν_m	1	0	0
	λ_m	0	0	0		K_a	-1	1	0
Transformation	M_s	**4**	**4**	**4**		K_m	0	0	0
	M_o	**4**	**4**	**4**		n_a	0	-1	0
	ΔH^{tr}	0	0	0		n_m	0	0	0
	ε^{tr}	**4**	**4**	**4**		$\sigma_a{}^\circ$	**-4**	2	0
	κ	0	0	0		$\sigma_m{}^\circ$	0	0	0

These results can be attributed to the reasons as following:

In the simulation of quenching, total strain rate ($\dot{\varepsilon}_{ij}$) were decomposed into five strain increments which were $\dot{\varepsilon}_{ij}^e$, $\dot{\varepsilon}_{ij}^p$, $\dot{\varepsilon}_{ij}^{th}$, $\dot{\varepsilon}_{ij}^{pt}$, $\dot{\varepsilon}_{ij}^{trip}$ (Eq. 2.11). Amongst these strains; the ones that are related with the volume change (ΔV) are dominant and these drastically affect dimensional changes. Sensitivity results are parallel to these facts, namely; material properties that are associated with $\dot{\varepsilon}_{ij}^{th}$ and $\dot{\varepsilon}_{ij}^{pt}$ (M_s, M_o, ε^{tr}, α_a, α_m) effect dimensional changes considerably. It should be noted that although transformation strains might be anisotropic due to several reasons [2, 13, 15, 16, 141], in the case of consideration these are not taken in to account. That is to say, both $\dot{\varepsilon}_{ij}^{th}$ and $\dot{\varepsilon}_{ij}^{pt}$ are assumed to be isotropic.

Other strain increment causing volume change is $\dot{\varepsilon}_{ij}^e$ (Eq. 2.11). However; its effect on total strain rate is very low compared to the other strains and, correspondingly, sensitivity of $\Delta V/V_o$ on elastic properties (E and υ) is almost zero. Elastic strains also have anisotropic components, the effects of which are seen on $\Delta D/D_o$ and $\Delta L/L_o$. Again sensitivities are quite low due to similar reason as before.

In equation 2.11, strain rates that bring in dimensional anisotropy to the system are $\dot{\varepsilon}_{ij}^{p}$ and $\dot{\varepsilon}_{ij}^{trip}$. Former, is due to stress state caused by thermal and transformation strains and it represents strains that are developed by classical plasticity (CP). Latter, on the other hand; represents strains coming from the plastification of austenite phase caused by newly formed martensite (transformation induced plasticity). $\dot{\varepsilon}_{ij}^{p}$ and $\dot{\varepsilon}_{ij}^{trip}$ are purely deviatoric strain rates and they do not cause any volume change. Accordingly; material properties related with $\dot{\varepsilon}_{ij}^{p}$ and $\dot{\varepsilon}_{ij}^{trip}$; $K, n, \sigma°$ and κ, do not have any effect on $\Delta V/V_{o}$ (Table 18 and Table 19). The main effect of these properties is on isotropy of the dimensional changes, which can be quantified by;

$$\Upsilon = \frac{\Delta L/L_0}{\Delta D/D_0} \tag{5.1}$$

Sensitivity results show that, $K, n, \sigma°$ and κ alter this ratio. However, magnitudes are very small compared to M_s, M_o, ε^{tr}, α_a, $\alpha_{m,}$, due to the fact that, plastic and trip strains are small compared to the transformation and thermal strain. On the other hand; the importance of these properties might depend on the Biot number. At higher Biot numbers; classical plasticity parameters and at lower Biot numbers; κ might gain importance.

In regards to the thermal properties (ρ, c, and λ); it is not straightforward to justify their effects on the system directly, since; all of the occurrences are triggered by temperature evolution during quenching. These properties affect temperature evolution and consequently progress of the physical occurrences (or kinetics). Results show that thermal properties influence the isotropy of dimensional changes (Table 18 and Table 19). This might be because of the change in the extent of plasticity due to the change in kinetics of the system. For instance, any change in temperature evolution alters thermal stress evolution which indirectly affects TRIP. Having "0" sensitivity in volume change might be owed to the fact that, final amount of martensite does not depend on the kinetics of the system.

In addition to aforementioned results, there are several points that are also observed;

o   There is no large difference between the results of kinematic and isotropic hardening rules. Only importance of mechanical properties slightly increase when kinematic hardening rule is used. This is probably due to the back stresses, but; it is not possible to reveal their effect on the system from current results.

o   Mechanical and thermal properties of austenite are more important than the properties of marteniste. This might be owed to the fact that, martensite does not exist in the initial stages of cooling when thermal stresses and classical plasticity are dominant and conduction is in its highest rate.

o   In contrast to the other transformation parameters, ΔH^{tr} has no significant effect on the simulation results. This might be because; in the case of consideration, heat dissipated during transformation has not significant effect in temperature evolution along the geometry. However; this might change with the geometric effects.

## 5.3.2. Effects of sensitive parameters on simulation results

The impact of sensitive parameters on the system can be characterized in terms of dilatation (Δ) and anisotropic dimensional changes (Υ; Eq. 5.1). In order to compare the effects of sensitive parameters on Δ, change in dilatation per 1% deviation of input parameters (x_o) is investigated (Eq. 5.2). Also, the effect of important input parameters on Υ is investigated with the help of changes in ε_{11} and ε_{22} per 1% deviation of input parameters (x_o) (Eq. 5.2). This is because, plasticity is the source of anisotropic dimensional changes (Υ)

$$\frac{\Delta_{x_o+\Delta x}-\Delta_{x_o-\Delta x}}{\left(\Delta x/x_o\right)\cdot 100}, \quad \frac{\left(\varepsilon_{11}\right)_{x_o+\Delta x}-\left(\varepsilon_{11}\right)_{x_o-\Delta x}}{\left(\Delta x/x_o\right)\cdot 100}, \quad \frac{\left(\varepsilon_{22}\right)_{x_o+\Delta x}-\left(\varepsilon_{22}\right)_{x_o-\Delta x}}{\left(\Delta x/x_o\right)\cdot 100} \qquad (5.2)$$

From Figure 38a-c. it can be seen that, deviation in M_s, M_o and ε^{tr} considerably alters volume change. This is expected since M_s and M_o determine the fraction of martensite and ε^{tr} determines dilatation due to austenite to martensite transformation. As a minor effect, these parameters alter isotropy of the dimensional changes (Υ) (Figure 38d-f). The effects of M_s and M_o on the isotropy (Υ) might be owed to the change in TRIP due to

the change in kinetics of the system and martensite fraction. ε^{tr}, on the other hand, alters isotropy by changing stress state that is originated from volume mismatch of austenite and martensite.

Sharp increase in M_s graphs are attributed to the time mismatch of martensite formation. When M_s is perturbed in positive direction (M_s), martensite forms earlier and so volume and strains change drastically. At the same instant of time, in negatively perturbed condition (M_s), only thermal strains are available. Therefore; direct subtraction of strains and dilatation gives peaks that are almost equal to the change in strain and dilatation at the instant when martensitic transformation starts (Figure 38 b and e) Therefore, it can be concluded that, these peaks are misleading, and they do not reveal the real differences between the two systems. On the other hand, from figures one can see that, effects of time mismatch are faded and almost disappear at later times. At 40th second dilatation change is slightly larger than ε^{tr} and M_s. In regards to plastic strain change, perturbation in M_s seems to bring larger anisotropy (Υ) compared to ε^{tr} and M_o. This might be because, M_s alters the duration of transformation more and consequently it affects the amount of TRIP more.
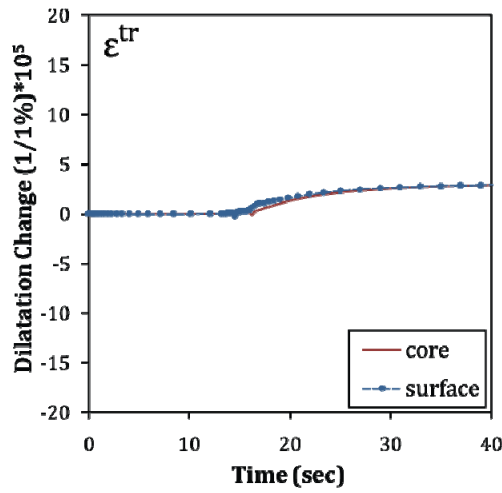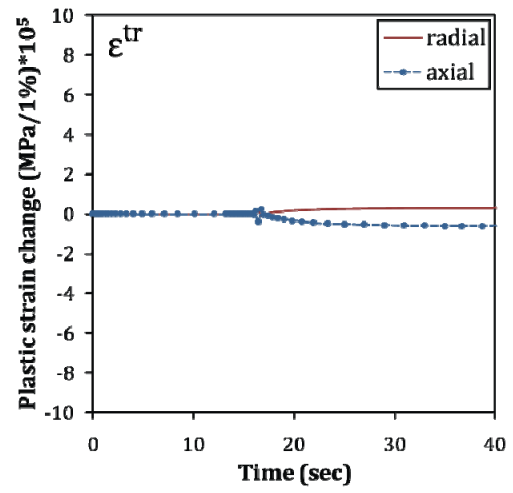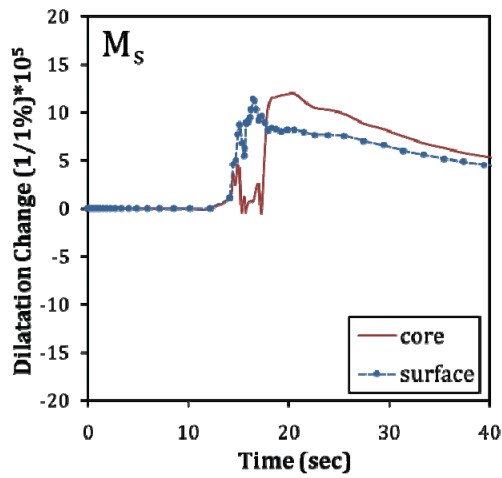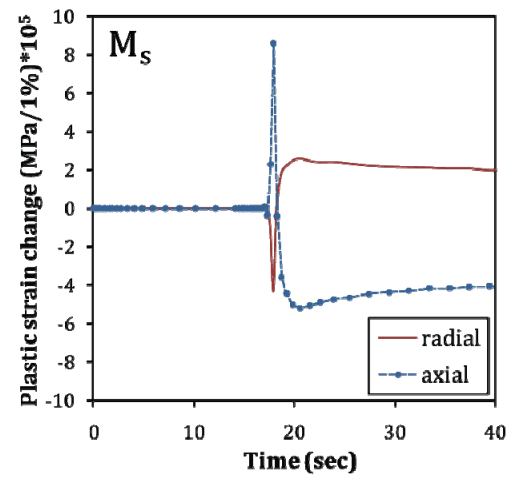
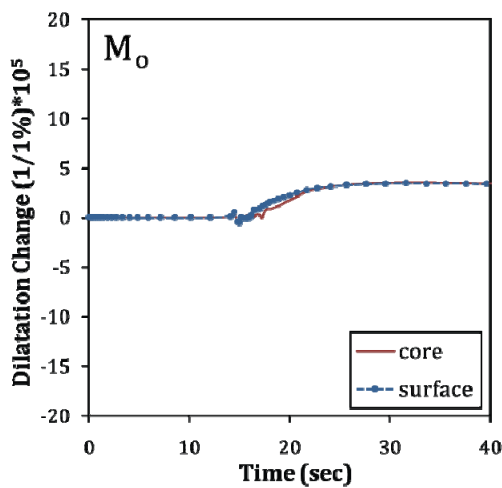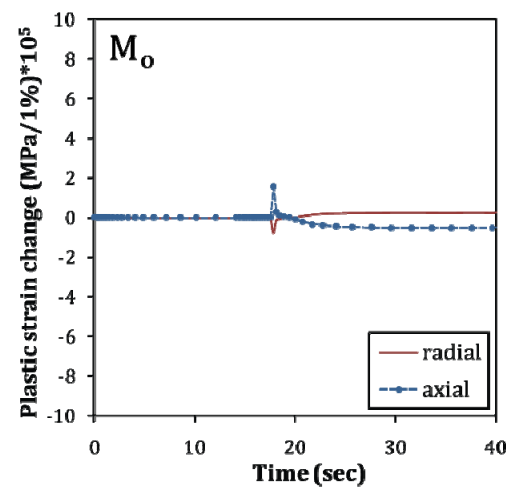**Figure 38: Effect of ε^{tr}, M_s, M_o on (a, b, c) dilatation change and (d, e, f) plastic strain at the core**

The effects of α_a and α_m on dilatation and plastic strains are presented in Figure 39a-b. When dilatation change is compared throughout the process, the impact of α_a and α_m on volume change is beyond the effects of transformation parameters. However, when final states of the systems are compared, it is seen that the effect of α_a on final volume change is similar to those of transformation parameters whereas; α_m has drastic effect on the final volume. These are expected results since effects of thermal expansion coefficients of the phases on ε_{ij}^{th} are correlated with their fraction according to the equation;

$$\varepsilon_{ij}^{th} = X_a \int_0^T \alpha_a dT + X_m \int_0^T \alpha_m dT \tag{5.3}$$

For instance; if M_s were lower, the effect of α_m on dilatation would be smaller due to the drop in martensite fraction.

In regards to the plastic strain change, the behavior is similar to the dilatation change, namely, the effects of thermal expansion coefficient of the phases on plastic strains are correlated with their fraction. On the case of α_a, thermal stresses increase drastically. Therefore, before M_s the extent of CP and after M_s the extents of both CP and TRIP changes considerably. Accordingly, isotropy of the dimensional changes (Υ) is significantly altered, which can also be seen from Table 18 and Table 19.

Perturbation of α_m causes deviations in two phenomena. When volume of martensite (V_m) at α_m^+ and α_m^- are compared, it is seen that V_m^+ is larger until room temperature. Therefore; transformation strain slightly increases when α_m increases. On the other hand, thermal stresses increase with an increase in α_m. Consequently, anisotropy of the system (Υ) is changed considerably (Figure 39d).
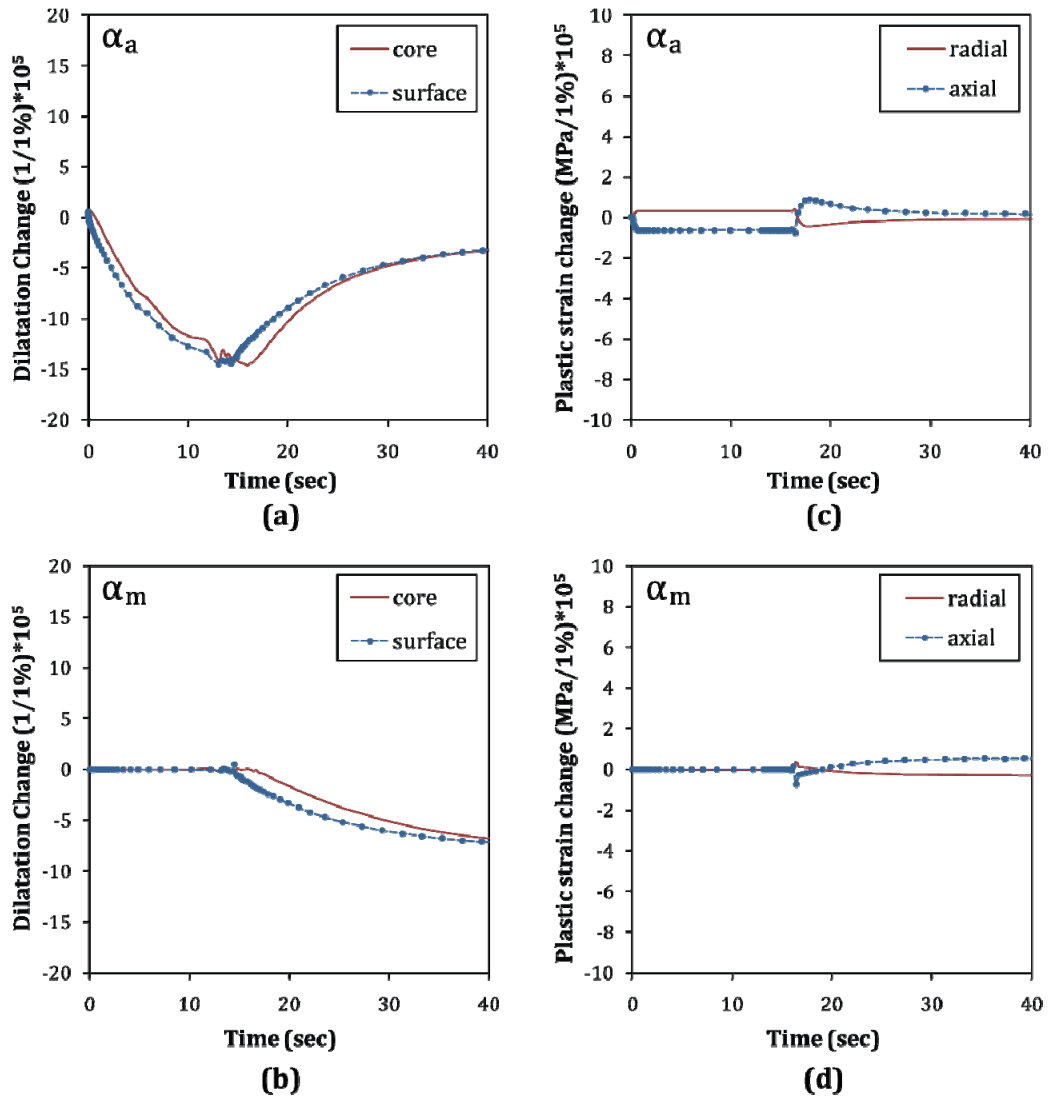
Figure 39: Effect of α_a and α_m on (a, b) dilatation change and (c, d) plastic strain at the core

Although it is not as significant as aforementioned parameters, yield strength of austenite brings in important deviations in dimensional changes. The major impact of σ_a^o is on the isotropy. It can be seen from Figure 40b that plastic strains change significantly with σ_a^o. On the other hand, σ_a^o does not have any effect on dilatation (Figure 40a).
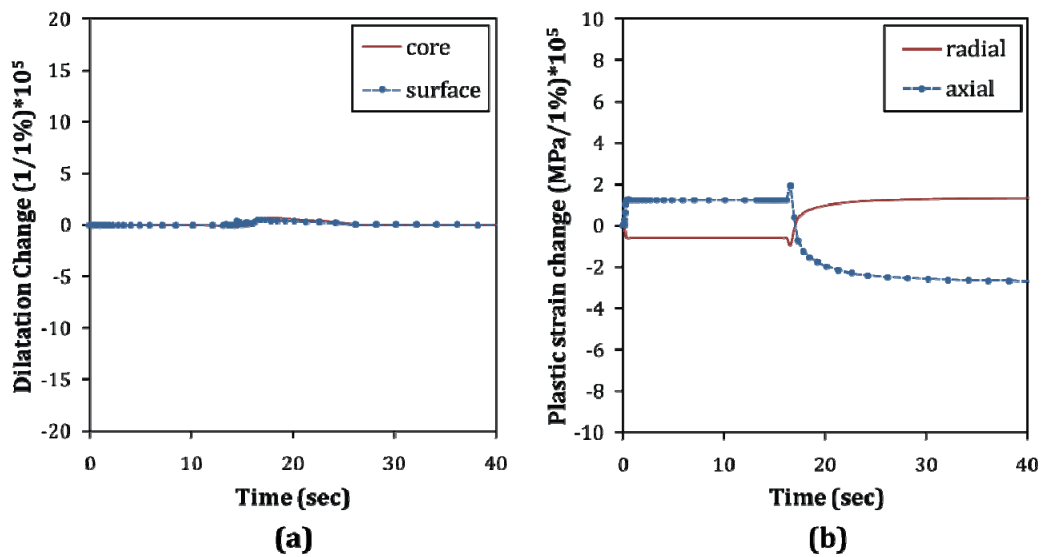

Figure 40: Effect of yield strength of austenite on (a) dilatation change and (b) plastic strain at the core

5.4. Dimensional analysis

In dimensional analysis part of the study, deviations in Biot number vs. relative dimensional change curves (*Bi vs. ΔY/Y_o*) were investigated with respect to the variations in dimensionless numbers that are in Ω_W. Here, what are meant by relative dimensional changes (or *ΔY/Y_o*) are; length change (*ΔL/L_o*), diameter change *(ΔD/D_o)* and volume change *(ΔV/V_o)*.

During this part of the study, temperature averaged material properties were used Therefore; effects of averaging of the material properties on simulation results should be discussed first.

5.4.1. The effect of averaging of the material properties

In Figure 41 comparison of *temperature dependent data set* (TDDS) and *averaged data set* (ADS) in terms of relative dimensional changes are presented.

In the case of isotropic hardening rule, TDDS and ADS curves have similar trends, but magnitudes of dimensional changes are significantly different (Figure 41a). Averaged data set can only be used up to $Bi_a \approx 0.2$ when tolerance is 0.1μm/mm. At higher Biot numbers, $\Delta L/L_o$ and $\Delta D/D_o$ that are obtained with ADS are less than half of the TDDS. Therefore, any investigation on averaged data set does not give quantitative result when $Bi_a > 0.2$ but it is valuable in understanding the behavior of the system qualitatively.

$\Delta L/L_o$ and $\Delta D/D_o$ curves of kinematic hardening are characterized by two peaks and a transition region. The major difference between the results of two data sets is in the first peak (P1). When TDDS is used, height of P1 is very low and it is restricted to a very small region. This peak is more visible in Figure 37. In the case of ADS, on the other hand, P1 is higher in magnitude and it is wider. This behavior might be attributed to the large differences in high temperature yield strengths. In ADS, σ_a^o at high temperatures is higher than that of TDDS which reduce the extent of classical plasticity at the first stage of quenching.

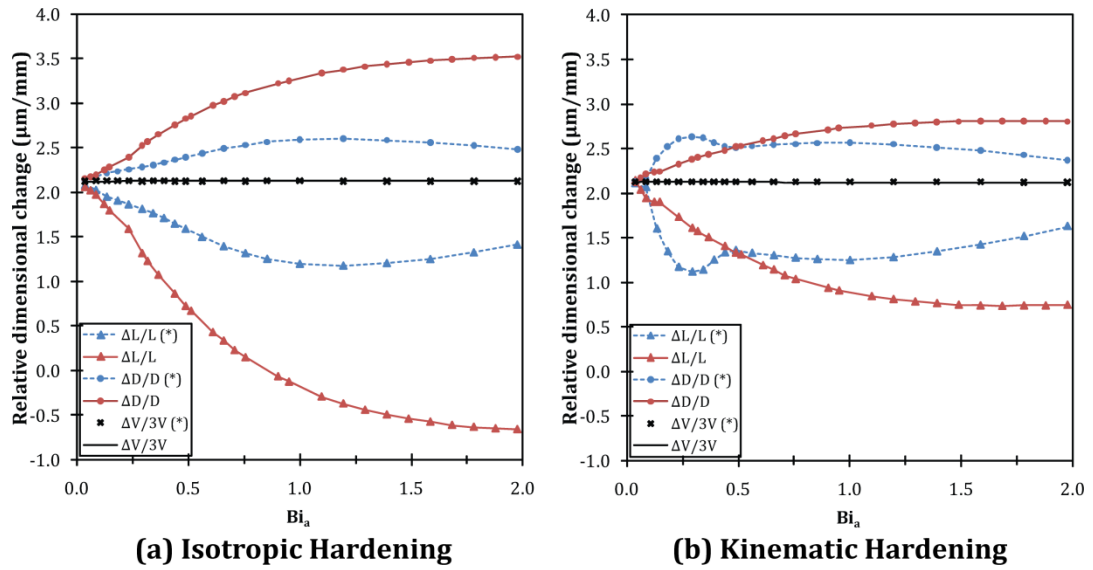(a) Isotropic Hardening   (b) Kinematic Hardening

Figure 41: Comparison of relative dimensional changes that are obtained by using temperature dependent and averaged (*) material data sets.

Curves of ADS and TDDS coincide at the transition region of TDDS curves ($Bi_a=Bi_a{}^{tr}$) and later on ($Bi_a>Bi_a{}^{tr}$) they differ. At $Bi_a>Bi_a{}^{tr}$, resultant dimensional changes of TDDS are larger than ADS, but the magnitude of the difference is low when it is compared to the case with isotropic hardening. Although, trend of relative dimensional change vs. Bi_a curves are similar for TDDS and ADS, differences are far above experimentally measurable range. Therefore; ADS curves can only be used for conceptual investigation of the system.

It should also be noted that ADS and TDDS yield same volumetric change at both hardening rules (Figure 41). This is expected, since material data related with volume change (α, M_s, M_o, ε^{tr}) are temperature independent.

5.4.2. Justification of the dimensionless number sets

In order to validate dimensionless number sets, input data was altered such that dimensionless numbers remain unchanged. Later, dimensionless behaviors of new set (Mod.) and standard set (Std.) are compared. These sets are listed in Table 20. Here it should be noted that this modification was utilized to verify both of the dimensionless number sets that are introduced in the mathematical framework section. That is to say, both sets remain constant after the modifications in material properties.

Some of the important output quantities for standard and modified input data are presented in Figure 42. For comparison, system responses were converted to dimensionless form:

- o Dimensionless temperature (θ) is defined as;

$$\theta = \frac{T - T_o}{T_a - T_o} \qquad (5.4)$$

where T, T_o and T_a are instantaneous, ambient and austenitization temperature, respectively.

- o Dimensionless time (τ) is defined as;

$$\tau = \frac{t}{t^*} \qquad (5.5)$$

where t* designates the time at which equilibrium condition is reached. In the case of consideration t* is taken as T_o+0.1°C.

- o Stresses are converted to dimensionless form by the equation;

$$\omega = \frac{\sigma}{\sigma_a^o} \qquad (5.6)$$

For normalization of the stresses, yield strength of austenite is not the only option. $\sigma_m^o, K_a, K_m, E_a$ and E_m could also be used. These yield same results since they were multiplied by the same factor in order to keep dimensionless numbers constant.

Table 20: Standard and modified input data.

	Parameter		Std.	Mod.				Std.	Mod.
Geo.	L	[mm]	200	200	**Process**	T_a	[°C]	850	**1214**
	D	[mm]	10	10		T_o	[°C]	20.0	**28.5**
Thermomechanical	α_a	[10^{-6} °C]	23.8	**16.7**		h	[W/m² °C]	1500	**1793**
	α_m	[10^{-6} °C]	10.9	**7.6**	**Thermal**	ρ_a	[kg/m³]	7798	7798
	E_a	[GPa]	170	**244**		ρ_m	[kg/m³]	7741	7741
	E_m	[GPa]	205	**292**		c_a	[J/kg °C]	561	561
	ν_a	[-]	0.33	0.33		c_m	[J/kg °C]	501	501
	ν_m	[-]	0.36	0.36		λ_a	[W/m °C]	20.1	**24.0**
	K_a	[MPa]	510	**729**		λ_m	[W/m °C]	42.7	**51.0**
	K_m	[MPa]	4943	**7062**	**Transformation**	M_s	[°C]	211	**301**
	n_a	[-]	0.12	0.12		M_o	[°C]	93	**134**
	n_m	[-]	0.14	0.14		ΔH^{tr}	[J/g]	-79	**-112**
	$\sigma_a°$	[MPa]	173	**274**		κ	[Pa]	70	**49**
	$\sigma_m°$	[MPa]	1278	**1826**					

In Figure 42a-c final states that are attained by using modified and standard data sets are presented. It can clearly be seen that phase fractions, residual stresses and plastic strains are almost the same for standard and modified data sets. Although these results are affirmative, they are not enough to justify dimensionless number sets. Kinetics of the systems should also be examined.

Temperature, phase and dilatation evolution are very important since these are the main reasons for stress and strain evolutions. Moreover, these two are expected to give parallel results since these are interrelated. From Figure 42 d-f it can be seen that standard and modified data sets yield same temperature and phase evolution. In Figure 42g-i, stress evolutions in radial, axial and tangential axes are presented. It can be seen from the figure that dimensionless stress evolution are also similar for both data sets.

To sum up; dimensionless behaviors of standard and modified input data sets give parallel results in terms of stress, strain and temperature evolution. Furthermore, final states of the output quantities are similar. From these results it can be concluded that dimensionless number sets in references [23, 133] are complete and independent.
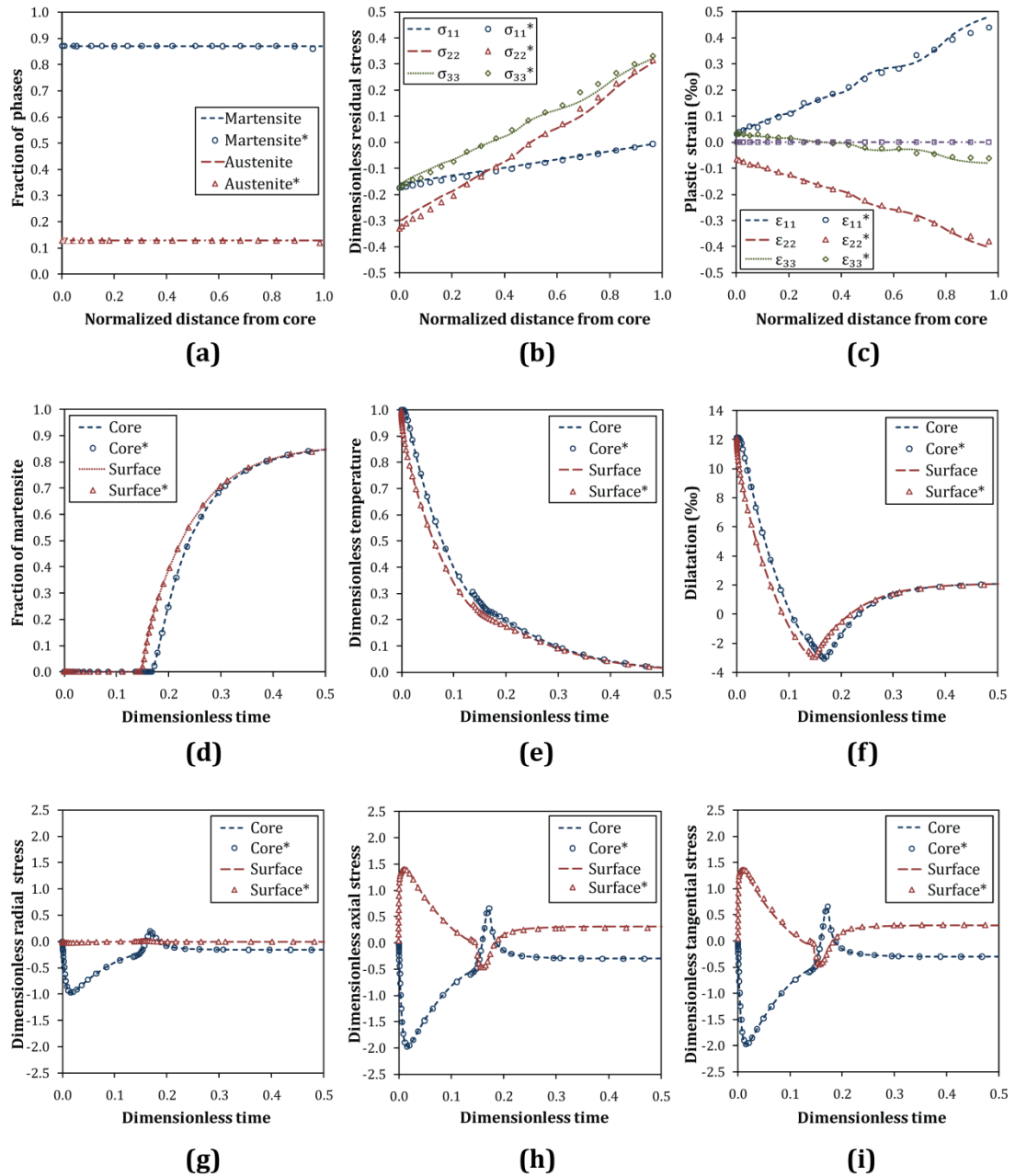

Figure 42: Justification of the dimensionless number sets. "*" refers modified data set.

5.4.3. Effect of Biot number on dimensional changes

In order to investigate the effect of Biot number on dimensional changes, heat transfer coefficient was varied (*h=300…16200W/m²°C*). Test cylinders had the dimensions of D=10mm and L=200mm). In Figure 43 results of these simulations are presented. It can be seen that relative dimensional changes significantly depend on Biot number. Volume change does not affected since this number does not have any influence on martensitic transformation and transformation strains.

Another parameter that can easily be varied is volume to surface ratio. For the validation of Bi_a, diameter is increased to 20mm and heat transfer coefficient is varied same as before (*Bi_a(h=300…16200W/m²°C, D=20mm)*) and resultant relative dimensional changes are compared with the previous case which is *Bi_a(h=300…16200W/m²°C, D=10mm)*. By this means, not only Bi_a is verified, but also behaviors of dimensional changes curves at higher Biot numbers are revealed. Results are presented in Figure 43a-b. From figure, one can see that, *Bi_a(h, D=20mm)* gives consistent results with *Bi_a(h, D=10mm)*. Moreover, smooth behavior of the dimensional changes curves continues to higher Bi_a.

Up to now Biot number is varied by altering heat transfer coefficient and diameter. These were relatively easy since heat transfer coefficient and diameter has an independent nature and they do not depend on the metallurgy of the material. Final parameter to be varied is thermal conductivity (λ). However, this is not an easy task since in the case of phase transformations thermal conductivity of the phase mixture continuously evolves. Therefore; an appropriate definition of λ in Biot number should be made.
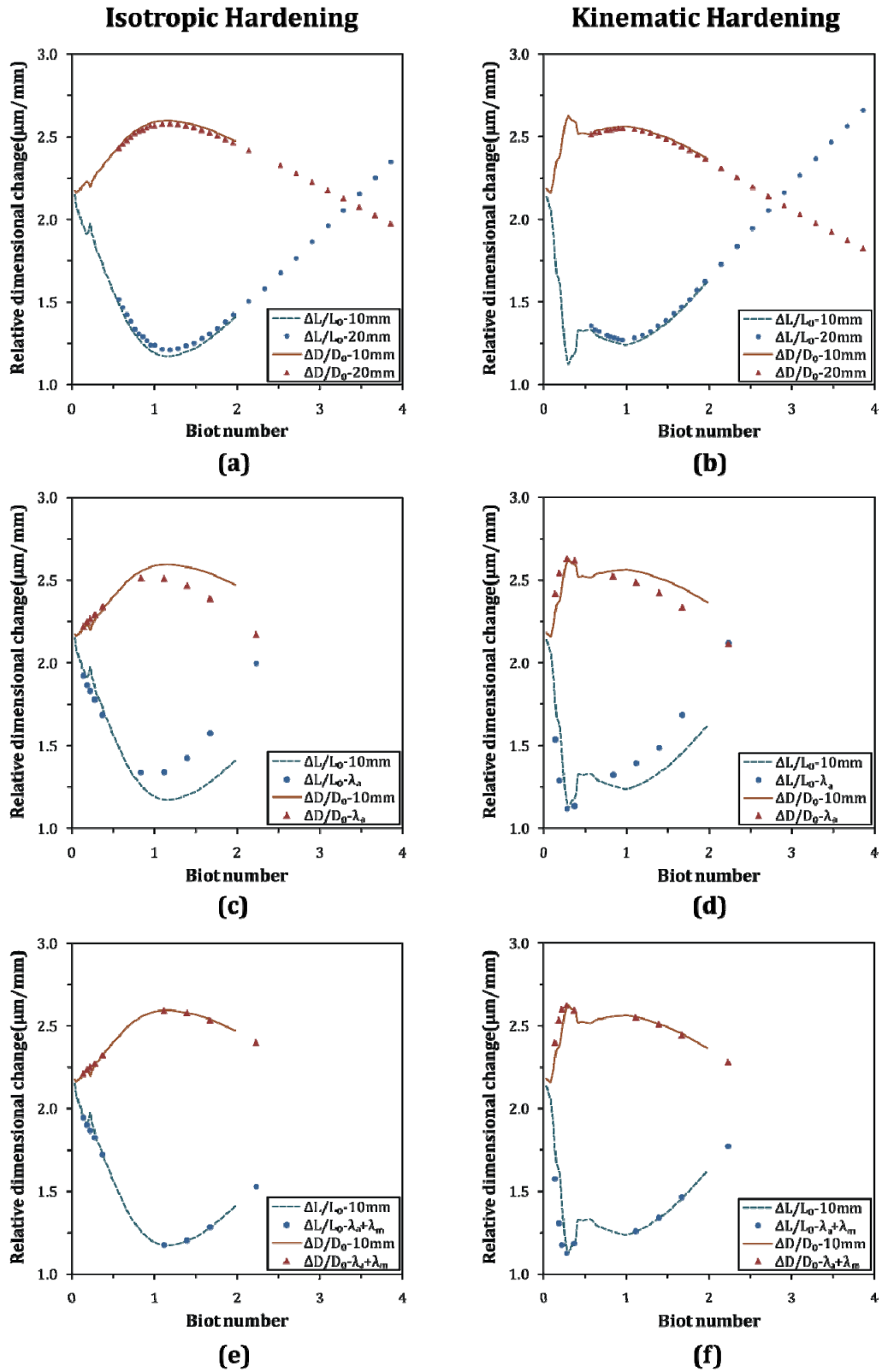
Figure 43: Relative dimensional changes when Biot number (Bi$_a$) is manipulated by changing (a, b) diameter, (c, d) λ_a and (e, f) both λ_a and λ_m.

116

First of all, λ in Biot number is defined as thermal conductivity of austenite and this number is named as *Biot number of austenite* (Bi_a). In order to check the validity of Bi_a definition, Biot number is varied by changing λ_a only. It is clearly be seen from Figure 43c-d that this gives reasonable results up to $Bi_a \approx 1$ with a tolerance of $0.1 \mu m/mm$ whereas; at higher Biot numbers this approach cannot be used. Therefore, Bi_a is not enough to describe the system and there is an undiscovered dimensionless number that effects the system. Based on the former experience, this number is predicted to be the ratio of thermal conductivities;

$$\Pi_{18} = \frac{\lambda_m}{\lambda_a}$$
(5.7)

In order to validate the existence of Π_{18}, thermal conductivities are multiplied with constant "c" in order to attain;

$$Bi_a' = Bi(h = 4600\,\mathrm{W}/\mathrm{m^{2o}C}, D = 10\mathrm{mm}, c\lambda_a)$$
(5.8)

and

$$\Pi_{18}' = \Pi_{18}^o = \Pi_{18}\left(c\lambda_a, c\lambda_m\right)$$
(5.9)

where "o"and "'" denotes standard and modified dimensionless numbers. Simulation results of this condition show that there is a good agreement between *Bi(h,D=10mm,λ_a)* and , *Bi(h,D=10mm, cλ_a)-Π_{18}(cλ_a, cλ_m)* couple. This proves that, inconsistency in Figure 43c-d is due to the change in Π_{18} which disturbs the equivalency of the systems.It can be concluded that Π_{18} is an important dimensionless number and should be included to the dimensionless number set. Moreover; the assumption of λ_a and λ_m equivalency (Section 4.2.2.1.) is quite severe. In Section 5.4.6.3. the effect of Π_{18} on dimensional changes is investigated in detail.

5.4.4. The behavior of Biot number versus relative dimensional change curves (Bi vs. $\Delta Y/Y_o$)

Before discussing the effects of dimensionless numbers on Bi vs. $\Delta Y/Y_o$ curves, behaviors of these curves should be clarified first. For better understanding of the system, Bi vs. $\Delta Y/Y_o$ curves was investigated in stepwise manner. Namely, several parameters (Phase transformations, TRIP, CP) were excluded from the model one by one and behaviors of the resultant curves are investigated.

First parameter that was excluded is phase transformations. In this condition, thermal stresses govern dimensional changes. Relative dimensional changes were determined with respect to Bi_a which was varied by changing heat transfer coefficient (h=300…16200W/m²°C). In Figure 44, simulation results of 10 mm diameter long cylinders (L=200mm) that were performed with averaged material data set is presented. Results show that when there is no phase transformation, $\Delta L/L_o$ increases until a certain Biot number and then start to decrease. These results are parallel to the findings in [19].
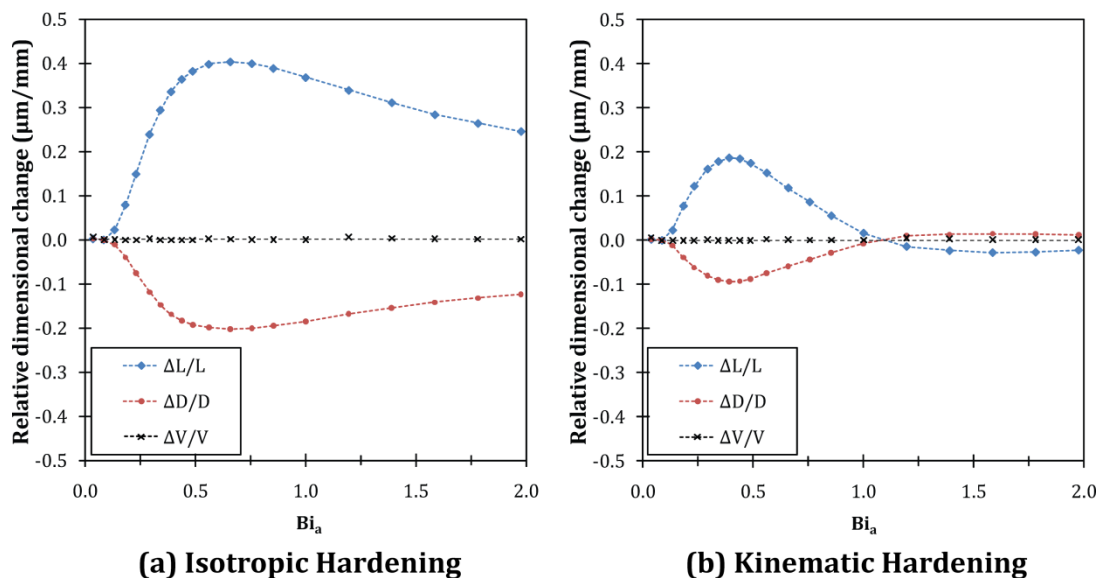

(a) Isotropic Hardening   (b) Kinematic Hardening

Figure 44: Bi vs. $\Delta Y/Y_o$ when there is no phase transformation (D=10mm)

In order to clarify the combined effect of classical plasticity, transformation strains and thermal strains on dimensional changes, phase transformations were included to the previous model. Here, transformation induced plasticity was excluded to distinguish the effect of classical plasticity (Figure 45). These results show that relative dimensional changes are totally different when there is phase transformation in the system.

First difference is in volume change. Volume drastically increase since volume of martensite is larger than volume of austenite. $\Delta V/V_o$ does not change with Biot number, since it does not depend on the cooling behavior. Volume change depends on material parameters that effect martensite fraction and transformation strain. In the case of phase transformations, material properties that are related with thermal strains are also included to this list since they affect transformation strains and final volume of the component. In regards to length and diameter change, it is observed that transformation strains significantly alter their magnitudes. In the range of Bi<2, maximum observed length change is more than ten times that of transformationless case. This shows that, transformation strains drastically alter stress state which significantly increases the extent of classical plasticity and hence anisotropic dimensional changes. Continuous increase of dimensional changes with increase in Biot number is most probably due to increase in thermal stresses.
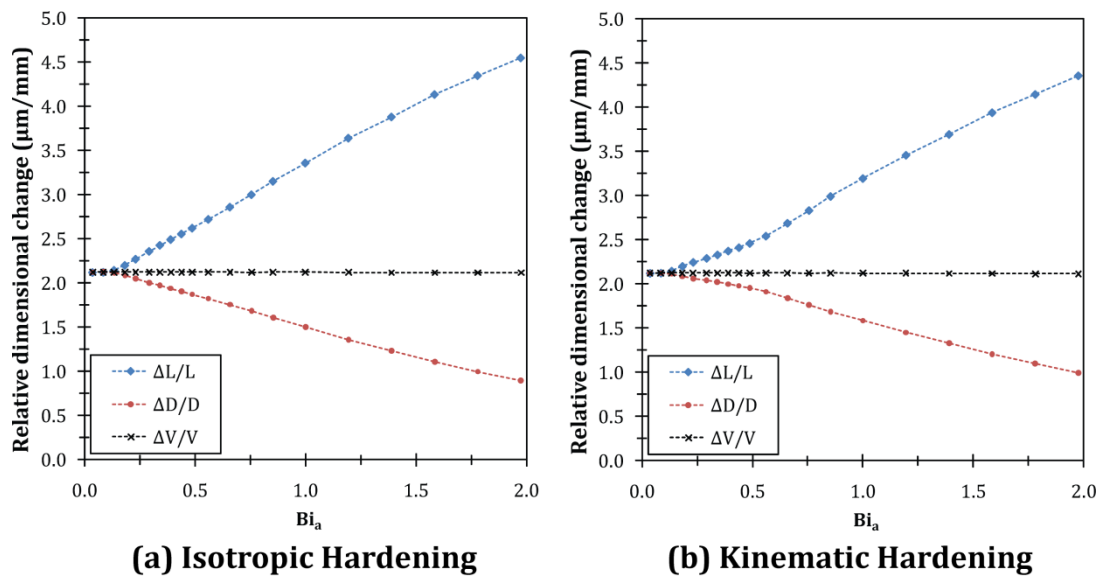

(a) Isotropic Hardening　　　　**(b) Kinematic Hardening**

Figure 45: Bi vs. $\Delta Y/Y_o$ when there is no transformation plasticity

In order to investigate the effect of TRIP on dimensional changes, classical plasticity was excluded from the previous model and instead TRIP option was opened. Results of these simulations are presented in Figure 46. The magnitude of anisotropic dimensional changes that is imposed by TRIP is low when it is compared to classical plasticity. Moreover, trend of the curves are very different. These two mechanisms effects dimensional changes in reverse manner. TRIP tends to decrease length and increase diameter whereas classical plasticity tends to increase length and decrease diameter. This behavior can be explained with the help of stress evolution:

Transformation induced plasticity, first appears in the system in Stage 2 when stresses change direction due to the initiation of transformation at the surface. At this stage transformation induced plasticity imposes strains in the reverse direction of classical plasticity. In the third stage when stresses again change direction due to transformation at the core, TRIP and classical plasticity are in the same direction. The direction of the total effect of TRIP depends on the competition between these two stages. From these results, it can be seen that at lower Biot numbers TRIP strains in Stage 2 is dominant, whereas; at higher Biot numbers TRIP strains at Stage 3 is dominant. However, it should be noted that, current results are not enough to clarify the mechanism and further post-processing is necessary to confirm these predictions.
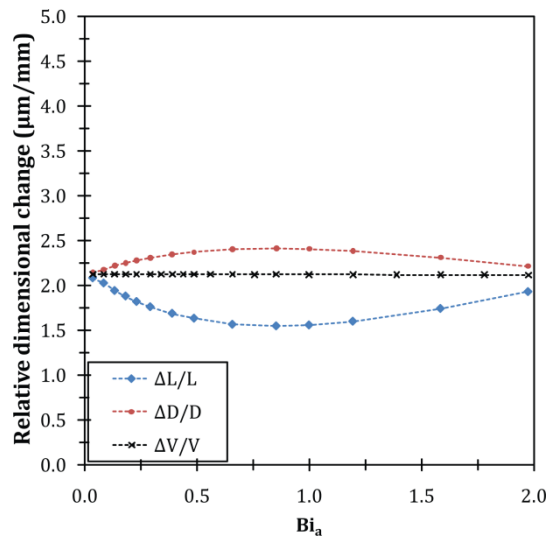

Figure 46: Bi vs. $\Delta Y/Y_o$ when there is no classical plasticity

In final series of simulations, all of the plasticity mechanisms were included to the model. This model will be referred as "*Standard*" throughout this study. In Figure 46 results of these simulations are presented. It can be seen from the figures that, direction of dimensional changes are similar to the case with TRIP (Figure 46). Namely, length tends to decrease and diameter tends to increase until Bi_a=2. However, magnitudes of dimensional changes are large when they are compared to the case with pure TRIP. On the other hand when these results are compared with the case with pure classical plasticity it is observed that direction of length and diameter changes are in reverse direction. Moreover, differences in the magnitude of relative dimensional changes increase at Biot numbers larger than 1.0.

These results show that TRIP dominates dimensional changes, and offsets the effect of classical plasticity. However, when previous results with "no TRIP" and with "no CP" are considered, this dominance is unexpected. This might be owed to the interaction between two plasticity mechanisms. Results show that, existence of classical plasticity in combination with TRIP magnifies dimensional changes in TRIP direction whereas; TRIP decreases the magnitudes of dimensional changes due to classical plasticity. But still there is a competition between TRIP and CP. At low Biot numbers, dominant plasticity mechanism is TRIP. This is because; thermal stresses are not high enough to cause large plastic deformation. At higher Biot numbers, on the other hand, dominant plasticity mechanism is classical plasticity. In this case, large temperature difference between core and surface causes large stresses and hence large plastic strains. As a result, magnitude of classical plasticity is higher when it is compared to the case with lower Biot numbers. Therefore; dominant factor determining the anisotropic dimensional changes is classical plasticity before martensitic transformation.

Up to now, the effect of phase transformations, CP and TRIP on dimensional changes were discussed. Another point that should be mentioned is the differences between the curves of isotropic and kinematic hardening, namely the effect of back stresses on dimensional changes.

In the case without martenisitic transformation, back stresses shift peak height to the left (Figure 44). Namely; critical Biot number at which length change is in its maximum, tends to decreases. This is probably because of the increase in plasticity in stress reversal when surface volume is stabilized and core starts to contract.
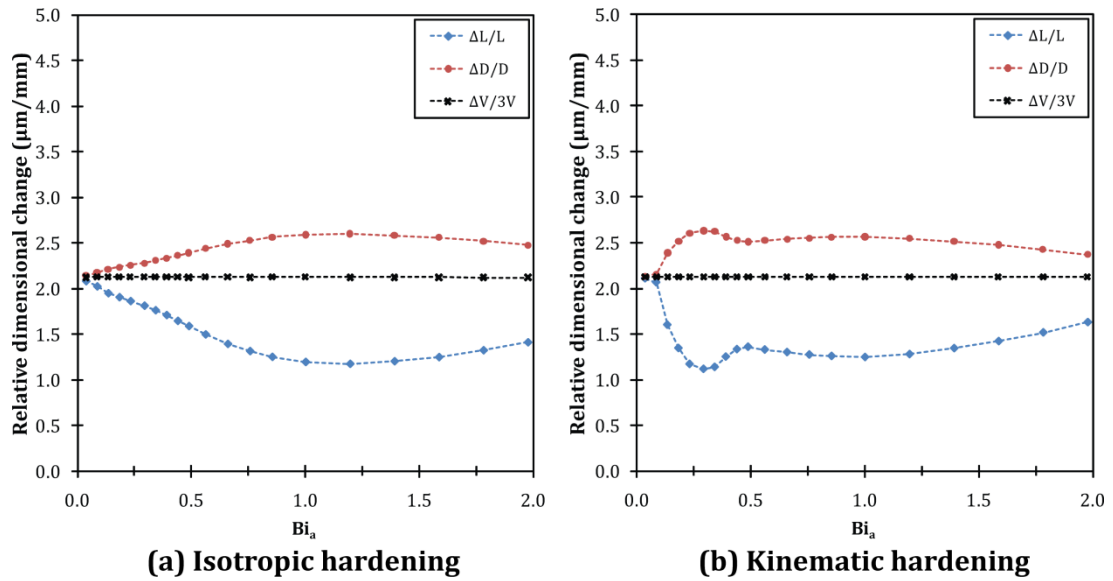
121

(a) Isotropic hardening　　　　　**(b) Kinematic hardening**

Figure 47: Bi vs. $\Delta Y/Y_o$ when all of the plasticity mechanisms are included to the model

In the case without TRIP, the major difference between kinematic and isotropic hardening is in the slope of the curves. Length and diameter change curves of isotropic hardening can be approximated to a straight line until Bi<2. Kinematic hardening curve has a similar behavior but the slope of the straight line changes at $Bi_a \approx 0.5$(Figure 45b). This change in slope might be attributed to the increase in plasticity in Stage 3 in which surface is totally cooled down and transformed whereas; transformation initiated at the core. Namely, after $Bi_a \approx 0.5$ back stresses are probably high enough to cause classical plasticity at Stage 3.

For the simulation set that all plasticity mechanisms are modeled, difference between isotropic and kinematic hardening rules is diverse (Figure 47). Isotropic hardening curves can be approximated to a second order polynomial in the investigated range of Biot number. On the other hand, for kinematic hardening, the behavior is more complicated and should be expressed in terms of piecewise functions.
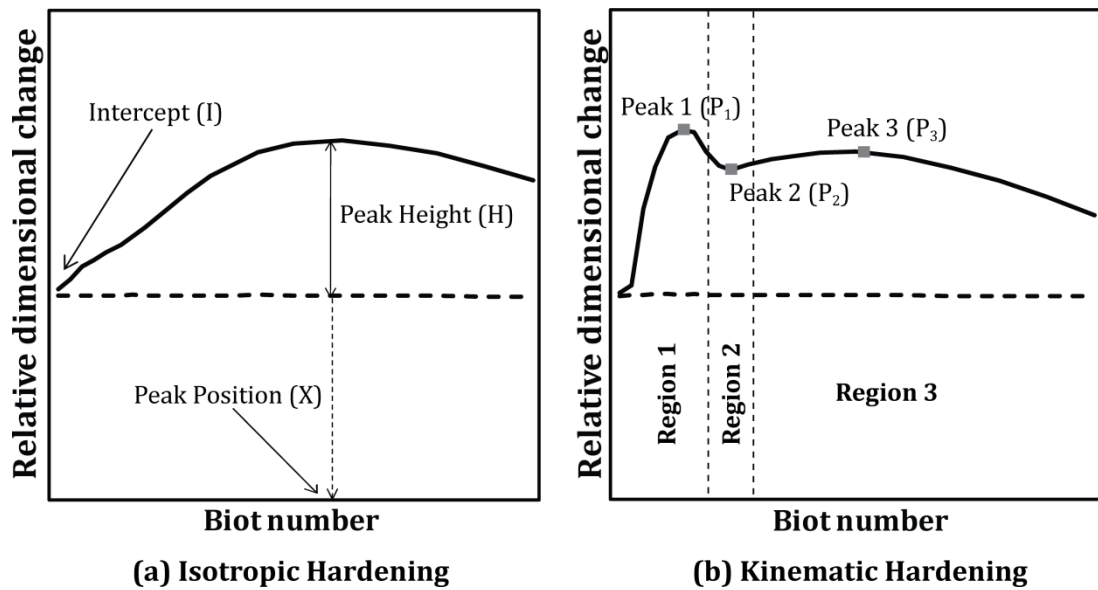
Figure 48: Characterization of Bi vs. ΔY/Y₀ curves

Bi vs. ΔY/Y₀ curves of kinematic hardening can roughly be divided in to three regions (Figure 48):

Region1: Narrow and relatively high peak. ($Bi_a \leq 0.4$)

Region2: Transition region ($0.4 < Bi_a < 0.5$)

Region3: Wide and lower peak. Behavior is much smoother. ($Bi_a > 0.5$)

This behavior is probably due to the back stresses that cause decrease in yield strength in reverse loading. During quenching there are two stress reversals. First one occurs when transformation starts at the surface, whereas; second stress reversal occurs when transformation starts at the core. Magnitude of back stresses during these stress reversal depends on previously accumulated strains in the material. Therefore, it is not straight forward to determine the effect of back stresses on dimensional changes.

However; results of "no TRIP" simulations provide a hint about this unusual behavior of kinematic hardening curves. Those results had shown that back stresses cause a drastic increase in plasticity above $Bi_a \approx 0.5$. This increase was attributed to increase in back stresses at high Biot numbers. After $Bi_a \approx 0.5$, back stresses increase such that, they cause yielding at Stage 3 where stresses change direction due to initiation of

transformation at the core. It is observed that Peak 2 in standard model is also located at $Bi_a \approx 0.5$. Thus, the piecewise behavior of kinematic hardening curves can be attributed to the change in the conditions of TRIP and CP competition due to yielding at Stage 3. Kinematic hardening curves are combination of two curves which are determined by two different TRIP-CP competitions. However, current results are not enough to explain complete mechanism. Further post-processing is necessary to explain the behavior of kinematic hardening curves.

5.4.5. Characteristics of Bi vs. ΔY/Y₀ curves

Biot number versus dimensional changes curves can be characterized by peak heights, peak positions an intercepts which are illustrated in Figure 48. In the case of consideration peak heights (H) can be interpreted as the extent of anisotropic dimensional change. Peak position, on the other hand, provides hint about TRIP-CP competition. For instance, right shift of the peak can be attributed to decrease in CP or increase in TRIP. Intercept of the curves interprets volume change. Since plasticity is theoretically zero at zero Biot number, intercepts of diameter and length change curves should be equal.

5.4.6. Effect of dimensionless numbers on dimensional changes

In this part of the study, dimensionless numbers individually were modified and their effects on the dimensional changes are investigated. Here dimensionless numbers are classified according to Table 13 and they are mentioned in the same order. In addition to these 18 numbers in Table 13, 6 dimensionless numbers (Table 12) those are included to Ω_W are mentioned in the order of relatedness.

5.4.6.1. Dimensionless number related with geometry

Π_0 - *Aspect Ratio:* $\left(\dfrac{L}{D} \right)$

Frerichs et. al. [19] has previously shown that austenitic cylinders with aspect ratio greater than 3, have similar Biot number vs. dimensional change curves. At this condition, cylinders were assumed to be infinitely long, and Π_0 can be considered as infinity. Although, in the case of consideration, material is totally different and there occur martensitic transformation, this assumption can still be valid since L/D ratio is well above this threshold (L/D=20).

5.4.6.2. Thermometallurgical dimensionless numbers

Π_2 - *Fourier Number:* $\left(\dfrac{\lambda t S}{\rho c D V} \right)$

Fourier number is an important dimensionless number that is related with the ratio between conduction rate and heat storage rate. This number is time dependent and can be considered as equal for systems that are in their equilibrium states. This is because; theoretically, infinite time is needed for equilibrium

As a result, Fourier number does not change the final state of the system, namely, distortion and residual stresses. But, it can be used as dimensionless time to compare stress, strain and temperature evolutions of two different systems.

Π_3 – *Latent Heat Number:* $\left(\dfrac{\Delta H_{tr}}{c(T_a - T_o)} \right)$

Latent heat number governs dissipated heat due to latent heat of transformation. The main influence of this number is on temperature evolution. Therefore; Π_3 has an indirect effect on plasticity mechanisms and hence anisotropic dimensional changes. This can also be deduced from Figure 49. At both hardening rules, Π_3 changes peak position and heights. However, this effect is very low since the sensitivity of relative dimensional changes on ΔH^{tr} is quite small. From Figure 49 one can also see that, latent heat number does not have any influence on intercept (I) and volume change. It is an anticipated result since this number does not have any connection with dilatational strain terms.

Π_3 - Isotropic hardening
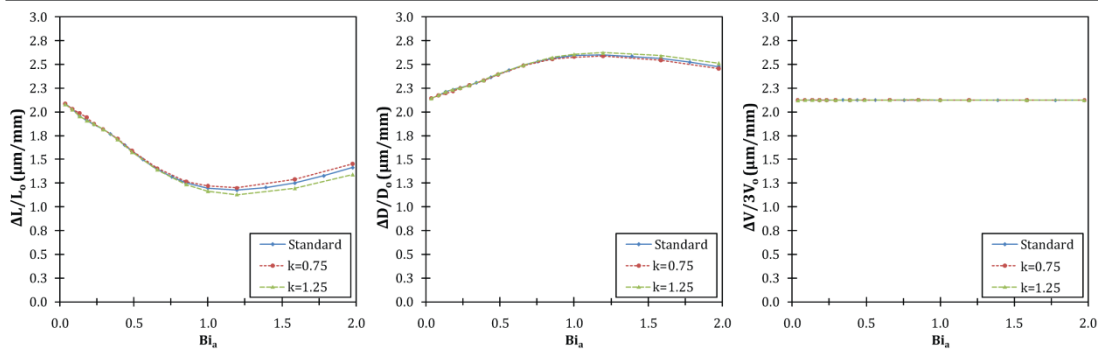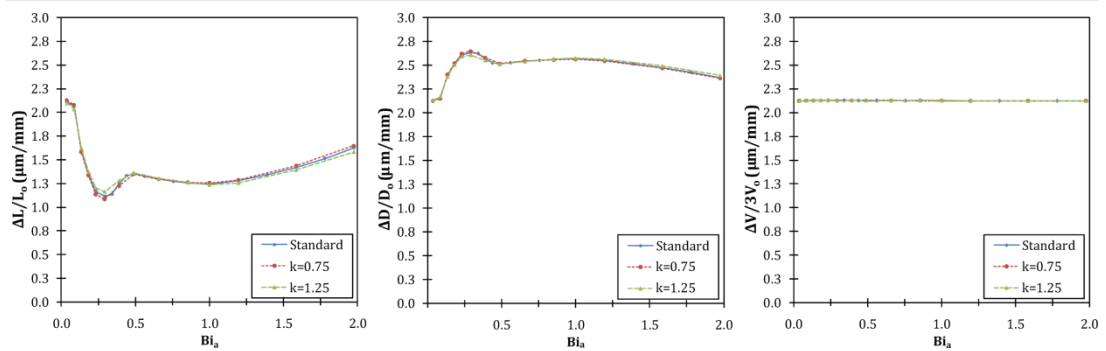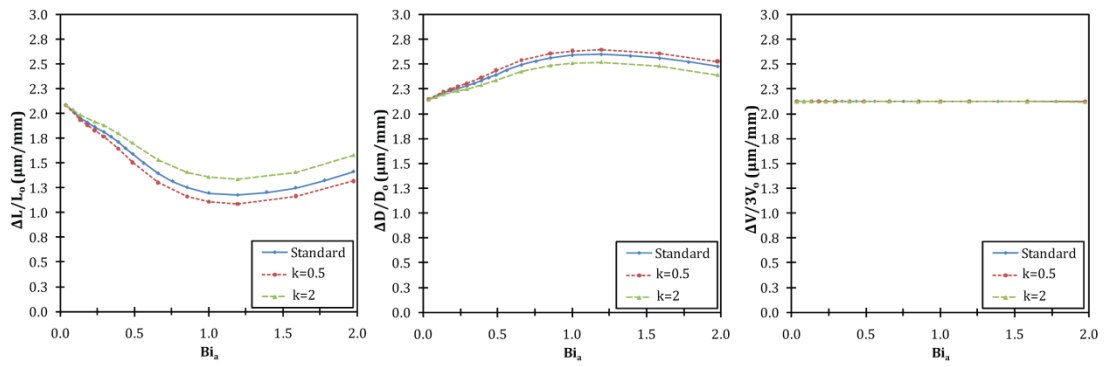

Π_3 - Kinematic hardening

Figure 49: Bi vs. $\Delta Y/Y_o$ curves when latent heat number (Π_3) is multiplied by k

5.4.6.3. Dimensionless numbers that are related with the thermal characteristics of the material

As it is discussed in Section 4.2.2.1. , during derivation of dimensionless numbers, two of the thermal properties, namely λ and c are assumed to be equal for austenite and martensite [23]. Although this assumption simplifies the problem, it has significant consequences on the simulation results. This is because; these properties exist in heat transfer equation and they directly affect temperature evolution. One of the consequences of this assumption was illustrated in Section 5.4.6.2. .

This problem is solved by including the ratio of these properties $(\Pi_{18} = \lambda_m/\lambda_a , \Pi_{19} = c_m/c_a)$ into Ω_W. Resultant dimensionless numbers are independent of the process; they purely depend on the material.
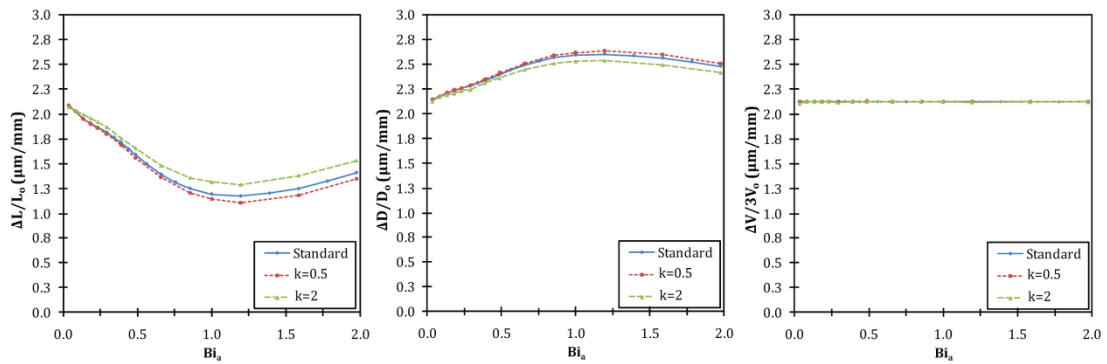
Π_{18}- Isotropic hardening

Π_{18}- Kinematic hardening
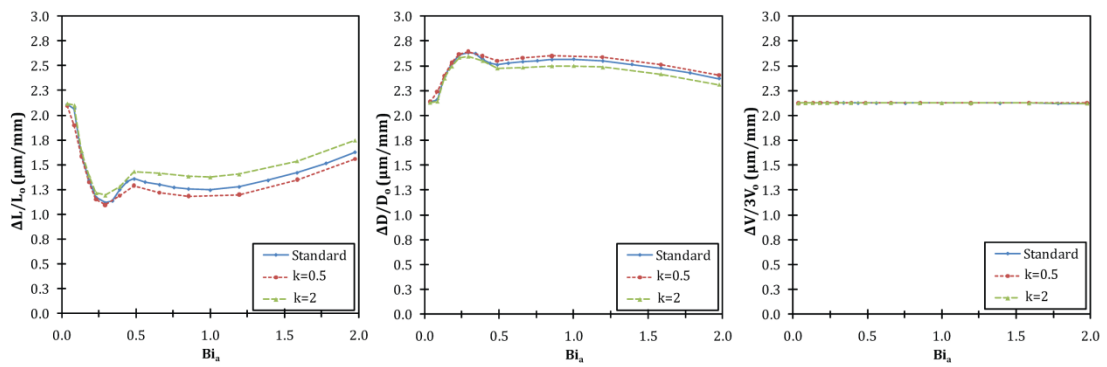
Π_{19}- Isotropic hardening
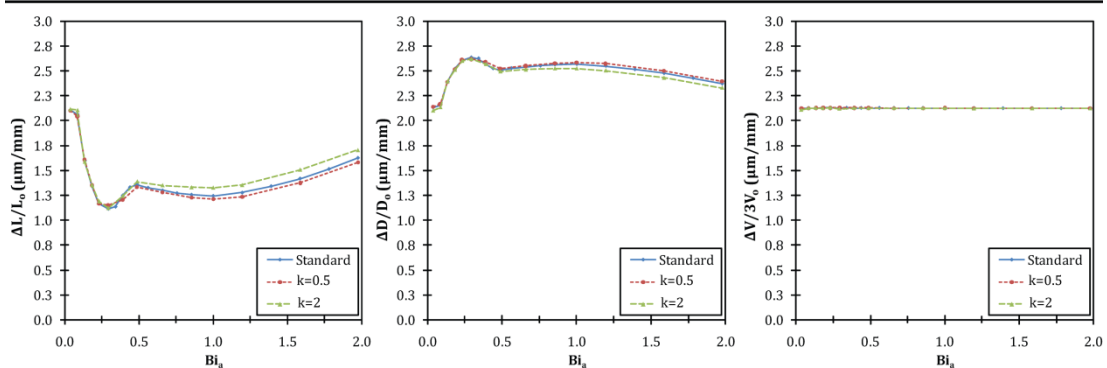

Π_{19}- Kinematic hardening

Figure 50: Bi vs. $\Delta Y/Y_o$ curves when ratio thermal conductivities (Π_{18}) and specific heats (Π_{19}) are multiplied by k

127

Π_{18} – *Ratio of Thermal Conductivities:* $\left(\dfrac{\lambda_m}{\lambda_a} \right)$

Thermal conductivity is one of the three material properties that determine temperature evolution. In heat transfer equation, thermal conductivity appears in heat flux term. SYSWELD® uses linear rule of mixtures to determine thermal conductivity of the phase mixture. Therefore, Π_{18} (with phase fractions) characterize the thermal conductivity of the material during quenching.

The influence of Π_{18} on dimensional changes is presented in Figure 50. Here thermal conductivity ratio is altered by changing λ_m. From figure it can be see that, an increase in Π_{18} causes a decrease in peak heights (H). There is not a significant change in peak position which shows that, increase in thermal conductivity decrease the extent of plasticity (both TRIP and CP). This is an anticipated result because when thermal conductivity increases, temperature gradient decreases and hence accumulated stresses decrease.

Π_{19} – *Ratio of Specific Heats:* $\left(\dfrac{c_m}{c_a} \right)$

Specific heat is another material property that determines temperature evolution. In heat transfer equation it is located in the "heat storage capacity" term. It can be seen from Figure 50 that ratio of specific heats has significant affect on plasticity. This is anticipated, since temperature evolution probably affects stress evolution which alters TRIP and CP.

On the other hand, it should also be noted that, dimensional changes might be influenced by the change in dissipated heat during transformation. That is to say; total dissipated heat is not constant since latent heat at different fractions of transformation is altered. Therefore; a minor change in latent heat number (Π_3) might have occurred. However, neither change in Π_3 nor its consequences are thought to be significant due to the following reasons.

- Enthalpy is averaged with respect to temperature which minimize (but not eliminate) the change in total dissipated heat.

- Latent heat number has negligible effect on dimensional changes (Figure 49). Its influence is very low even at 25% alterations. In the case of consideration change in Π_3 is predicted to be well below 25%.

- In Section 5.4.2. it was shown that this variation procedure yield exactly the same dimensionless respond which show that it is sufficient and does not make any significant change in Π_3.

However, detailed post processing is necessary to clarify the influence of the change in Π_3 on dimensional changes.

5.4.6.4. Dimensionless numbers related with transformation

Π_4 – *Martensite Start Number:* $\left(\dfrac{M_s - T_o}{T_a - T_o} \right)$

Martensite start number is the dimensionless form of martensite start temperature (M_s). This number "*locates the onset of martensitic transformation in the temperature domain*" [23]. Π_4 comes from Koistinen-Marburger equation and it directly determines fraction of martensite and the temperature at which martensite transformation starts. Therefore, it has strong influence on volume change. Effect of Π_4 on Biot number versus relative dimensional change curves are presented in Figure 51.

Besides its effect on volume change, martensite start number alters peak positions (X) and heights (H) considerably. In the case of isotropic hardening peak positions shift left and peak heights decrease with increasing Π_4. This might be attributed to the decrease in thermal strains due to early initiation of transformation. However; this also causes a decrease in TRIP. These results show that change in classical plasticity offsets the decrease in TRIP.

At kinematic hardening, Π_4 also has considerable influence on plasticity. But, it is not possible to deduce the effect of Π_4 on TRIP and CP competition from current results. Further post-processing is necessary. However; the change in kinematic hardening might be owed to the alterations in the extent of TRIP, back stresses and classical plasticity which are caused by the changes in (1) accumulated thermal strains, (2) fraction of martensite, and (3) stress state during transformation.
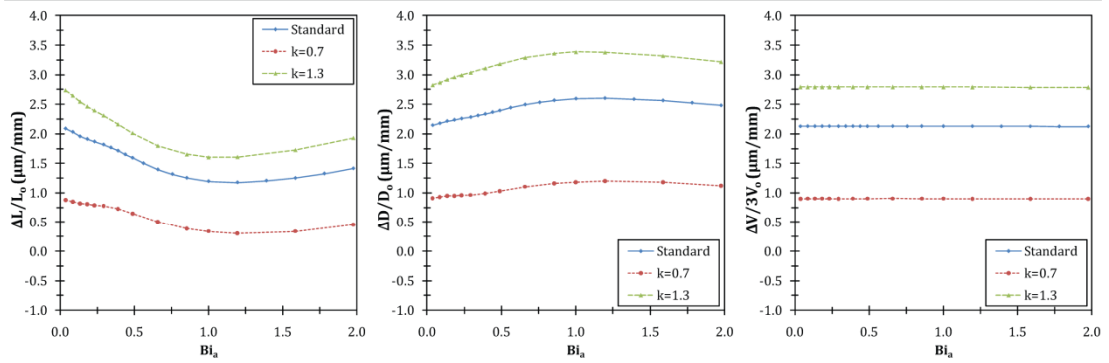
Π_4 - Isotropic hardening
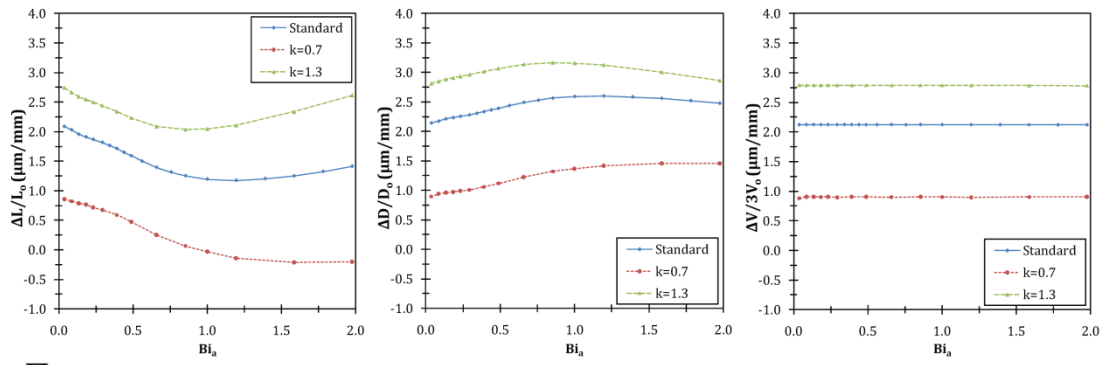
Π_4 - Kinematic hardening
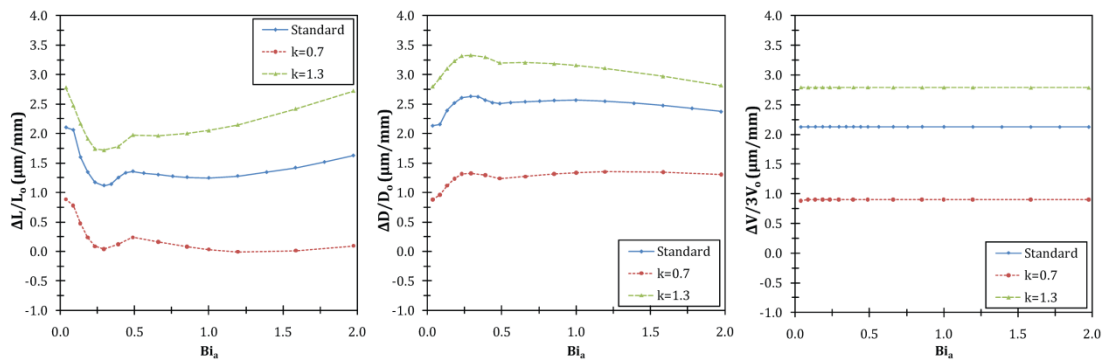
Π_5 - Isotropic hardening
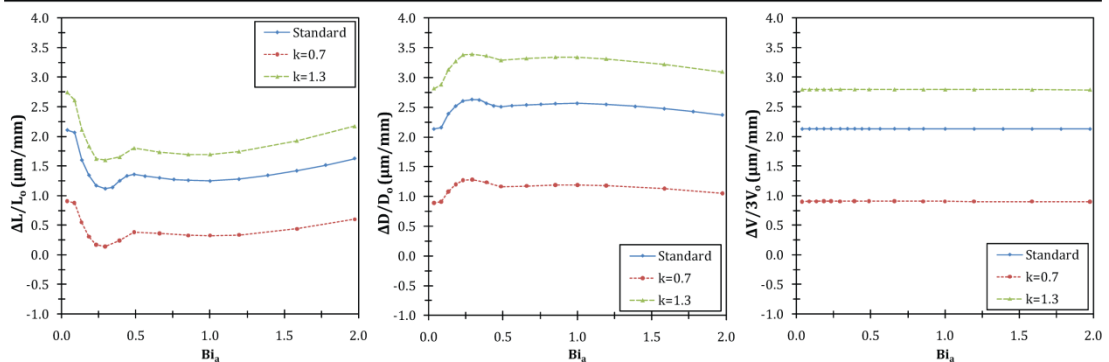

Π_5 - Kinematic hardening

Figure 51: Bi vs. $\Delta Y/Y_o$ curves when martensite start number (Π_4) and Koistinen-Marburger number (Π_5) are multiplied by k

Π_5 – *Koistinen-Marburger Number:* $\left(\dfrac{T_a - T_o}{M_o}\right)$

Koistinen-Marburger number is another important dimensionless number that effect kinetics of martensite formation and martensite fraction. As anticipated, Π_5 significantly alters volume change and intercepts (I) (Figure 51). In regards to peak positions, trend is similar to martensite start number at both hardening rules, but peak heights show large distinction. In contrast to Π_4, heights of all of the peaks increase. This shows that, although Π_4 and Π_5 stem from same equation and their affect on martensite fraction is almost equal, they have different effects on the plasticity which might be because these numbers alter evolution of phase transformation in different manner. It is not possible to understand the effect of Π_5 on dimensional changes from current results. These are most probably due to the changes in three numbered items that are mentioned in section *"Martensite Start Number"* above.

5.4.6.5. Dilatational dimensionless numbers

Π_6 – *Thermal Strain Number:* $\left(\dfrac{(1+v)\,\alpha\,(T_a - T_o)}{1 - 2v}\right)$

Thermal strain number is one of the dilatational numbers that governs thermal strain that is accumulated in austenite phase. Therefore, it has significant effect on volume change which can also be seen from Figure 52.

Π_5 also alters peak heights (H) and positions (X). This might be due to its effect on thermal stresses, and hence the extent of classical plasticity and TRIP:

As thermal stain number decreases, peak heights decrease which is due to decrease in thermal stresses and hence CP and TRIP. Another salient deviation is observed in the first peak (P1) of kinematic hardening curves. As thermal strain number decreases, P1 becomes wider. This is probably because, TRIP dominance range increases, since thermal stresses at initial stages of cooling drops to lower levels even at high Biot numbers.

In the derivation of this number, thermal expansion coefficients of austenite and martensite were assumed to be equal [23]. However, this assumption is not safe since, α_a is larger than two times of α_m. Moreover, when thermal component of volume change is expressed as;

$$\left(\frac{\Delta V}{V_o}\right)_{th} = -3\left(\alpha_a\left(T_a - M_s\right) + \int_{T_a}^{M_s}\left(\alpha_a X_a(T) + \alpha_m X_m(T)\right)dT\right) \qquad (5.10)$$

it can clearly be seen that thermal expansion coefficient of martensite has important contribution to dilatation. Moreover, sensitivity analysis showed that thermal expansion coefficient has significant effects on dimensional changes. As a result, another dimensionless number Π_{20};

$$\Pi_{20} = \frac{\alpha_m}{\alpha_a} \qquad (5.11)$$

should be included to dimensionless numbers to complete the dimensionless number set. In the next section influence of this number on dimensional changes is discussed.

Π_{20} – *Ratio of Thermal Expansion Coefficients:* $\left(\dfrac{\alpha_m}{\alpha_a}\right)$

Due to the reasons that are discussed above, this number has significant effects on dimensional changes (Figure 52). The major impact is on volume change and hence on intercept. Since α_m determines the volume of martensite at T_o its effect on volume change is more than that of other dimensionless numbers.

Π_{20} also affects plasticity. When Π_{20} is increased, plasticity significantly decreases. This might be due to the decrease in volume mismatch of austenite and martensite at low temperatures.
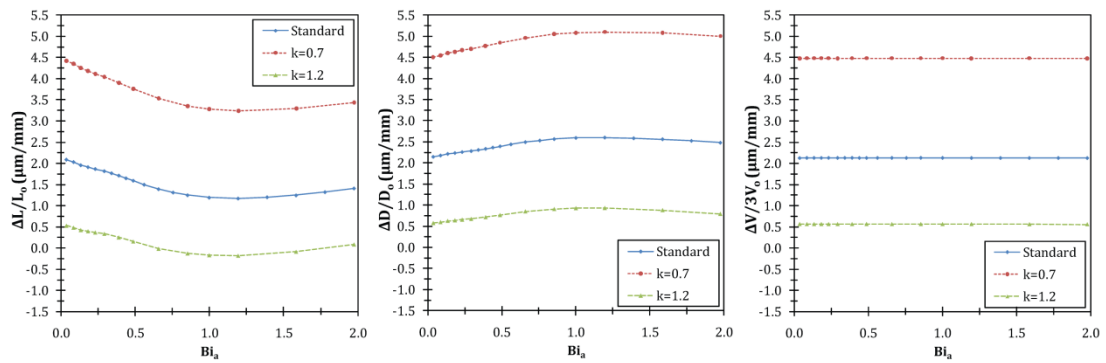
Π_6 - Isotropic hardening
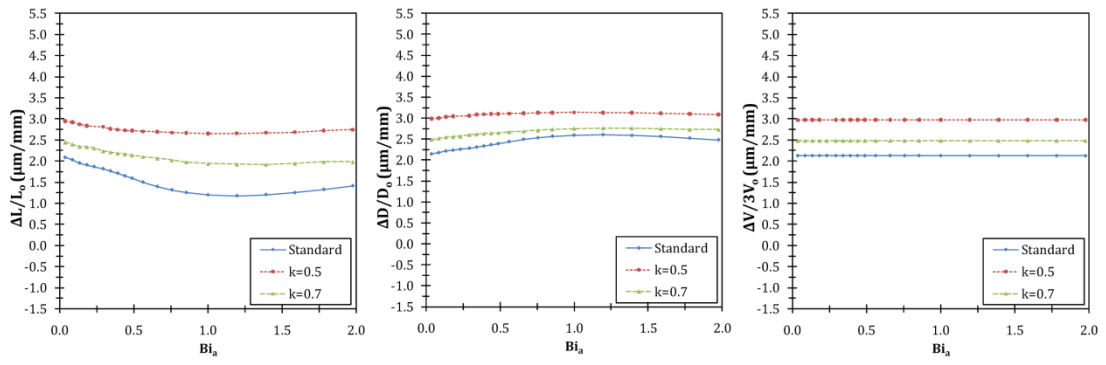
Π_6 - Kinematic hardening
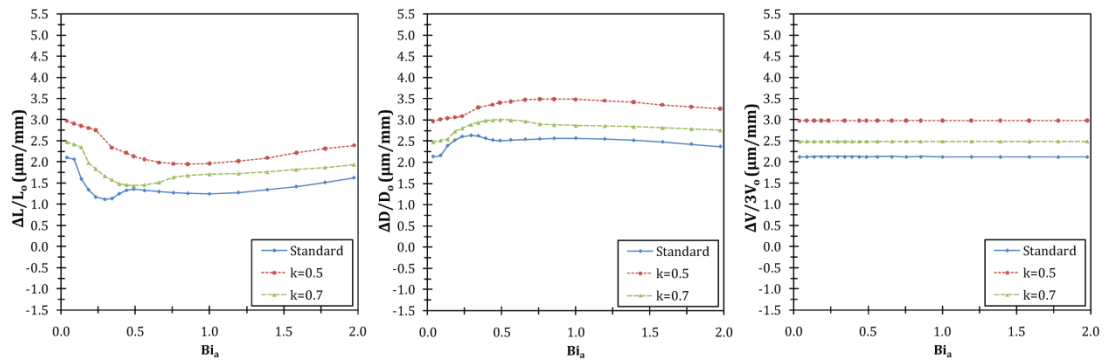
Π_{20}- Isotropic hardening
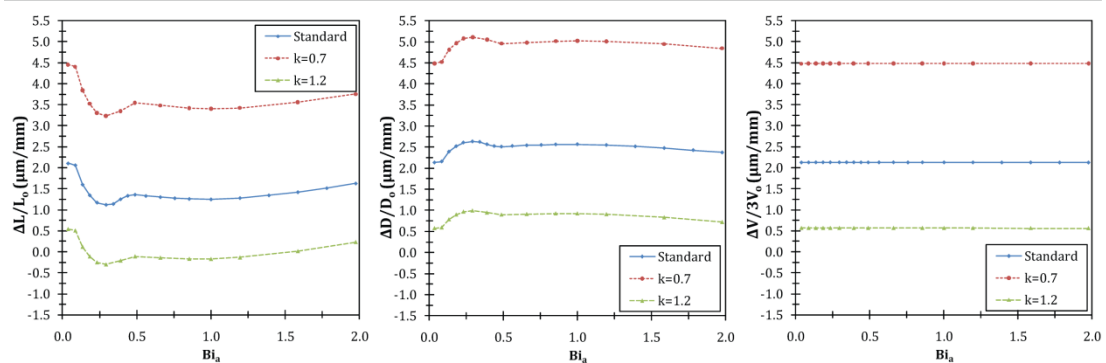
Π_{20}- Kinematic hardening

Figure 52: Bi vs. ΔY/Y$_o$ change curves when thermal strain number (Π_6) and ratio of thermal expansion coefficients (Π_{20}) are multiplied by k
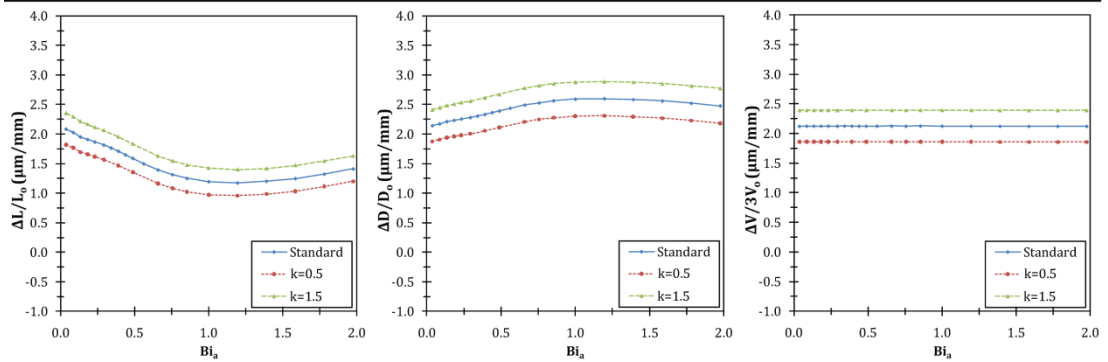
Π_7 – *Transformation Strain Number:* $\left(\dfrac{(1+v)(\rho_a - \rho_m)}{3(1-2v)\rho_m} \right)$

Transformation strain number determines volume change due to martensitic transformation. It directly stems from the expression:

$$\left(\frac{\Delta V}{V_o} \right)_{tr} = 3\varepsilon^{tr} X_m = 3\frac{\rho_a - \rho_m}{3\rho_m} X_m \qquad (5.12)$$

As anticipated, the major impact of this number is on volume change and hence the intercepts (I) (Figure 53). Π_7 only slightly increase peak positions and heights. The influence of this number on plasticity is small compared to aforementioned dimensionless numbers.
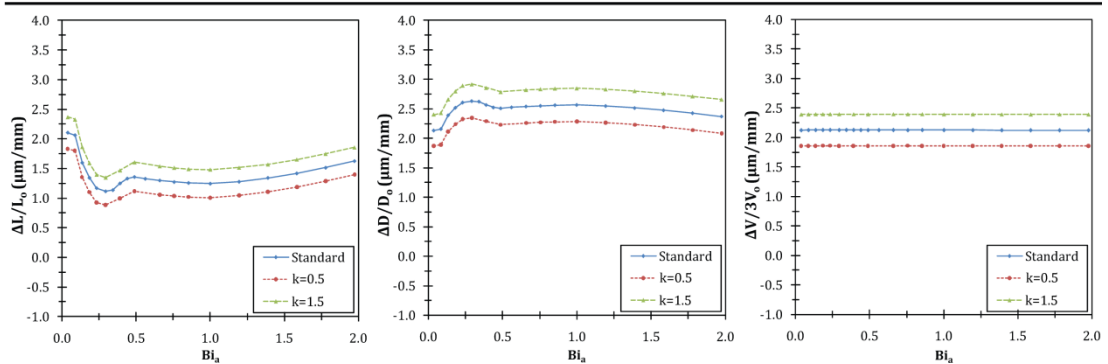

Figure 53: Bi vs. $\Delta Y/Y_o$ curves when transformation strain number (Π_7) is multiplied by k

5.4.6.6. Dimensionless numbers related with thermo-elasto-plasticity

Π_8 –*Thermo-elastic Fourier Number:* $\left(\dfrac{(1+\nu)\lambda^2 S}{E\rho c^2 (T_a - T_o)V} \right)$

This number governs inertial forces due to acceleration. These forces are quite small and can be neglected. Moreover, SYSWELD® uses quasi-static approach and hence it neglects inertial forces. Therefore, it is anticipated that this number does not have any influence on simulation results. Figure 54 confirms this prediction. Frerichs et. al. [131] also found same results in the case of quenching without phase transformations.
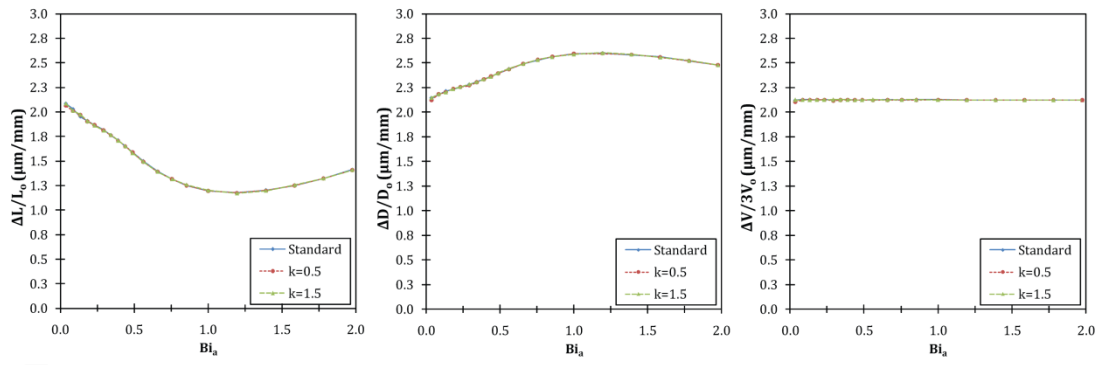
Π_9 – *Thermo-elastic Dissipation Number:* $\left(\dfrac{E\alpha T_a}{(1-2\nu)\rho c (T_a - T_o)} \right)$

Thermo-elastic dissipation number is related with temperature drop due to adiabatic expansion. Since, increase in volume during quenching is very low, effect of this number on temperature evolution is negligible. Moreover, quench model that is used during this study is not fully coupled and hence SYSWELD® does not simulate this effect. On the other hand, it is not practically possible to make prominent modifications in this number within physical limitations. This number can only be modified independently by changing austenitization temperature (T_a) and it is not possible to make extreme changes in T_a due to physical limitations. Moreover, this number limits modifications in plastic dissipation number (Π_{10}) and yield number (Π_{11}). It is not possible to make prominent modifications in Π_{10} and Π_{11} when this number is kept constant. Because of these reasons, this number was not investigated. However it is predicted that this number has no influence on dimensional changes.
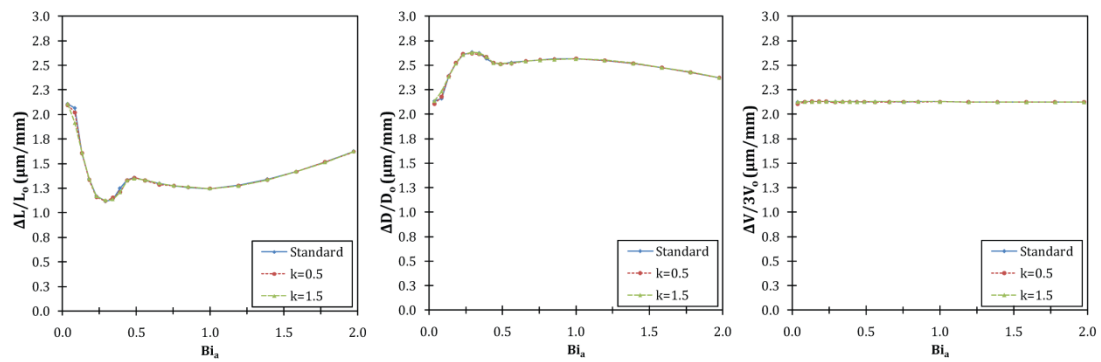
Π_{10} – *Plastic Dissipation Number:* $\left(\dfrac{\sigma^o}{\rho c (T_a - T_o)} \right)$

Plastic dissipation number governs heat dissipation due to plastic deformation. In quenching the extent of plastic deformation is relatively low (2-3%) Therefore, this term does not have significant effect on temperature evolution. As it is also mentioned above; quenching model that is used is not fully coupled. Thus, SYSWELD® does not simulate this term. As a result, it is not anticipated to have any change in dimensional changes with variations in Π_{10}. In fact, simulation result confirms this prediction (Figure 54).

Π_8 - Isotropic hardening

Π_8 - Kinematic hardening

Π_{10}- Isotropic hardening
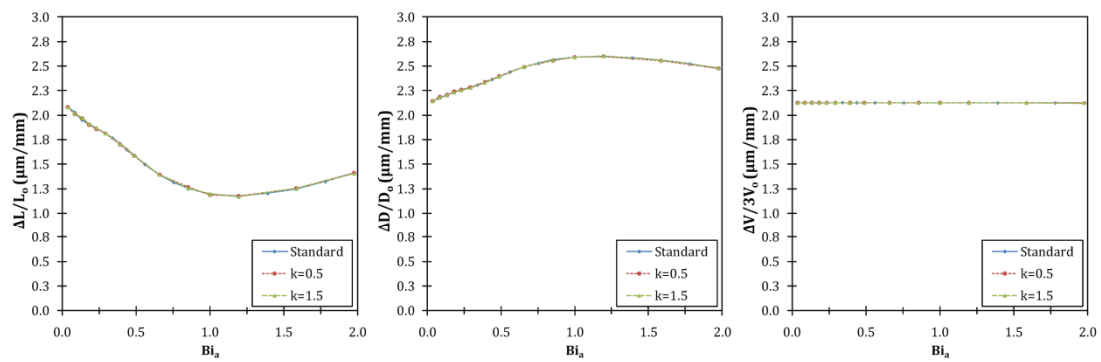
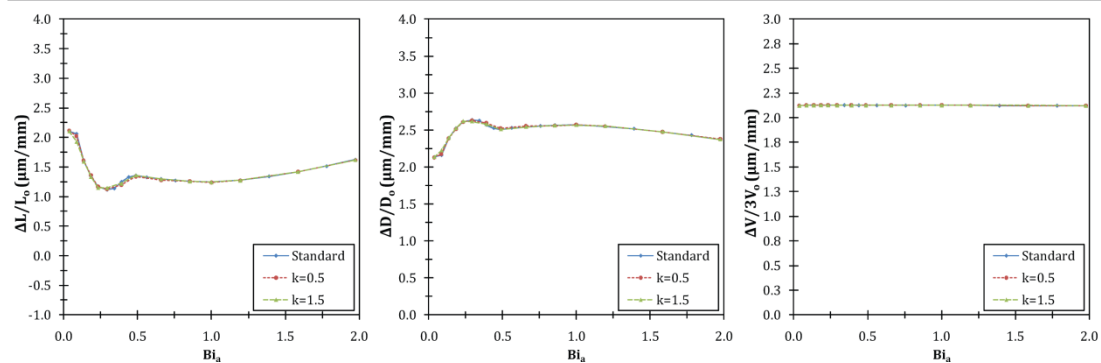## Π_{10}- Kinematic hardening

Figure 54: Bi vs. $\Delta Y/Y_o$ change curves when thermo-elastic Fourier number (Π_8) and plastic dissipation number (Π_{10}) are multiplied by k

### 5.4.6.7. Dimensionless numbers related with elasto-plasticity

Π_{11} - *Yield Number:* $\left(\sqrt{\dfrac{2}{3}} \dfrac{(1+\nu)\sigma^o}{E} \right)$

Yield number is one of the dimensionless numbers that are independent of the process parameters and purely depends on material. It governs the magnitude of elastic strains that is accumulated in the material in a certain stress state. Consequently, this number is anticipated to affect the extent of plasticity. Figure 55 confirms this prediction by illustrating the effect of this number on peak heights (H).

In the case of isotropic hardening, as yield number increases H decreases which show that the extent of plasticity and anisotropy of the dimensional changes decrease. At kinematic hardening curve, effect of this number is quite different. Major impact is observed in first peak (P1).

In Section 5.4.3. , the formation of the first peak is predicted to be a consequence of the influence of back stresses on TRIP-CP competition. Also it was mentioned that, TRIP intends to increase the height and width of P1 whereas, CP has reverse effect. Results in Figure 55 confirm these predictions. P1 widens such that it is not possible to see third peak in investigated Biot number range. Any attempt to decrease magnitude of classical plasticity seems to increase height and width of P1 and vice versa.

Π_{11}- Isotropic hardening
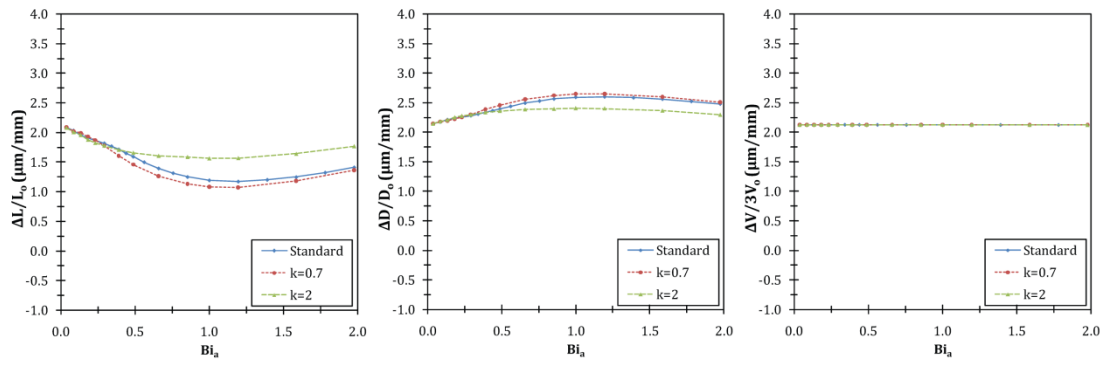
Π_{11}- Kinematic hardening
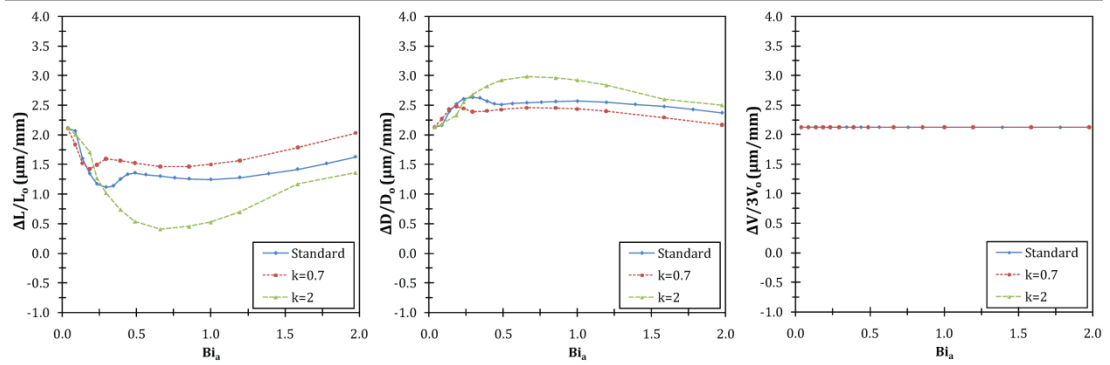
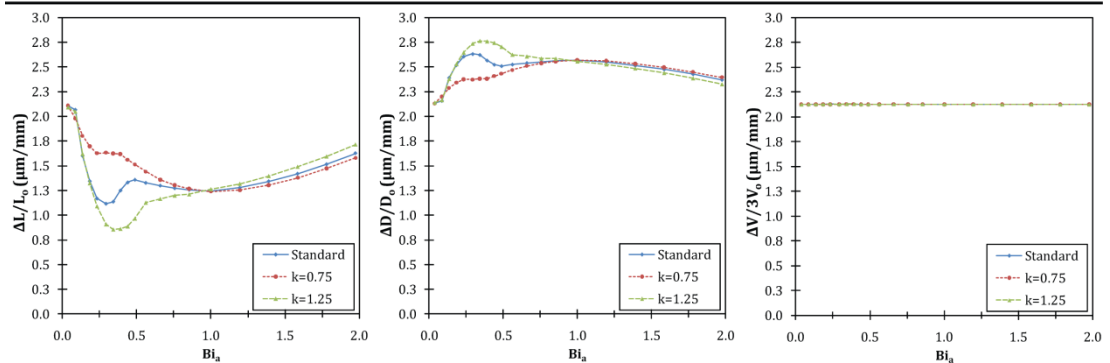## Π_{12}- Isotropic hardening
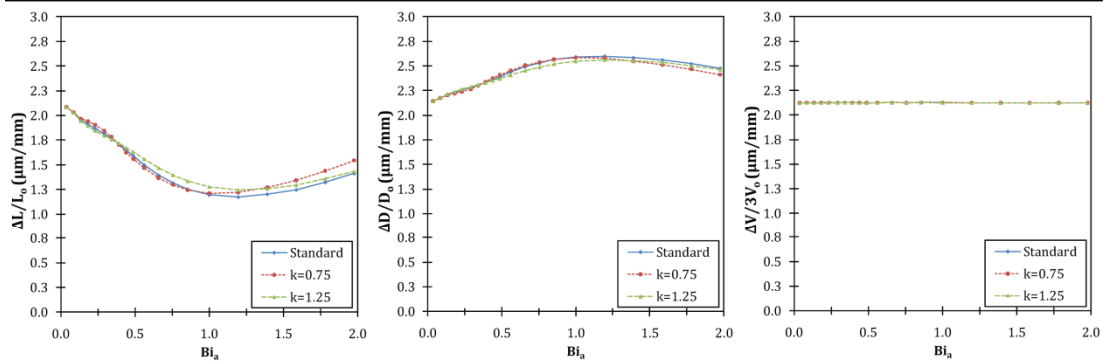
Π_{12}- Kinematic hardening

Figure 55: Bi vs. $\Delta Y/Y_o$ change curves when yield number (Π_{11}) and isotropic hardening number (Π_{12}) are multiplied by k

138

Π_{12} – *Isotropic Hardening Number:* $\left(\sqrt{\dfrac{2}{3}} \dfrac{(1+v)K_a}{E} \right)$

Isotropic hardening number directly stems from Ramberg-Osgood model. Similar to Π_{11}, this number is independent of the process and it purely depends on material property. It is a simple index that gives the ratio of plastic deformation resistance to elastic deformation resistance. Therefore, it is anticipated that peak heights will be affected from its variation. Figure 55 confirms this prediction. It can be seen that peak heights (H) decreases with increasing Π_{12}.

Π_{12} also has significant affect on peak positions (X). In the case of isotropic hardening, X increases with increasing Π_{12}. This is most probably because, the dominance of classical plasticity shifts to higher Biot numbers since plasticity becomes harder.

One of the material parameters that determines back stresses is K_a. Therefore, effect of isotropic hardening number on kinematic hardening curves is more severe. It is seen that relative dimensional change curves become almost identical to isotropic curve when Π_{12} is decreased. This is due to the decrease in back stresses. It is also seen that second peak shifts left and its height significantly increases when Π_{12} is decreased. This confirms that the range of TRIP dominance decreases with increasing classical plasticity. Also; increase in peak height might be attributed to the increase in backstresses, but further post-processing is necessary to clarify the mechanism.

Π_{13} – *Transformation Plasticity Number:* $\left(\dfrac{3\kappa E}{2(1+v)} \right)$

TRIP number, as its name implies, governs the extent of transformation plasticity. This number is very important since it gives hints about

- the differences in the plasticity mechanisms of right and left hand side of the peak positions.

- the reasons behind the first peak in the kinematic hardening curves.

Π_{13}- Isotropic hardening
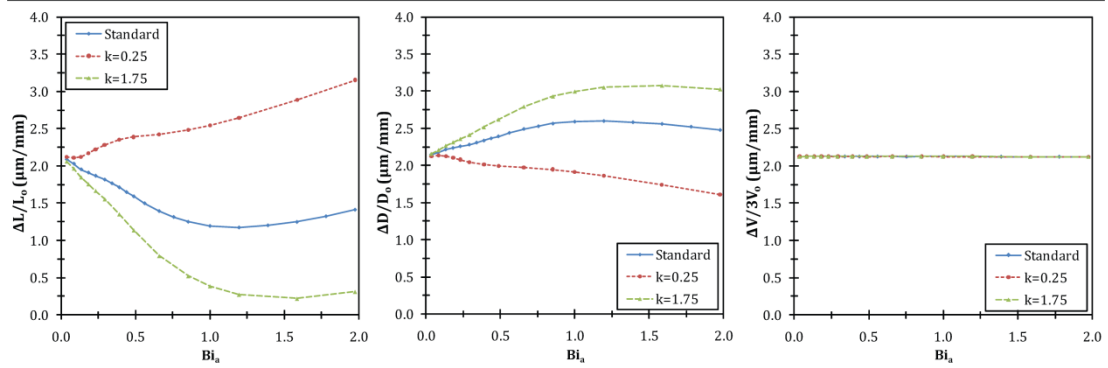
Π_{13}- Kinematic hardening
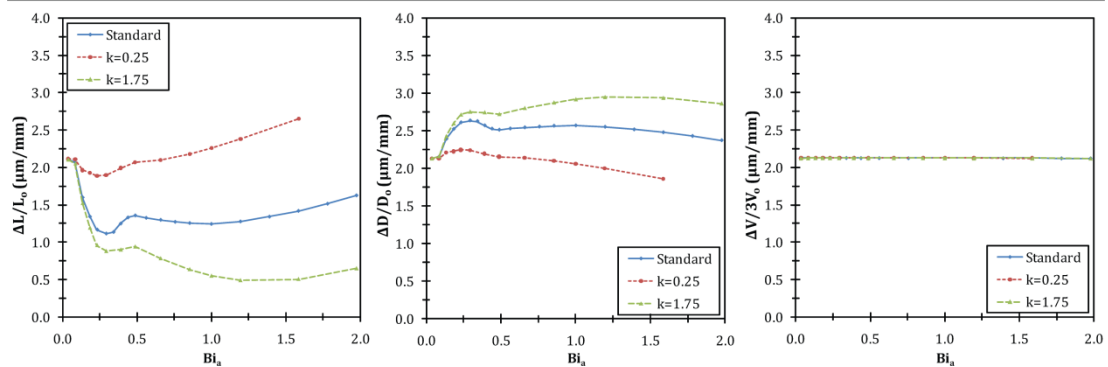
Figure 56: Bi vs. ΔY/Yₒ curves when transformation induced plasticity number (Π₁₃) is multiplied by k

Similar to the case without TRIP, trend of the isotropic hardening curves change considerably at low TRIP numbers. Classical plasticity does not dominate at the investigated range of Biot number. At higher TRIP numbers, on the other hand, peak position shifts right. These results confirm the prediction about the reasons behind the formation of first peak (Section 5.4.3.), by illustrating the increase in range of TRIP dominance.

In the case of kinematic hardening, first peak tends to disappear at lower TRIP numbers. This result together with the results of isotropic hardening number (Π_{12}) confirms the predictions in Section 5.4.3. . However, further, investigations and post processing is necessary for complete understanding of the mechanism.

5.4.6.8. Dimensionless numbers related with plasticity

Π_{14} – *Ramberg-Osgood Exponent of Austenite:* $\left(n_a \right)$

Ramberg-Osgood exponent is a dimensionless material property. It stems from Ramberg-Osgood equation. It governs work hardening and it can be considered as a kind of strain hardening rate $\left(n = d\log\sigma / d\log\varepsilon \right)$. As it is illustrated in Figure 57, magnitude of stress occurring at a certain magnitude of strain (ε) decreases with increasing n when ε<1. Quenching strains are well below this threshold. Therefore, increasing Ramberg-Osgood exponent eases the classical plasticity and decreases TRIP. Namely, its effect is opposite to the isotropic hardening number (Π_{12}). Another influence of n_a is on back stresses. Together with Ramberg-Osgood coefficient (K_a), n_a determines back stresses. This can also be seen from Figure 58. Peak hights (H) increase, and peak position (X) decrease when n_a is increased. First peak in kinematic hardening curves are also affected significantly. This might be because of the changes in the magnitude of TRIP and back-stresses..

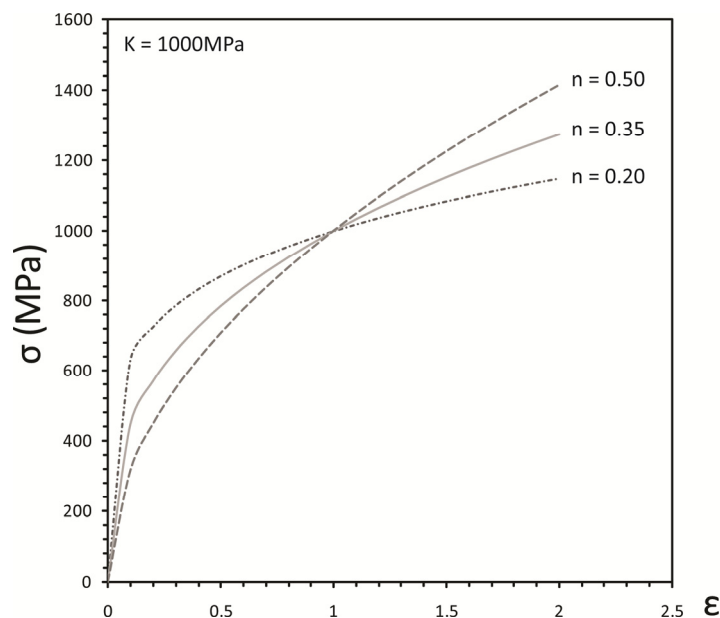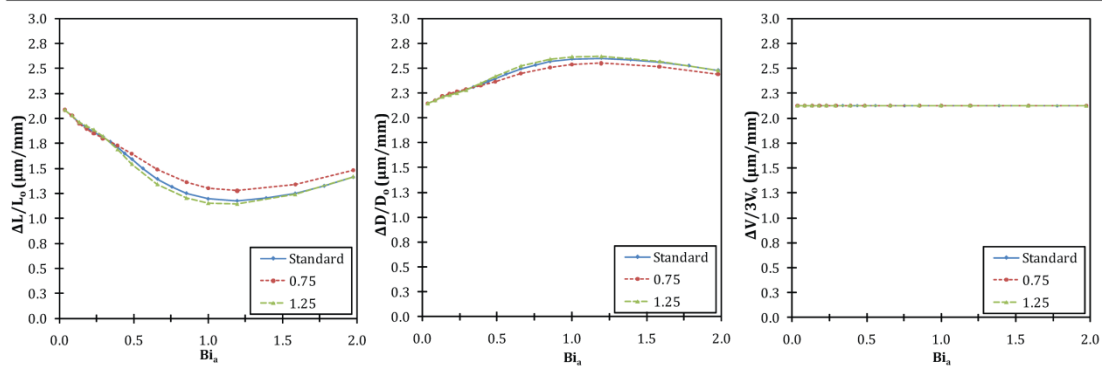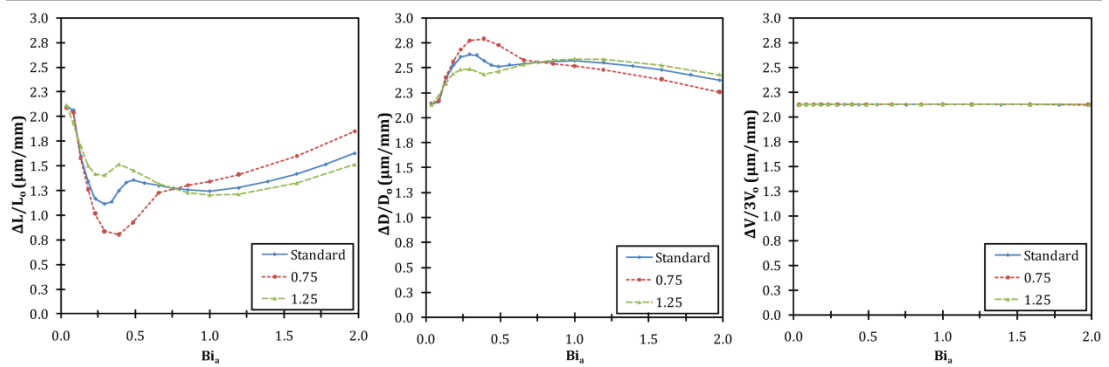**Figure 57: Stress-strain diagram for different values of Ramberg-Osgood exponent (n). (Ramberg-Osgood coefficient is equal to 1000MPa)**
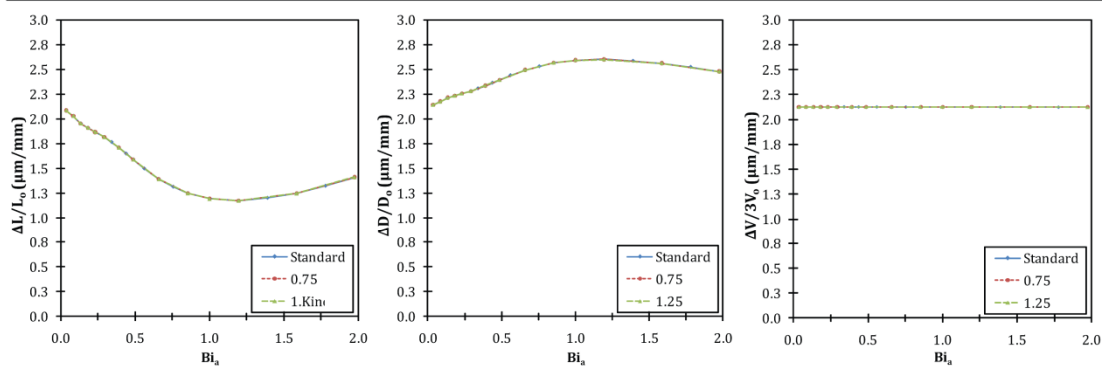
Π_{14}- Isotropic hardening

Π_{14}- Kinematic hardening

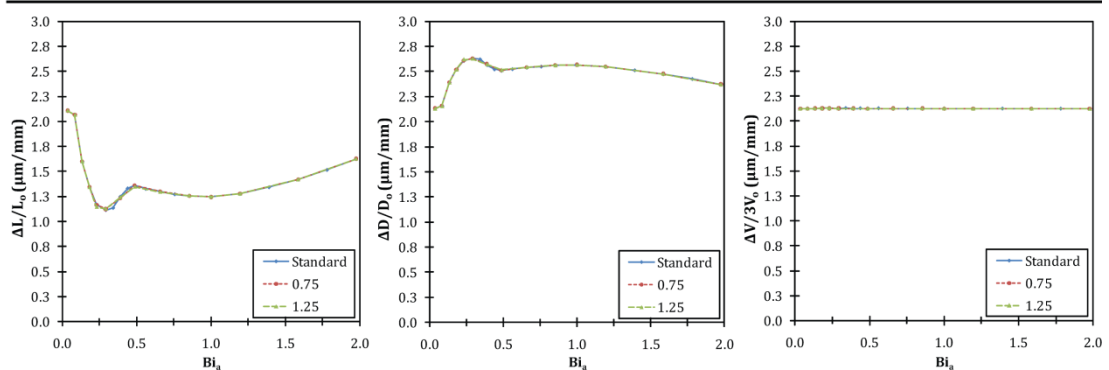Π_{21}- Isotropic hardening

Π_{21}- Kinematic hardening

Figure 58: Bi vs. $\Delta Y/Y_o$ curves when Ramberg-Osgood exponent of austenite (Π_{14}) and martensite are multiplied by k=0.75 and k=125

Π_{21} – *Ramberg-Osgood Exponent of Martensite:* $\left(n_m \right)$

In addition to n_a, the effect of n_m on the dimensional changes were also investigated. From Figure 58 it can be seen that this number does not have any effect, as anticipated. This is because; martensite does not yield due to its high yield strength. However, it should be noted that, the affect of n_m depends on σ_m^o. If yield strength of martensite were lower, it would be an important parameter that effect anisotropic dimensional changes.

Π_{15} – *Yield Strength Ratio:* $\left(\dfrac{\sigma_m^o}{\sigma_a^o} \right)$

This number depends purely on material property. It is an index comparing the yield strength of austenite and martensite. It can be seen from Figure 59 that increasing yield strength ratio does not have any effect on dimensional changes. This is because; there is no plasticity in martensite and increasing the yield strength of martensite does not make any difference in the plasticity. On the other hand, when Π_{15} is decreased, behavior of the curve changes at higher Biot numbers. This is because, at these Biot numbers, the magnitudes of stresses are high enough to exceed decreased yield strength of martensite.

Π_{16} – *Isotropic Hardening Ratio:* $\left(\dfrac{K_m}{K_a} \right)$

Isotropic hardening number is an index that compares the hardening coefficients of austenite and martensite. Due to the similar reasons in Π_{21}, this number does not have any influence on dimensional changes (Figure 59). However, this might change at higher Biot numbers and lower σ_m^o.

Π_{15}- Isotropic hardening
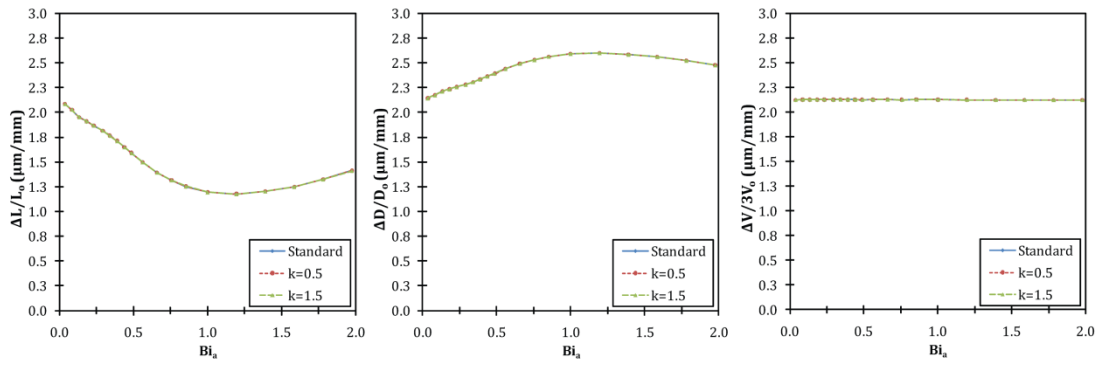
Π_{15}- Kinematic hardening
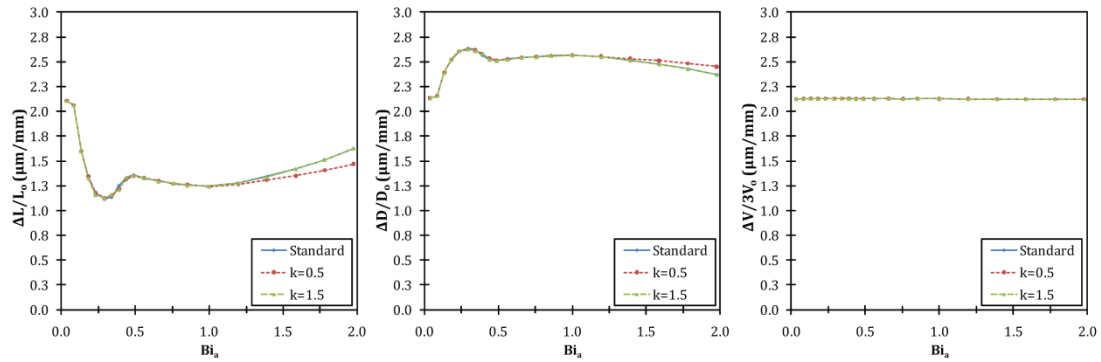
Π_{16}- Isotropic hardening
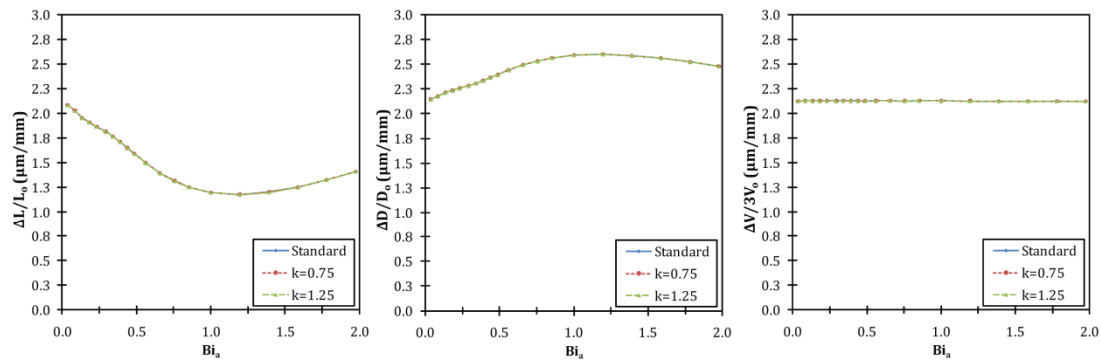
Π_{16}- Kinematic hardening
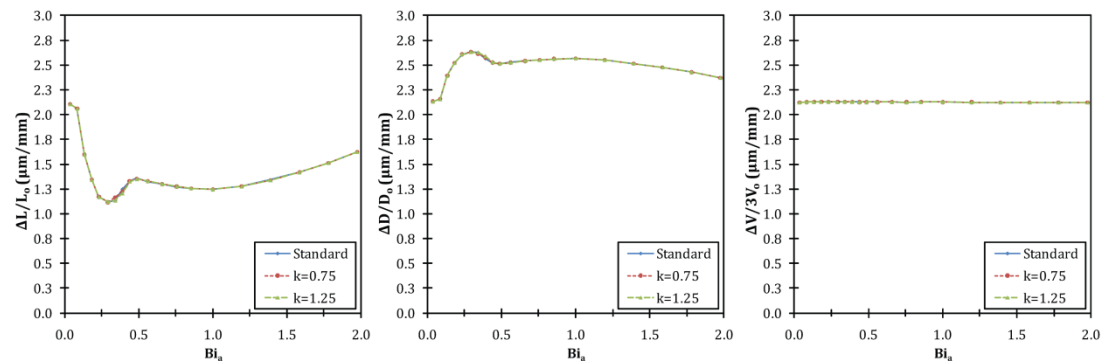
Figure 59: Bi vs. $\Delta Y/Y_o$ curves when yield strength ratio (Π_{15}) and isotropic hardening ratio (Π_{16}) are multiplied by k

5.4.6.9. Dimensionless numbers related with elasticity

Π_{17} – *Poisson's Ratio Number of Austenite and* Π_{22} - *Martensite:* $\left(\dfrac{v_a}{1-2v_a}\right), \left(\dfrac{v_m}{1-2v_m}\right)$

Poisson's ratio is an important material property that determines anisotropic dimensional changes in elastic deformation. This number alters plastic deformation since it affects stresses that are accumulated in the component.

It can be seen from Figure 60 that Poisson's ratio of austenite has significant effects on isotropy of the dimensional changes. As anticipated, increasing Poisson's ratio, increase the anisotropy of dimensional changes.

Behavior of first peak of kinematic hardening curve is altered significantly by Biot number. However, it is not possible to predict the reason behind this behavior without post-procession of the simulations.

Poisson's ratio of martensite does not cause any significant change in dimensional changes which might be because; there is no plasticity in martensite phase.

Π_{23} – *Ratio of Elastic Moduli:* $\left(\dfrac{E_m}{E_a}\right)$

Ratio of elastic moduli is another important material parameter. Similar to Poisson's ratio it affects accumulated stresses in the component. Therefore, it alters TRIP and CP strains which alter anisotropic dimensional changes (Figure 61). Increasing this number increases anisotropic dimensional changes, as predicted.

Π_{17}- Isotropic hardening
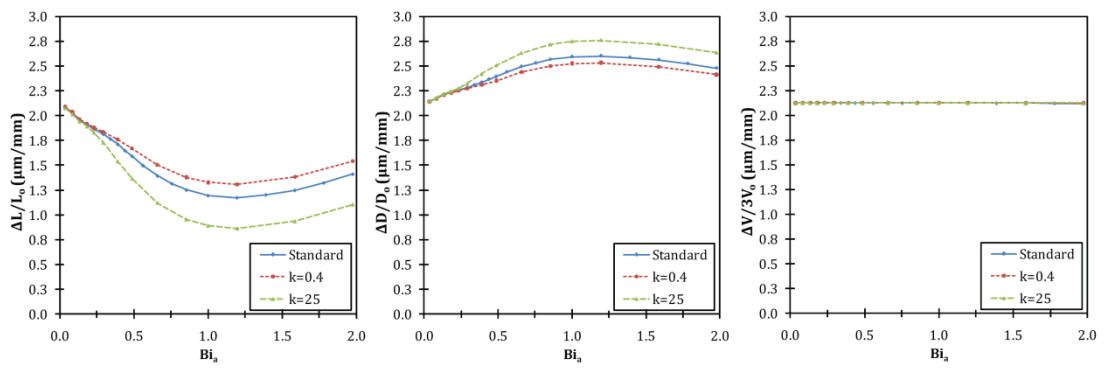
Π_{17}- Kinematic hardening
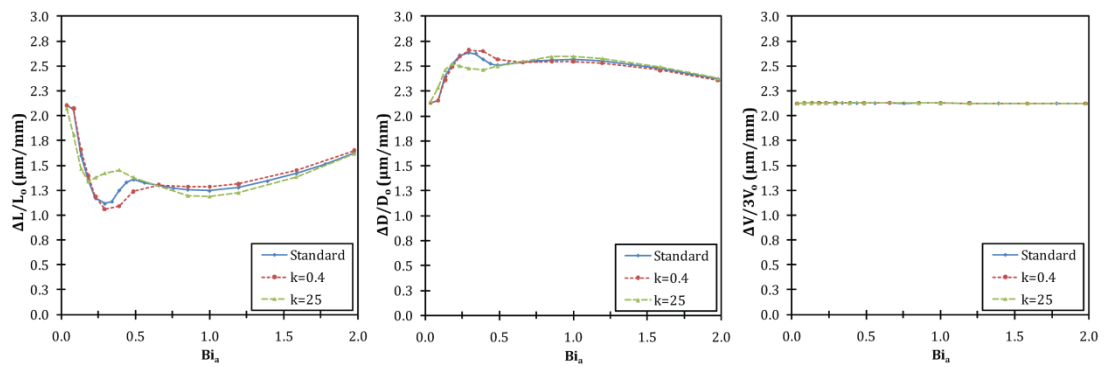
Π_{22}- Isotropic hardening
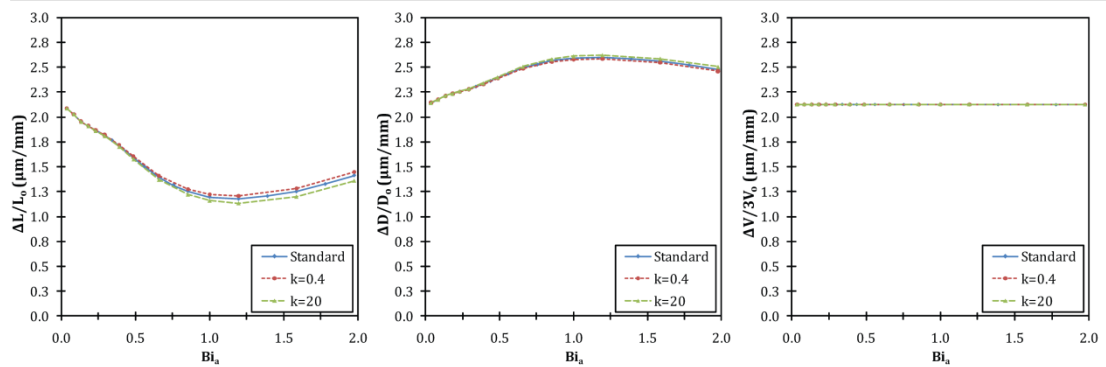
Π_{22}- Kinematic hardening
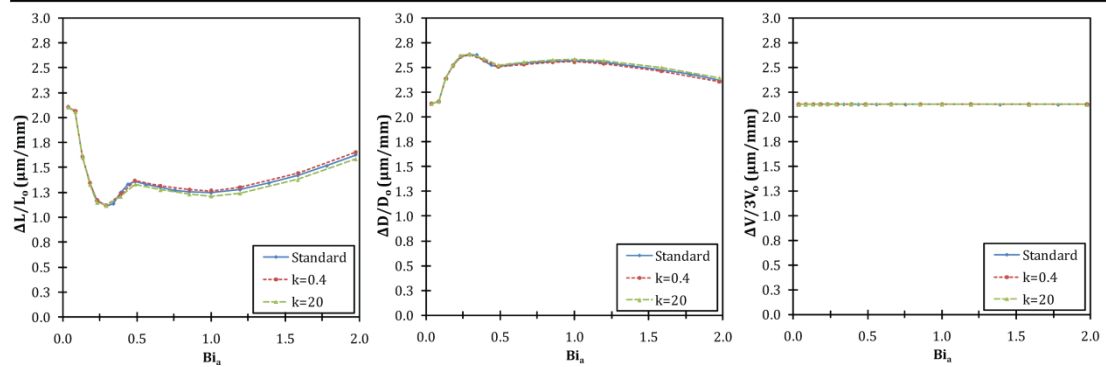
Figure 60: Bi vs. $\Delta Y/Y_o$ curves when Poisson's ratio number of austenite (Π_{17}) and martensite (Π_{22}) are multiplied by k

Π_{23}- Isotropic hardening
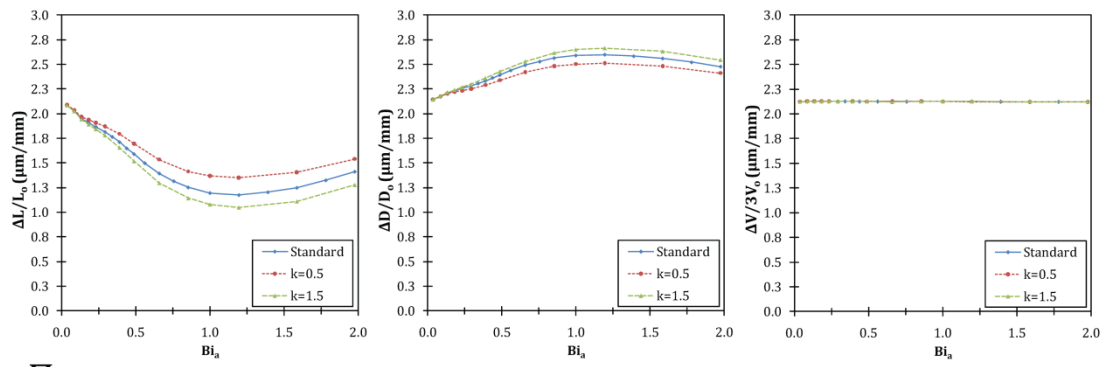
Π_{23}- Kinematic hardening
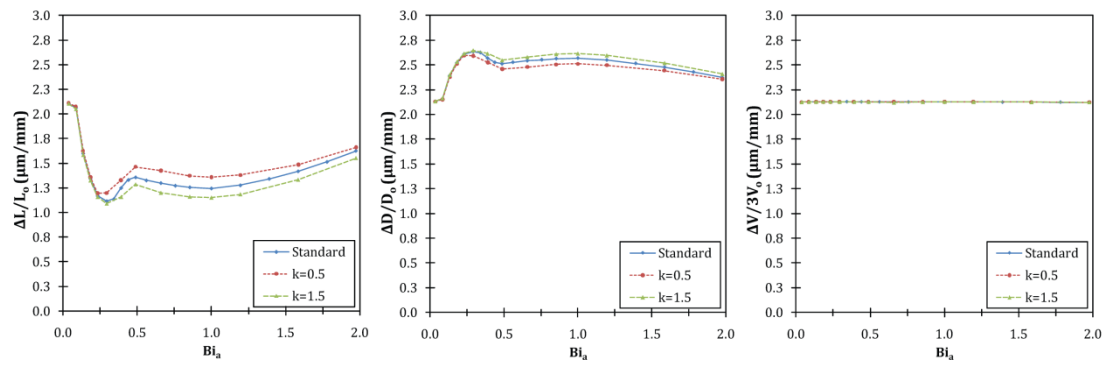
Figure 61: Bi vs. ΔY/Y₀ curves ratio of elastic moduli (Π₂₃) is multiplied by k

CHAPTER 6

CONCLUSION AND OUTLOOK

6.1. Experimental

In this part of the study, SAE52100 long cylinders were through hardened by gas nozzle field, salt bath and high speed quenching techniques. Specimens were machined from different positions of the initial billet in order to investigate effects of segregation distribution on distortion. According to the results it can be concluded that;

o Dimensional changes deviate significantly with machining positions. This might be owed to the inhomogeneous distribution of Martensite start (M_s) temperature, spatially asymmetric variation of material properties and anisotropy in the transformation strains [15] due to inhomogeneous distribution of Cr and C.

o Since there is large scatter in the experimental data, it is not possible to correlate bending magnitudes with heat transfer coefficient and diameter of the cylinders.

o Similar to SAE 5120 steel [15], bending directions of SAE52100 exhibits an orientation relationship with microstructure. However. bending magnitudes of SAE52100 steel is lower than that of SAE 5120 [15]. This might be because of the differences in the type of the inclusions. In SAE 5120 the reason of bending is systematic distribution of anisotropic transformation strain (ATS) resulting from the development of banded microstructures. In the case of SAE52100 there is no such structure. Reason of bending in this steel might be due to the inhomogeneous distribution of C and Cr which results in deviations in volume change throughout the component.

148

Beside clarified points about the bending behavior of SAE52100, there remain several questions to be uncovered. In the outlook, additional dilatometer and mechanical tests can be considered as a future task to verify the predictions about the bending behavior of SAE52100 steel.

Unfortunately, during processing of the results, it was observed that, symmetric cooling could not be achieved in gas-nozzle-field. Also, there were excessive bainite in salt bath quenching experiments. Therefore, bending results from these experiments are not totally reliable. They only provide hints about the behaior. In order to ensure repeatability of the results, further quenching experiments can be considered in the outlook of this study.

6.2. Sensitivity analysis

In this part of the study, the main aim was to determine the effects of uncertainties in material data on quenching simulation and distinguish input parameters that significantly alter simulation results. For this purpose, each material property perturbed around a reference state and a dimensionless (local) sensitivity measure was used to compare the effects of these on simulation results. Finally, a sensitivity ranking system was utilized to classify the parameters according to their importance. Sensitivity analysis results showed that;

o   Regardless of the hardening rule, the most significant material properties are the ones that affect dilatation which are M_s, M_o, ε_{tr}, α_a and α_m. Amongst these, M_s, M_o and ε_{tr} alter phase transformation strains (ε_{ij}^{pt}), whereas; α_a and α_m affect thermal strains (ε_{ij}^{th}). These properties also have various affects on stress field and hence isotropy of dimensional changes.

o   In contrast to the other transformation parameters, ΔH^{tr} has no significant effect on the simulation results. This might be because; in the case of consideration, heat dissipated during transformation has not significant effect in temperature evolution along the geometry. However; this might change with the geometric effects such as section thickness or symmetry.

- o Plasticity and thermal parameters does not affect volume change. Amongst plasticity parameters the most important one is yield strength of austenite. It significantly alters anisotropic dimensional changes since it directly affects the extent of classical plasticity. Thermal parameters also have slight influence on dimensional changes. This might be because they affect heat gradient within the material.

- o There is no large difference between the results of kinematic and isotropic hardening rules. Only importance of mechanical properties slightly increase when kinematic hardening rule is used. This is probably due to the back stresses, but; it is not possible to reveal their effect on the system from current results.

- o Mechanical and thermal properties of austenite are more important than the properties of marteniste. This might be owed to the fact that, martensite does not exist in the initial stages of cooling when thermal stresses and classical plasticity are dominant and conduction is in its highest rate.

In the outlook of this study, sensitivity analysis can be considered to be performed at two or more Biot numbers. This might provide valuable information about the dependence of sensitivities of material properties on cooling behavior.

6.3. Dimensional analysis

In dimensional analysis part of this study, the validity and completeness of dimensionless number sets that were determined by Buckingham π theorem and non-dimensionalization of weak form of the governing equations were verified. Later, influences of the dimensionless numbers on relative dimensional change were investigated. Results of the investigations on dimensionless number sets and dimensionless numbers can be summarized as following:

- o Dimensionless number sets are valid and completely govern quenching with martensitic transformation.

- o Biot number is an important dimensionless number that determines dimensional changes after quenching.

o In the case of isotropic hardening model relative dimensional changes vs. Biot number curves can simply be approximated to second order parabola, whereas; in the case of kinematic hardening behavior of the curve is more complicated. It is combination of two parabolas and a transition region.

o The behavior of relative dimensional change vs. Biot number curves can be attributed to competition between classical plasticity (CP) and transformation plasticity (TRIP). In isotropic hardening curves peak can be interpreted as the critical Biot number at which classical plasticity starts to offset TRIP. In the case of kinematic hardening, back stresses cause formation of a second peak at higher Biot numbers. This might be because of drastic increase in plasticity in Stage 3 due to back stresses.

o Dimensionless numbers that govern with transformation (Π_4-Martensite start number, Π_5-Koistinen-Marburger number) and dilatation (Π_6-Thermal strain number, Π_7-Transformation strain number, Π_{20}-Ratio thermal expansion coefficients) influence intercept of Bi vs. $\Delta Y/Y_o$ curves and hence volume change significantly. These numbers also have various influences on isotropy of dimensional changes depending on their effects on stress state.

o Dimensionless numbers related with heat conduction (Π_{18}-Ratio of thermal conductivities, Π_{19}-Ratio of specific heats) considerably alter isotropic dimensional changes. This might be attributed to their effects on heat evolution and therefore stress state.

o Dimensionless numbers that determine thermo-elasto-plasticity (Π_8-Thermo-elastic Fourier number, Π_{10}-Plastic dissipation number) have no effect on dimensional changes. The reason why Π_8 has no influence is that, SYSWELD® uses quasi-static approach and therefore, it neglects inertial terms. Π_{10} is also unimportant since heat dissipated due to plastic strains are negligible and SYSWELD® does not simulate it since thermo-metallurgical and mechanical fields are not fully coupled.

o Dimensionless numbers that determine plasticity of austenite (Π_{11}-Yield number, Π_{12}-Isotropic hardening number, Π_{14}-Ramberg Osgood exponent of austenite) have various influences on isotropy of dimensional changes. Amongst these numbers, Π_{11} has most importance. In the case of kinematic hardening these numbers have drastic effects on first peak. This is because they, effect plasticity. Also, Π_{12} and Π_{14} alters back stresses.

o Dimensionless numbers that are related with plasticity of martensite (Π_{15}-Yield strength ratio, Π_{16}-Isotropic hardening ratio, Π_{21}-Ramberg Osgood exponent of martensite) does not have any influence on dimensional changes. This is anticipated since; stresses usually do not exceed yield strength of martensite.

o TRIP number (Π_{13}) is one of the most important dimensionless numbers. It significantly alters plasticity. It can change even the behavior of the curves.

o Dimensionless numbers that govern elasticity (Π_{17}-Poisson's ratio of austenite, Π_{22}-Poisson's ratio of martensite, Π_{23}-Ratio of elastic moduli) affect isotropy of the dimensional changes. This might be attributed to their indirect effect on plasticity. These numbers affect accumulated stresses and hence plasticity and TRIP in the component.

o If insignificant dimensionless numbers are eliminated from the dimensionless number set, there remain 14 numbers that alter dimensional changes:

Π_1-Biot number	Π_{13}-Transformation plasticity number
Π_4-Martensite start number	Π_{15}-Yield strength ratio
Π_5-Koistinen-Marburger number	Π_{17}-Poisson's ratio number
Π_6-Thermal strain number	Π_{18}-Ratio of thermal conductivities
Π_7-Transformation strain number	Π_{19}-Ratio of specific heats
Π_{11}-Yield number	Π_{20}- Ratio of th. expansion coefficients
Π_{12}-Isotropic hardening number	Π_{23}-Ratio of elastic moduli

Depending on the required accuracy further elimination of the dimensionless numbers is possible. It should also be noted that, this list is valid only when there is no plasticity in martensite. At very high Biot numbers, plasticity parameters of martensite should be included to this list.

Beside aforementioned clarified points, in the outlook of this study, several points can be considered which are

- o Derivation of a rough expression that approximates dimensional changes by processing current results,

- o Derivation of a new dimensionless number set in which temperature dependency of sensitive material parameters is included.

REFERENCES

[1]   Zoch H-W. Distortion engineering: vision or ready to application? 2nd. International Conference on Distortion Engineering. Bremen, Germany, 2008. p.13.

[2]   Clausen B, Frerichs F, Kohlhoff T, Th L, Prinz C, Rentsch R, Sölter J, Surm H, Stöbener D, Klein D. Identification of process parameters affecting distortion of disks for gear manufacture Part I: casting, forming and machining. Materialwissenschaft und Werkstofftechnik 2009;40:354.

[3]   Şimşir C. 3D Finite Element Simulation of Steel Quenching in order to Determine the Microstructure and Residual Stresses. Metallurgical and Materials Engineering Depatment, vol. PhD. Ankara, Turkey: Middle East Technical University, 2008.

[4]   Wolf M, Bohm M, M. D, Lowisch G. Validation of Tp Model with Backstress for the Pearlitic Transformation of the Steel 100Cr6 under Step-Wise Loads. Comput. Mater. Sci. 2007;39:49.

[5]   Serajzadeh S. Modelling of Temperature History and Phase Transformations During Cooling of Steel. J. Mater. Process. Technol. 2004;146:311.

[6]   Taleb L, Cavallo N, Waeckel F. Experimental Analysis of Transformation Plasticity. Int. J. Plast. 2001;17:1.

[7]   Wolf M, M. B, G. L, Schmidt A. Modelling and Testing of Transformation-Induced Plasticity and Stress-Dependent Phase Transformations in Steel Via Simple Experiments. Comput. Mater. Sci. 2005;32:604.

[8]   Luiggi NJ. Comments on the Analysis of Experimental Data in Nonisothermal Kinetics. Metall. Mater. Trans. A-Phys. Metall. Mater. Sci. 2003;34A:2679.

[9]   Tszeng TC, Schi G. A Global Optimization Technique to Identify Overall Transfomation Kinetics Using Dilatometry Data – Applications to Austenitization of Steels. Mater. Sci. Eng. A-Struct. Mater. Prop. Microstruct. Process. 2004;380:123.

[10]   Wolf M, Bohm M, M. D, G. L, N. L, Rath J. Parameter Identification for a Trip Model with Backstress. Comp. Mater. Sci. 2006;37:37.

[11]   Acht C, Dalgic M, Frerichs F, Hunkel M, Irretier A, Lübben T, Surm H. Ermittlung der Materialdaten zur Simulation des Durchhärtens von Komponenten aus 100Cr6 - Teil 2. (German) Heat Treatm. Mat. 2008;64:362.

[12]   Acht C, Dalgic M, Frerichs F, Hunkel M, Irretier A, Lübben T, Surm H. Ermittlung der Materialdaten zur Simulation des Durchhärtens von Komponenten aus 100Cr6 - Teil 1. (German) Heat Treatm. Mat. 2008;63:234.

[13]   Krauss G. Principles of Heat Treatment of Steel. Metalspark, Ohio: American Society of Metals, 1980.

[14]   Gür CH, Pan J. Handbook of Thermal Process Modelling of Steels. Boca Raton, FL: CRC Press, 2008.

[15]   Hunkel M, Hoffmann F, Zoch H-W. Simulation of the distortion of cylindrical shafts during heat treatment due to segregations. Int. J. Microstructure and Materials Properties 2008;3:162.

[16]   Jaramillo RA, Lusk MT, Mataya MC. Dimensional anisotropy during phase transformations in a chemically banded 5140 steel. Part I: experimental investigation. Acta Materialia 2004;52:851.

[17]   Frerichs F, Lübben T, Fritsching U, Lohner H, Rocha A, Löwisch G, Hoffmann F, Mayr P. Simulation of gas quenching. Journal de Physique IV 2004;120:727.

[18]   Nallathambi AK, Kaymak Y, Specht E, Bertram A. Sensitivity of material properties on distortion and residual stresses during metal quenching processes. Journal of Materials Processing Technology 2010;210:204.

[19]   Frerichs F, D. Landek, Lübben T. Prediction of Distortion of Cylinders without Phase Transformations. Mat/-wiss u. Werkstofftech. 2006;37:63.

[20]   Frerichs F, Landek D, Lübben T, Hoffman F, Zoch HW. Prediction of Distortion of Cylinders Without Phase Transformations. In: Zoch HW, Lübben T, editors. 1st International Conference of Distortion Engineering. Bremen, Germany, 2005. p.415.

[21]   Landek D, Lisjak D, Frerichs F. Prediction of unavoidable distortions in transformation free cooling by a newly developed dimensionless model. 2nd International Congress on Distortion Engineering. Bremen, Germany,, 2008. p.237.

[22]   Wolff M, Böhm M, Frerichs F. Dimensional analysis of a model problem in thermoelasto-plasticity for cylindrical bodies under heating and cooling. Z. Angew. Math. Mech. (ZAMM) 2008;10:758.

[23]   Simsir C, Lübben T, Hoffmann F, Zoch H-W. Dimensional analysis of the thermomechanical problem arising during through-hardening of cylindrical steel components. Computational Materials Science 2010;49:462.

[24]   Totten GE, Tensi HM, Canal LCF. Chemistry of Quenching : Part II - Fundamental Thermophysical Processes Involved in Quenching. Proceedings of the 22nd Heat Treating Society Conference and the 2nd International Surface Engineering Congress. Indianapolis, Indiana. USA: ASM International, 2003. p.148.

[25]   Totten GE, Tensi HM, Canale LCF. Chemistry of Quenching : Part I - Fundemental Interfacial Chemical Processes Involved in Quenching. Proceedings of the 22nd Heat Treating Society Conference and the 2nd International Surface Engineering Congress. Indianapolis, Indiana, USA: ASM International, 2003. p.141.

[26]   Denis S, Farias D, Simon A. Mathematical-Model Coupling Phase-Transformations And Temperature Evolutions In Steels. ISIJ Int. 1992;32:316.

[27]   Denis S, Gautier E, Sjostrom S, Simon A. Influence Of Stresses On The Kinetics Of Pearlitic Transformation During Continuous Cooling. Acta Metallurgica 1987;35:1621.

[28]   Stouvenot F, Denis S, Simon A, Denis JP, Ducamp C. Experimental-study and prediction of structural transformations and cracking in a solidified thin-walled low-carbon steel. Memoires Et Etudes Scientifiques De La Revue De Metallurgie 1988;85:508.

[29]   Denis S, Gautier E, Simon A, Beck G. Stress-Phase-Transformation Interactions - Basic Principles, Modelling, And Calculation Of Internal Stresses. Mater. Sci. Technol. 1984;1:805.

[30]   Denis S, Sjostrom S, Simon A. Coupled Temperature, Stress, Phase Transformation Calculation; Model Numerical Illustration Of The Internal Stresses Evolution During Cooling Of A Eutectoid Carbon Steel Cylinder. Metallurgical transactions. A, Physical metallurgy and materials science 1987;18 A:1203.

[31]   Gautier E, Simon A. Transformation plasticity mechanisms for martensitic transformation of ferrous alloys. Phase Transformation 1988;87:285.

[32]   Avrami M. Kinetics of phase change. I. General theory. J. Chem. Phys. 1939;7:1103.

[33]   Avrami M. Kinetics of phase change. II. Transformation-time relations for random distribution of nuclei. J. Chem. Phys. 1940;8:212.

[34]   Avrami M. Kinetics of phase change III. Granulation, phase change, and microstructure. J. Chem. Phys. 1941;9:177.

[35]   Johnson WA, Mehl RF. Reaction kinetics in processes of nucleation and growth. Trans. AIME 1939;135:416.

[36]   Kolmogorov AN. On the statistical theory of the crystallization of metals. Izv. Akad. Nauk SSSR, Ser. Mat. 1937:355.

[37]   Scheil E. Anlaufzeit der austenitumwandlung. Arch. Eisenhuttenwes (German) 1935;8:565.

[38]   Cahn JW. Transformation kinetics during continous cooling. Acta Metallurgica 1956;4:572.

[39]   Christian JW. The Theory of Transformations in Metals and Alloys. Oxford: Pergamon Press, 1975.

[40]   Ahrens U, Maier HJ, Maksoud AEM. Stress affected transformation in low alloy steels - factors limiting prediction of plastic strains. J. Phys. IV 2004;120:615.

[41]   Bhadeshia H. Martensite and bainite in steels: Transformation mechanism & mechanical properties. J. Phys. IV 1997;7:367.

[42]   Cherkaoui M, Berveiller M, Lemoine X. Couplings between plasticity and martensitic phase transformation: overall behavior of polycrystalline TRIP steels. Int. J. Plast. 2000;16:1215.

[43]   Liu CC, Yao KF, Lu Z, Gao GF. Study of the effects of stress and strain on martensite transformation: Kinetics and transformation plasticity. J. Comput-Aided Mater. Des. 2000;7:63.

[44]   Todinov MT. Influence of some parameters on the residual stresses from quenching. Model. Simul. Mater. Sci. Eng. 1999;7:25.

[45]   Scott MD. Advances in quenching- A discussion of present and future technologies. 22nd Heat Treating Society Conference and the 2nd International Surface Engineering Congress. Indianapolis, Indiana, USA: ASM International, 2003. p.228.

[46]   Gajen DP. Salt bath quenching. Advanced materials and processes 1999.

[47]   Lior N. The cooling process in gas quenching. Journal of Materials Processing Technology 2004;155-156:1881.

[48]   Kobasko NI, Prokhorenko NI. Quenching cooling rate effect on crack formation of 45 steel. Metallovedenie and Thermicheskaya Obrabotka Metallov 1964:53.

[49]   Kobasko NI. Basics of intensive quenching. Adv. Mater. Process. 1995;148:W42.

[50]   Kobasko NI. Basics of intensive quenching. Adv. Mater. Process. 1999;156:H31.

[51]   Kobasko NI. Basics of intensive quenching .2. Adv. Mater. Process. 1996;150:CC40.

[52]   Kobasko NI. Method of overcoming self-deformation and cracking during quenching of metal parts. Metallovedenie and Thermicheskaya Obrabotka Metallov 1975:12.

[53]   Kobasko NI, Aronov MA, Powell JA, Canale LCF, Totten GE. Intensive quenching process classification and applications. Heat Treat. Met. 2004;31:51.

[54]   Sjostrom S. Interactions and Constitutive Models for Calculating Quench Stresses In Steel. Mater. Sci. Technol. 1984;1:823.

[55]   Geijselaers HJM. Numerical Simulation of Stresses due to Solid State Transformations. vol. PhD. Twente: University of Twente.

[56]   Stringfellow RG, Parks DM. A Self-Consistent Model of Isotropic Viscoplastic Behavior in Multiphase Materials. Int. J. Plast. 1991;7:529.

[57]   Koistinen DP, Marburger RE. A general equation prescribing the extent of the austenite-martensite transformation in pure non-carbon alloys and plain carbon steels. Acta Materialia 1959;7:55.

[58]   Belytscko T, Liu WK, Moran B. Nonlinear Finite Elements for Continua and Structures. Chicester: John Wiley & Sons, 2000.

[59]   Antretter T, Fischer FD, Cailletaud G. A numerical model for transformation induced plasticity (TRIP). J. Phys. IV 2004;115:233.

[60]   Cherkaoui M. Transformation induced plasticity: Mechanisms and modeling. J. Eng. Mater. Technol.-Trans. ASME 2002;124:55.

[61]   Cherkaoui M, Berveiller M. Micromechanical modeling of the martensitic transformation induced plasticity in steels. Smart Mater. Struct. 2000;9:592.

[62]   Cherkaoui M, Berveiller M. Special issue: Mechanics of martensitic phase transformation in SMA and TRIP steels. Int. J. Plast. 2000;16:1133.

[63]   Cherkaoui M, Berveiller M. Mechanics of materials undergoing martensitic phase change: A micro-macro approach for transformation induced plasticity. Z. Angew. Math. Mech. 2000;80:219.

[64]   Cherkaoui M, Berveiller M. Moving inelastic discontinuities and applications to martensitic phase transition. Arch. Appl. Mech. 2000;70:159.

[65]   Cherkaoui M, Berveiller M, Sabar H. Micromechanical modeling of martensitic transformation induced plasticity (TRIP) in austenitic single crystals. Int. J. Plast. 1998;14:597.

[66]   Fischer FD, Oberaigner ER, Tanaka K, Nishimura F. Transformation induced plasticity revised an updated formulation. Int. J. Solids Struct. 1998;35:2209.

[67]   Fischer FD, Schlogl SM. The Influence of Material Anisotropy on Transformation-Induced Plasticity in Steel Subject to Martensitic-Transformation. Mech. Mater. 1995;21:1.

[68]   Grostabussiat S, Taleb L, Jullien JF, Sidoroff F. Transformation induced plasticity in martensitic transformation of ferrous alloys. J. Phys. IV 2001;11:173.

[69]   Jacques P, Furnemont Q, Mertens A, Delannay F. On the sources of work hardening in multiphase steels assisted by transformation-induced plasticity. Philos. Mag. A-Phys. Condens. Matter Struct. Defect Mech. Prop. 2001;81:1789.

[70]   Jacques P, Furnemont Q, Pardoen T, Delannay F. On the role of martensitic transformation on damage and cracking resistance in trip-assisted multiphase steels. Acta Mater. 2001;49:139.

[71]   Marketz F, Fischer FD, Tanaka K. Micromechanics of transformation-induced plasticity and variant coalescence. J. Phys. IV 1996;6:445.

[72]   Meftah S, Barbe F, Taleb L, Sidoroff F. Parametric numerical simulations of TRIP and its interaction with classical plasticity in martensitic transformation. Eur. J. Mech. A-Solids 2007;26:688.

[73]   Suiker ASJ, Turteltaub S. Computational modelling of plasticity induced by martensitic phase transformations. Int. J. Numer. Methods Eng. 2005;63:1655.

[74]   Taleb L, Cavallo N, Waeckel F. Experimental analysis of transformation plasticity (vol 17, pg 1, 2001). Int. J. Plast. 2001;17:1029.

[75]   Taleb L, Cavallo N, Waeckel F. Experimental analysis of transformation plasticity. Int. J. Plast. 2001;17:1.

[76]   Taleb L, Petit S. New investigations on transformation induced plasticity and its interaction with classical plasticity. Int. J. Plast. 2006;22:110.

[77]   Taleb L, Petit-Grostabussiat S. Elastoplasticity and phase transformations in ferrous alloys: Some discrepencies between experiments and modeling. J. Phys. IV 2002;12:187.

[78]   Taleb L, Sidoroff F. A micromechanical modeling of the Greenwood-Johnson mechanism in transformation induced plasticity. Int. J. Plast. 2003;19:1821.

[79]   Tanaka K, Nishimura F, Fischer FD, Oberaigner ER. Transformation thermomechanics of alloy materials in the process of martensitic transformation: A unified theory. J. Phys. IV 1996;6:455.

[80]   Tjahjanto DD, Turteltaub S, Suiker ASJ, van der Zwaag S. Modelling of the effects of grain orientation on transformation-induced plasticity in multiphase carbon steels. Model. Simul. Mater. Sci. Eng. 2006;14:617.

[81]   Turteltaub S, Suiker ASJ. Transformation-induced plasticity in ferrous alloys. J. Mech. Phys. Solids 2005;53:1747.

[82]   Turteltaub S, Suiker ASJ. Grain size effects in multiphase steels assisted by transformation-induced plasticity. Int. J. Solids Struct. 2006;43:7322.

[83]   Leblond JB. Mathematical-modeling of transformation plasticity in steels .2. Coupling with strain-hardening phenomena. International Journal of Plasticity 1989;5:573.

[84]   Leblond JB, Devaux J, Devaux JC. Mathematical-modeling of transformation plasticity in steels .1. Case of ideal-plastic phases. Int. J. Plast. 1989;5:551.

[85]   Fischer FD, Reisner G, Werner E, Tanaka K, Cailletaud G, Antretter T. A new view on transformation induced plasticity (TRIP). Int. J. Plast. 2000;16:723.

[86]   Greenwood GW, Johnson RH. The deformation of metals under small stresses during phase transformations. Proc. Roy. Soc. 1965;283:403.

[87]   Abrassart F. Stress-Induced Gamma-Alpha' Martensitic Transformation In 2 Carbon Stainless-Steels - Application To Trip Steels. Metallurgical Transactions 1973;4:2205.

[88]   Sjöström S. Calculation of Quench Stresses in Steel. vol. PhD. Linköping, Sweden: University of Linköping, 1982.

[89]   Dasalos Y. Comportement dilatometrique et mecanique de l´austenite metastable d´un acier A 533. IRSID, 1981.

[90]   Leblond JB, Devaux J, Devaux JC. Mathematical modelling of transformation plasticity in steels: I. Case of ideal-plastic phases. Int. J. Plast. 1989;5:551.

[91]   Saltelli A, Tarantola S, Campolonga F, Ratto M. Sensitivity analysis in practice: a guide to assessing scientific models. West Sussex: Wiley, 2004.

[92]   Helton J, Davis F. Illustration of sampling-based methods for uncertainty and sensitivity analysis. Risk Anal 2002;22:591.

[93]   Iman R, Helton J. An investigation of uncertainty and sensivitiy analysis techniques for computer models. Risk Anal 1988;8:71.

[94]   Saltelli A, Chan K, Scott M. Sensitivity analysis. West Sussex: Wiley, 2000.

[95]   Cukier R, Fortuin C, Shuler K, Petschek A, Schaibly J. Study of the sensitivity of coupled reaction systems to uncertainties in rate coefficients. I. Theory. J Chem Phys 1973;59:3873.

[96]   Cukier R, Levine H, Shuler K. Nonlinear sensitivity analysis of multiparameter model systems. J Phys Chem 1977;81:2365.

[97]   Cukier R, Levine H, Shuler K. Nonlinear sensitivity analysis of multiparameter model systems. J Computat Phys 1978;26:1.

[98]   Cukier R, Schaibly J, Shuler K. Study of the sensitivity of coupled reaction systems to uncertainties in Rate coefficient. III. Analysis of teh approximations. J Chem Phys 1975;63:1140.

[99]   McRae G, Tilden J, Seinfeld J. Global sensitivity analysis-a computational implementation of the Fourier amplitude sensivity test (FAST). Comput Chem Eng 1982;6:15.

[100]   Saltelli A, Andres T, Homma T. Sensitivity analysis of model output: performance of the iterated fractional factorial design method. Comput Stat Data Anal 1995;20:387.

[101]   McCarthy MA. Stochastic Population Models for Wildlife Management. vol. PhD: The Unversity of Melbourne, 1995.

[102] McCarthy MA, Burgman MA, Ferson S. Sensitivity analysis for models of population viability. Biological Conversation 1995;73:93.

[103] Helton J. Uncertainty and sensitivity analysis techniques for use in performance assessment for radioactive waste disposal. Reliab Eng Syst Saf 1993;42:327.

[104] Helton J, Johnson J, Sallabery C, Storlie C. Survey of sampling-based methods for uncertainty and sensitivity analysis. Reliab Eng Syst Saf 2006;91:1175.

[105] Sobol I. Sensitivity estimates for nonlinear mathematical models. Math Model Comput Exp 1993;1:407.

[106] Cacuci D, Ionescu-Bujor M. A comparative review of sensitivity and uncertainty analysis of large-scale systems-II: statistical methods. Nucl Sci Eng 2004;147:204.

[107] Frey H, Patil S. Identification and review of sensitivity analysis methods. Risk Anal 2002;22:553.

[108] Ionescu-Bujor M, Cacuci D. A comparative review of sensitivity and uncetainty analysis of large-scale systems-I: deterministic methods. Nucl Sci Eng 2004;147:189.

[109] Ravalico JK, Maier HR, Dandy GC, Norton JP, Croke BFW. A Comparison of Sensitivity Analysis Techniques for Complex Models for Environmental Management.

[110] Saltelli A, Marivoet J. Non-parametric statistics in sensivity analysis for model output: a comparison of selected techniques. Reliab Eng Syst Saf 1990;28:229.

[111] Saltelli A, Ratto M, Tarantola S, Campolonga F. Sensitivity analysis for chemical models. Chem Rev 2005;105:2811.

[112] Bruno JE, Doctorow O, Kappner CH. Use of dimensional analysis in social science research. Socio-Economic Planning Sciences 1981;15:95.

[113] Campos I, Torres R, Ramírez G, Ganem R, Martínez J. Growth kinetics of iron boride layers: Dimensional analysis. Applied Surface Science 2006;252:8662.

[114] Cariñena JF, Santander M. Dimensional Analysis. Advances in Electronics and Electron Physics 1988;72:181.

[115] Chavan A, Mukherji S. Dimensional analysis for modeling oxygen transfer in rotating biological contactor. Bioresource Technology 2008;99:3721.

[116] Dixit RK, Mandal JN. Dimensional analysis and modelling laws for bearing capacity of reinforced and unreinforced soil. Construction and Building Materials 1993;7:203.

[117]   Giever PM, Sack RL. Similitude considerations for roof snow loads. Cold Regions Science and Technology 1990;19:59.

[118]   Jeswani ML. Dimensional analysis of tool wear in electrical discharge machining. Wear 1979;55:153.

[119]   Karbhari VM, Wilkins DJ. A dimensional analysis approach to notch sensitivity and fracture of composites with applications to design. Engineering Fracture Mechanics;42:139.

[120]   Kowalczyk W, Delgado A. Dimensional analysis of thermo-fluid-dynamics of high hydrostatic pressure processes with phase transition. International Journal of Heat and Mass Transfer 2007;50:3007.

[121]   Legendre P, Legendre L. Developments in Environmental Modelling. vol. 20: Elsevier, 1998. p.97.

[122]   Mazzeo NA, Venegas LE. An application of generalized similarity analysis to atmospheric diffusion. Atmospheric Research 1997;43:157.

[123]   Messina G, Paoletti A, Santangelo S, Tucciarone A. A single quality factor for electron backscattering from thin films. Microelectronic Engineering 1995;27:183.

[124]   Salam MA, Ahmad H, Tamsir T. Calculation of time to flashover of contaminated insulator by Dimensional Analysis technique. Computers & Electrical Engineering 2001;27:419.

[125]   Salokhe VM, Ninh NT. Modelling soil compaction under pneumatic tyres in clay soil. Journal of Terramechanics 1993;30:63.

[126]   Thurairajasingam E, Shayan E, Masood S. Modelling of a continuous food pressing process by dimensional analysis. Computers & Industrial Engineering 2002;42:343.

[127]   Buckingham E. On Physically Similar Systems; Illustrations of the Dimensional Equations. Physical Review 1914;4:345.

[128]   Rayleigh L. The Principal of Similitude. Nature 1915;95.

[129]   Tolman RC. The Measurable Quantities of Physics. Physical Review Ser. 2 1917;9:237.

[130]   Ameen E. Dimension changes of tool steels during quenching and temperig. Trans. ASM 1940;28:472.

[131]   Frerichs F, Lübben T, Hoffmann F, Zoch H-W, Wolff M. Unavoidable Distortion due to Thermal Stresses. 5th International Conference on Quenching and Control of Distortion. Berlin, 2007.

[132]   Wolff M, Böhm M, Frerichs F. Dimensional Analysis of a Model Problem in Thermoelasto-plasticity for Cylinderical Bodies under Heating and Cooling. Z. Angew. Math. Mech. 2008;88:758.

[133]   Wolff M, Böhm M, Suhr B. Dimensional analysis of a model problemfor cylinderical steel work-pieces in the case of phase transformations. Proceedings of IFHTSE. Dubrovnik-Cavtati, Croatia, 2009. p.247.

[134]   Simsir C, Lübben T, Hoffman F, Zoch HW, Wolf M. Prediction of Distortions in Through Hardening of Cylinderical Steel Workpieces by Dimensional Analysis. New Challanges in Heat Treatment and Surface Engineering. Dubrovnik, Croatia, 2009. p.351.

[135]   Epp J, Surm H, Kessler O, Hirsch T. In situ X-ray phase analysis and computer simulation of carbide dissolution of ball bearing steel at different austenitizing temperatures. Acta Materialia 2007;55:5959.

[136]   Wever F, Rose A. Atlas Fur Waermbehandlung Der Staehle, 1954.

[137]   Frerichs F, Lübben T, Fritsching U, Lohner H, Rocha A, Löwisch G, Hoffmann F, Mayr P. Simulation of gas quenching. Journal De Physique. IV : JP 2004;120:727.

[138]   Lübben T, Rath J, Krause F, Hoffman F, Zoch H-W. Determination of heat transfer coefficient during high-speed quenching (accepted manuscript). IMMC. İstanbul, Turkey, 2010.

[139]   Rajhi R, Taleb L, hami AE. Sensitivity of structural analyses to material parameters and appliation to elastoplastic constitutive equations through a case study. International Journal of Pressure Vessels and Piping 2007;84:430.

[140]   Maradit BP, Şimşir C, Lübben T, Gür CH. Metallurgical influence on quench distortion of SAE52100 long cylinders. 18th Congress of International Federation of Heat Treatment and Surface Engineering, July 26th -30th Rio de Janeiro, Brazil, 2010.

[141]   Prinz C, Hunkel M, Clausen B, Hoffmann F, Zoch H-W. Characterization of segregations and microstructure and their influence on distortion of low alloy SAE 5120 steel. 2nd Internation conference on distortion engineering. Bremen, Germany, 2008. p.61.